ABSTRACT

CHEMOSTRATIGRAPHY OF HEMIPELAGIC FACIES OF THE MONTEREY FORMATION AND EQUIVALENT SEDIMENTARY ROCKS, LOS ANGELES BASIN, CALIFORNIA

By

Rebecca K. Lanners

August 2013

The submarine-fan-dominated, proximal Los Angeles basin contains interstratified hemipelagic strata coeval with the widespread Miocene Monterey Formation that accumulated in other California margin basins. Although more detrital-rich and containing greater abundance of plagioclase and muscovite than more distal, outboard basins, a four-part compositional zonation is recognized in the fine-grained facies, similar to the stratigraphic succession of the Santa Barbara coastal area. In ascending stratigraphic order, these include a basal interbedded calcareous-siliceous zone, a phosphatic zone, a calcareous-siliceous zone, and an uppermost siliceous zone. To establish these zonations, 125 samples from five wells in a north-south transect across the western basin from East and West Beverly Hills, Inglewood, and Wilmington oil fields were analyzed for bulk chemical composition by XRF and quantitative mineralogy by XRD and FTIR. The mineralogic composition of the fine-grained detrital fraction makes use of geochemical equations for sedimentary components developed elsewhere unsuitable to the Los Angeles basin.

CHEMOSTRATIGRAPHY OF HEMIPELAGIC FACIES OF THE MONTEREY FORMATION AND EQUIVALENT SEDIMENTARY ROCKS, LOS ANGELES BASIN, CALIFORNIA

A THESIS

Presented to the Department of Geological Sciences

California State University, Long Beach

In Partial Fulfillment

of the Requirements for the Degree

Master of Science in Geology

Committee Members:

Richard J. Behl, Ph.D. (Chair)
Thomas Kelty, Ph.D.
Scott Prior, M.S.

College Designee:

Robert D. Francis, Ph.D.

By Rebecca K. Lanners

B.S., 2010, California State University, Long Beach

August 2013

WE, THE UNDERSIGNED MEMBERS OF THE COMMITTEE,

HAVE APPROVED THIS THESIS

CHEMOSTRATIGRAPHY OF HEMIPELAGIC FACIES OF THE MONTEREY FORMATION AND EQUIVALENT SEDIMENTARY ROCKS, LOS ANGELES, CALIFORNIA

By

Rebecca K. Lanners

COMMITTEE MEMBERS

Richard J. Behl, Ph.D. (Chair)	Geological Sciences
Thomas Kelty, Ph.D.	Geological Sciences
Scott Prior, M.S.	Occidental Oil and Gas Corporation

ACCEPTED AND APPROVED ON BEHALF OF THE UNIVERSITY

Robert D. Francis, Ph.D.
Department Chair, Department of Geological Sciences

California State University, Long Beach

August 2013

ACKNOWLEDGEMENTS

I would like to take the time to thank everyone who supported me through this lengthy and at times challenging endeavor.

To my advisor, Dr. Richard Behl, a very heartfelt thank you for the opportunity to continue my education and be a part of the Monterey and Related Sediments (MARS) consortium. Hearing you lecture still inspires me to be a better geologist. I am incredibly fortunate to have had the opportunity to be under your instruction over the last few years.

To Janice Tomson, I owe my passion for geology to you. You introduced me to geology my first semester in college. Your enthusiasm is infectious and challenges me to strive to be a better geologist in and out of the classroom. Little did I know that my thesis would follow the very work you did years ago when you worked at USGS. I felt so proud to see your name on so many of the papers that I read countless times. I am so thankful to have you as a mentor, you are truly amazing. Thank you, for everything.

To my coworkers at Occidental Oil and Gas, thank you for all the support over the last few years. There is no greater motivation than working and going to school full time!! That said, it would not have been possible without the support of my team. Hilario Camacho, you have believed in me from the very beginning. Thank you for telling me I could work and go to school at the same time, when so many others said I could not. I am so fortunate to have you as a Manager, you have the ability to see one's potential and have unwavering support for it. Don Clarke, you introduced me to Petroleum geology, and Oxy. Your support and advice over the last few years has been

so helpful. To Scott Prior, thank you for agreeing to be on my thesis committee. Your knowledge of the geology of the LA basin and "ability to write the King's English" has helped me vastly.

To Dr. Charles Herzig, you were such a blessing over the last year. You were there with me nearly every day, raiding offices and labs for the right equipment, picking samples, figuring out new analytical techniques, and as my sound board. Thank you for all of your time, expertise, and support. Students at El Camino College are fortunate to have a professor like you. To Dr. Tom Kelty, a big thank you for the guidance and structure as an undergrad and now as a graduate student. Your smart comments kept me on my feet.

To my undergrad assistants, Bennet Trotter and Rane Anderson, I am incredibly grateful. Bennet, you are well on your way to becoming a wonderful geologist. I had no idea I was going to get such great help when Dr. Behl asked if I would like some assistance. I would probably still be picking samples if it were not for you guys!

I would like to thank all of the affiliate members of the MARS consortium for your support and membership. Use of your samples allowed me to work full time, and focus my time in the lab. Your generous advice knowledge helped make this project a success!

To my family, there are not enough words to express my appreciation for you all. Your support allowed me to focus on school, and accommodations let me put school first, after work. Thank you for taking an interest in what I do, wanting to see the easy-bake oven (XRD), asking if there was anything you could do to help, and listening to my rants of grad school. I love you guys and could not have a better family, I am truly fortunate!

To Ryan, my best friend, thank you for always telling me that I could do it, even when I doubted myself. You've been by my side from the start. Being a student requires a certain amount of selfishness, and you never questioned that. I cannot wait to start our lives together

TABLE OF CONTENTS

CHAPTER Page

Page

LIST OF TABLES

LIST OF FIGURES

FIGURE Page

FIGURE Page

CHAPTER 1

INTRODUCTION

Continental margin depositional systems can be dominated by basinward distribution of siliciclastic sediments from land or, alternately, by the oceanic and climatic processes that control the sedimentation and preservation of primarily biogenic components in the open ocean, or a combination of both (Teng and Gorsline, 1989)). In tectonically active margins, there exists the potential for development of a system of different depocenters in which sedimentation is controlled by these variables to different degrees depending on their proximity to the shoreline, rivers, banktops, oceanic currents or upwelling centers (Schwalbach and Gorsline, 1985). The middle to late Miocene California margin consisted of just this kind of network of tectonically formed sedimentary basins (Figure 1) into which was deposited the organic-rich, petroliferous Monterey Formation (Blake et al., 1978; Ingle, 1980). In several basins where the Monterey deposits are primarily fine-grained and hemipelagic in character (e.g., Santa Barbara, Santa Maria, San Joaquin, and Salinas basins), a widespread compositional lithostratigraphy has been documented by previous workers and interpreted to reflect major changes in ocean circulation and climate (Ingle, 1980; Pisciotto and Garrison, 1981), or alternately, position on a prograding margin (Isaacs, 2001). These lithofacies have not been identified in inner, proximal basins that were dominated by coarse-grained

siliciclastic sedimentation where the hemipelagic signal would be expected to be weak or absent. Yet, as fine-grained "shales" become increasingly important in an economic sense as unconventional reservoirs for hydrocarbons (USGS Reserve-Growth Assessment Project, 2012), the ability to characterize and correlate them in a regional framework becomes ever more important. Whereas compositional or chemostratigraphic correlation can be relatively straightforward in continuous fine-grained deposits, extending these kinds of stratigraphic correlation into mixed clastic-biogenic depositional systems is considerably more challenging. This is the focus of this thesis.

This study uses mineralogic and chemostratigraphic techniques to characterize the Monterey Formation and equivalent sedimentary rocks in the Los Angeles basin, one of the innermost, proximal basins of the Neogene. Although the Los Angeles basin is an inboard basin with a much greater detrital input than outboard basins like the Santa Barbara and Santa Maria basins, this thesis develops a method to investigate whether a similar hemipelagic lithostratigraphic succession exists within the inboard Los Angeles basin to that in other basins, albeit disrupted and diluted by the abundance of turbiditic sand and silt.

This study is the first of this kind in the Los Angeles basin. The purpose of this study is to determine if there are compositional lithostratigraphic zones in the hemipelagic strata of the Los Angeles basin and, if so, are, they similar to those in the other Neogene basins of California? Vertical stratigraphic variation of the fine-grained middle to late Miocene rocks is determined from cuttings samples from four oil fields within the Los Angeles basin–East and West Beverly Hills, Inglewood, and offshore

Wilmington oil fields (Figure 2 –by geochemically and mineralogically analyzing samples that were cleaned of all coarse clastic material (sand, sandstone, and siltstones containing grains greater than 0.0625 mm). Newly discovered compositional lithostratigraphic facies (zones) are then compared and correlated within the Wilmington field and across the subsurface of the Los Angeles basin in a north-south transect.

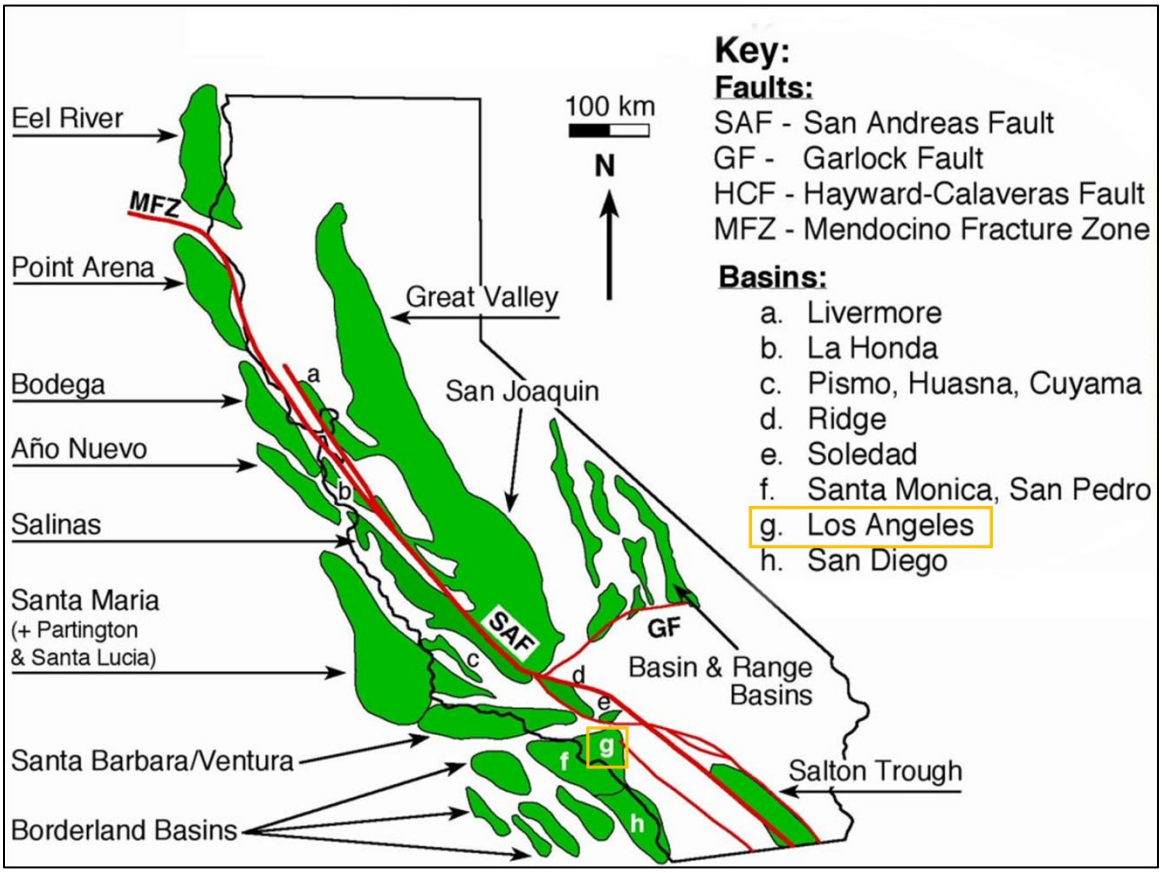

FIGURE 1. Locations of Neogene sedimentary basins. Los Angeles basin is boxed in yellow, after Behl (1999).

This investigation tests two separate hypotheses: 1) that the global oceanic and climatic controls of hemipelagic sedimentation were strong enough to leave a detectible record in a proximal, clastic-dominated basin during the middle to late Miocene similar to that found in the Monterey Formation and equivalent rocks in the Santa Barbara-Ventura, San Joaquin, Santa Maria and Salinas basins, and 2) that the composition of fine-grained lithofacies, even within highly localized submarine fan depositional systems such as existed in the Los Angeles basin, are distinct enough to support the use of chemostratigraphy as a tool to correlate within and between other oil fields across the Los Angeles basin. If such a compositional zonation can be developed, then it would aid in correlation across the Los Angeles basin, which is very challenging owing to its complex tectonic and structural history, and the environmental sensitivity and time-transgressive nature of benthic foraminifera – the primary biostratigraphic tool in the basin.

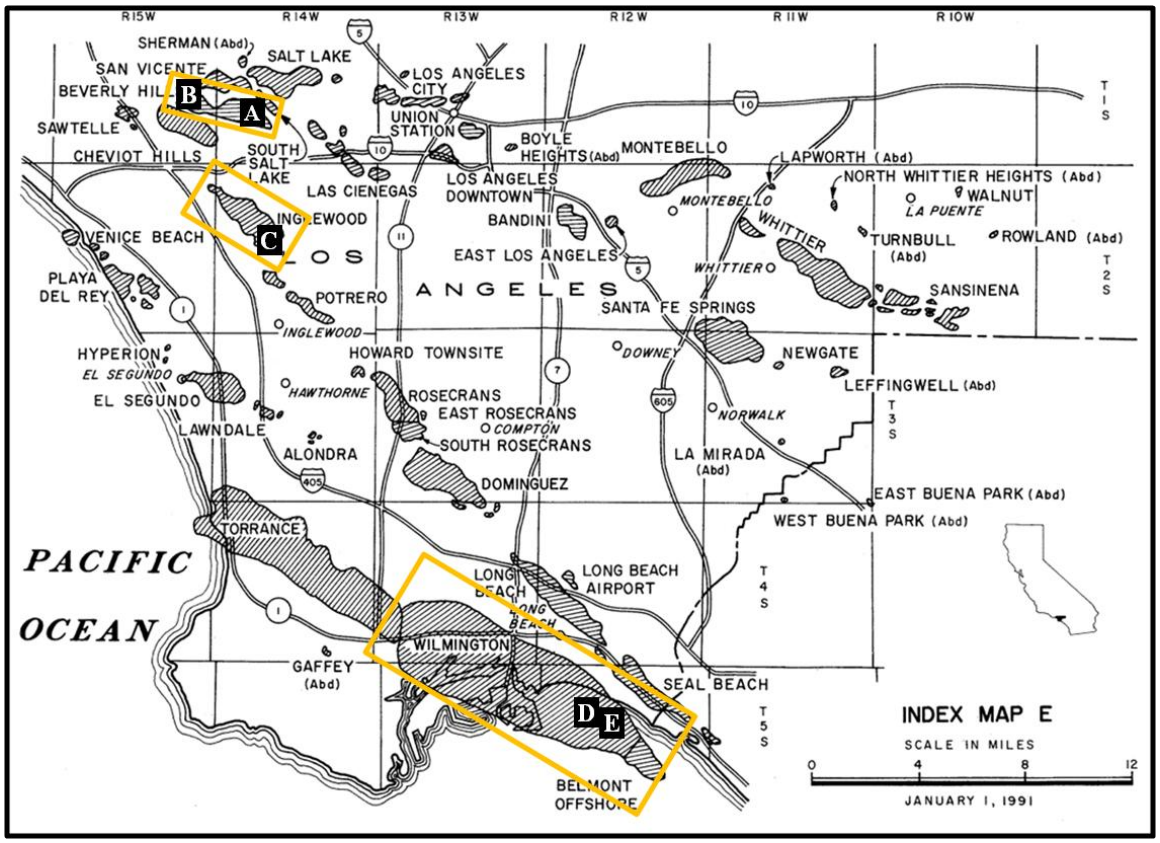

FIGURE 2. Map of Los Angeles basin and study areas. A = East Beverly Hills well A, B = West Beverly Hills B, C = Inglewood well C, D = Wilmington well D, E =Wilmington well E, modified from DOGGR (1991).

CHAPTER 2

BACKGROUND

Monterey Formation

The Miocene Monterey Formation consists of siliceous and organic-rich hemipelagic sediments with very distinctive physical properties (Bramlette, 1946; Isaacs, 1980). It is a proven source rock as well as a reservoir for many petroleum fields in California (Isaacs and Petersen, 1987; Behl, 1999; Isaacs and Rullkötter, 2001). The Monterey Formation and its equivalent rocks were deposited between 17.5 to 5 Ma in a series of basins that formed under similar tectonic conditions (Barron, 1986). During this time interval, major climatic and tectonic shifts occurred, including: a rise in global sea level during the warmest interval of the Miocene, followed by the transition to a glacial world as the Antarctic ice sheet formed and sea level fell (Kennett, 1977; Ingle, 1981). The formation of the Antarctic ice sheet changed the distribution of nutrient-rich waters in the world's ocean (Pisciotto & Garrison, 1981; Woodruff and Savin, 1989) as coastal upwelling brought these cold, nutrient-rich waters to the surface along the perimeter of the Pacific Ocean, where diatoms out-competed other organisms (Ingle, 1981). Similar deposits have been found in Japan, Korea, Sakhalin Island and elsewhere around the Pacific Rim (Barron, 1986), suggesting that oceanographic conditions were widespread enough to extend across the Pacific Ocean. The mid-Miocene rise in eustatic sea level,

enhanced by the widespread tectonic formation of isolated basins along the California margin (Blake et al., 1978), led to an initial and widespread decrease in the deposition of terrigenous detritus (Ingle, 1981). Differences in timing of basin evolution and sediment fill resulted in facies variations amongst the basins (Pisciotto & Garrison, 1981), although there are considerable similarities that are the basis for this thesis research. Work completed in the Santa Barbara, Santa Maria, San Joaquin, and Salinas basins suggests that an approximately time-equivalent, three-part stratigraphy exists across these basins (Pisciotto & Garrison, 1981; Isaacs, 1985; Graham and Williams, 1985). Figure 3 shows a compilation of these workers' stratigraphies in the Coast Ranges, Santa Barbara area and San Joaquin basin.

The three main compositional zones of the Monterey Formation found in most of the Neogene basins in California are a lower calcareous member, a middle organic-phosphatic rich member, and an upper siliceous member (Pisciotto & Garrison, 1981). The middle member may also have a substantial amount of chert (Bramlette, 1946; Hornafius, 1991; Isaacs, 2001). More detailed stratigraphies have been identified locally (e.g., Isaacs, 1980). The different members reflect shifts in climatic and oceanographic patterns relative to tectonic induced changes in sedimentation and subsidence rates (Pisciotto and Garrison, 1981; Figure 3). The calcareous member was deposited during the early to middle Miocene when relatively warm, nutrient poor waters produced foraminifera-coccolithic shales and mudstones with both biogenic and authigenic carbonate (Pisciotto and Garrison, 1981). Although more distinctly carbonate-rich than other members, this lithofacies still includes siliceous and other rock types. The

phosphatic member was deposited during the middle to late Miocene and is composed of organic-rich shale or mudstone with an abundance of phosphatic laminations and nodules, reflecting phosphitization along the slope and bathymetric highs near the oxygen minimum zone boundaries (Pisciotto and Garrison, 1981; Föllmi and Garrison, 1991; Föllmi et al., 2005). Dolostone beds and nodules are also closely associated with the phosphatic member, although they are found within the other members, as well. Both dolomite and phosphate are early diagenetic products of organic-rich sediment, occurring less than a meter below the ocean floor (Garrison et al., 1994). In general, the phosphatic member represents a time of extremely slow sedimentation coupled with an increase in organic productivity (Hoots, 1935; Pisciotto and Garrison, 1981; Föllmi et al., 2005). The upper "clayey" siliceous member is composed of both biogenic and diagenetic silica-rich shales and mudstones, porcelanite and minor chert (Isaacs, 1981). The deposition of the upper siliceous member reflects deposition of diatom ooze, a result of intensification in coastal upwelling that leads to an increase in plankton productivity (Pisciotto & Garrison, 1981), with the overall absence of calcareous nanno- and microfossils likely being due to deposition above the Carbonate Compensation Depth.

Although the Monterey, overall, is very organic-rich, source rock potential and kerogen type of organic- rich Monterey Formation vary between basins. Samples from Naples Beach in the Santa Barbara-Ventura basin contain a mixture of both Type II/III kerogen, with the highest abundance of Type II kerogen in the carbonaceous marl member of Isaacs' classification, Figure 3 (Michael, 2001). Samples from Lion's Head in the Santa Maria basin contain primarily Type II kerogen (Michael, 2001). Samples

from the San Joaquin basin contain Type-II kerogen (Peters et al., 2007). Samples from Los Angeles basin contain a mixture of Type II/III kerogen, within shales from Divisions D and E (Delmontian and Mohnian) (Philippi, 1975; Jeffery et al., 1991). Oil gravities vary greatly in the Los Angeles basin, shallow producing zones can have oil gravities of less than 10˚API, deeper producing zones yield condensate, with oil gravity as great or greater than 50˚ API, though, most of the oil produced has a gravity of approximately 25˚ API with a sulfur content of greater than 1% (Jefferey et al., 1991).

Los Angeles Basin Evolution and Stratigraphy

Basin Evolution

The Los Angeles basin is one of some twenty distinct sedimentary basins (Figure 1) that formed as a result of the Neogene reorganization of western California during the transition of the North American margin from a convergent to transform boundary (Atwater, 1970; Blake, 1978). It is estimated that more than 10 km of late Cenozoic sediments were deposited in the basin's depocenter (Blake et al., 1978; Wright, 1991). The Monterey Formation and its chronostratigraphic equivalents – the Puente, Modelo, and Topanga Formations are important components of the basin fill within the Los Angeles basin.

The Los Angeles basin has undergone three main stages of development; each phase contributing to the basin's petroleum productivity (Biddle, 1991, Rumelhart and Ingersoll, 1999), although timing and bathymetry varied greatly across the region. Middle Miocene subsidence formed a deep, silled basin allowing for the accumulation and preservation of organic matter (Wright, 1991). A shift from Miocene regional

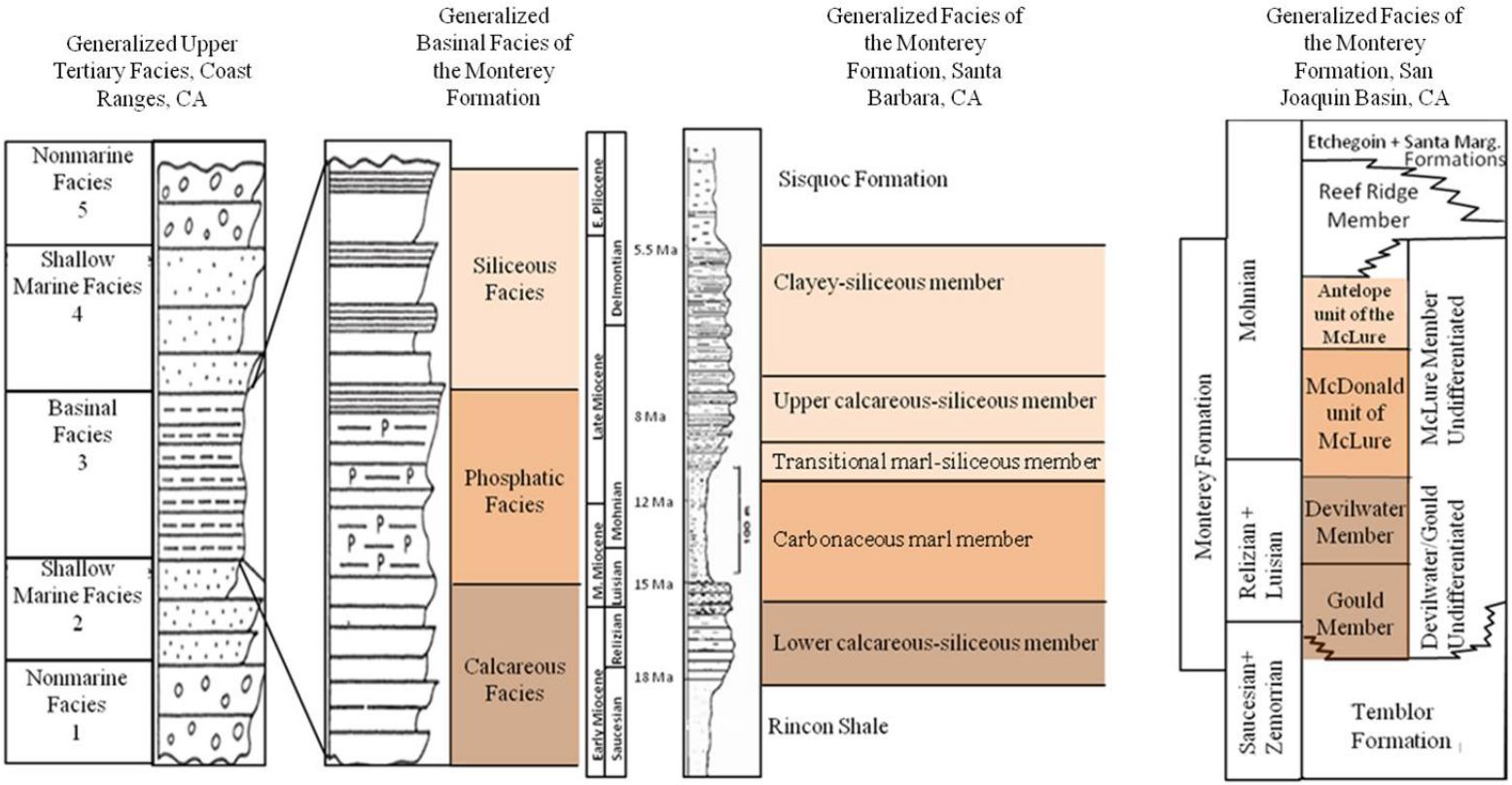

FIGURE 3. Summary of previous work in the Coast Ranges, Santa Barbara, and San Joaquin basin. After Pisciotto and Garrison (1981), Isaacs (1980), and Graham and Williams (1985).

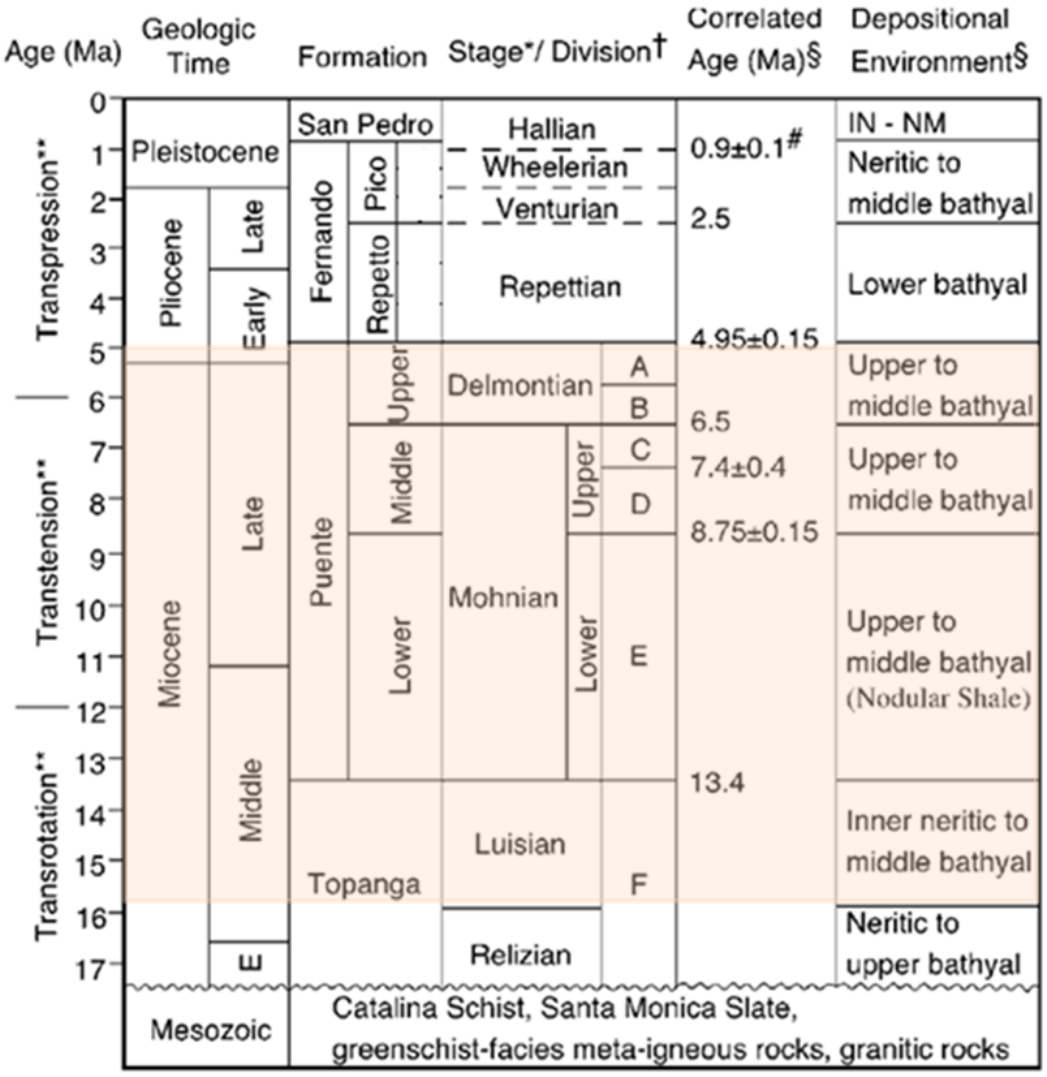

FIGURE 4. Major phases of deformation within the Los Angeles basin. Deposition of Monterey Formations-equivalent rocks is highlighted, after Tsutsumi et al. (2001).

transtension to Pliocene transpression later led to many of the structural traps within the basin (Biddle, 1991). The Los Angeles basin underwent three main phases of deformation of deformation during Neogene time (Rumelhart and Ingersoll, 1997; Ingersoll and Rumelhart, 1999). These stages coincide with the evolving transform-fault system, the first stage consisted of transrotation (18-12 Ma), transtension (12-6 Ma), and most recently transpression (6-0 Ma) (Ingersoll and Rumelhart, 1997; Ingersoll, 1999). Figure 4 gives the stratigraphic context and timing for the three phases of deformation. The first stage began in early Miocene and consisted of transrotation, with 60° clockwise rotation of the western Transverse Ranges, localized extension in the Los Angeles basin, and subsequent basin subsidence (Luyendyk and Hornafius, 1987; Luyendyk, 1991; Nicholson et al., 1994; Ingersoll and Rumelhart, 1999). During this time coastal sediments were deposited in neritic to middle to upper bathyal environments (Critelli et al., 1995; Tsutsumi et al., 2001). The second phase consisting of transtension began in or during latest middle Miocene in association with the formation of the releasing bend of the San Gabriel-Chino Hills-Christianitos fault zone, which separated the Santa Ana Mountains on the east from a deep basin to the west (Ingersoll and Rumelhart, 1999). This fault served as the principal transform boundary in the area at the time (Ingersoll and Rumelhart, 1999). Fine-grained hemipelagic sediments and deep-water turbidites were deposited into the basin as additional basin subsidence resulted from normal faulting in the basin (Tsutsumi et al., 2001). The third phase began near the Miocene-Pliocene boundary with a shift to transpression, and deposition from neritic to lower to middle bathyal environments. This last stage of deformation led to the reactivation of some

Miocene normal faults into Pliocene thrust faults and the Santa Monica fault systems (Tsutsumi et al., 2001). East and West Beverly Hills oil fields are found at the northern extension of the Newport-Inglewood fault zone (NIFZ). The main structures are associated with the Santa Monica fault system. Inglewood oil field lies along the main trace of the NIFZ. Wilmington oil field is associated with the THUMS-Huntington Beach fault, Palos Verde fault and NIFZ.

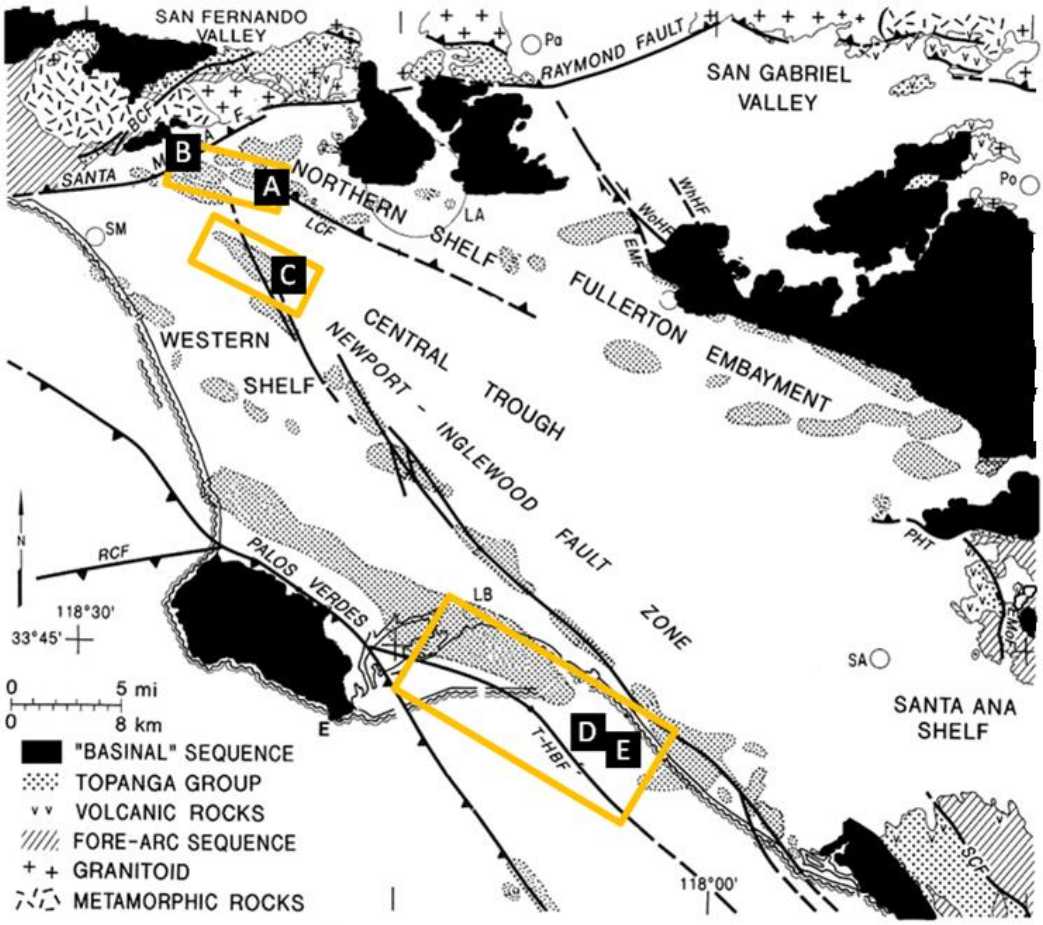

FIGURE 5. Map showing major faults and fault zones affecting the study areas, oil fields, and surface geology and outcrops of Monterey Formation-equivalent rocks. East Beverly Hills = A, West Beverly Hills = B, Inglewood = C, Wilmington well D = D, Wilmington well E = E, modified from Wright (1991).

Stratigraphy

The stratigraphy of the Los Angeles basin has been described by Hoots (1931), Woodring et al. (1946), Yerkes et al. (1965), Yerkes (1972), Yerkes and Campbell (1979), Schoellmer et al. (1981), and Yeats and Beall (1991). During Miocene time, the Los Angeles basin ranged from a non-marine to deep marine environment (Figure 4). Deposition into the basin in middle to late Miocene time were of two modes: (1) hemipelagic settling from the water column of fine-grained, biogenic-rich sediment, reflecting the oceanic conditions at the time, and (2) coarse-grained gravity flows, including turbidity currents, debris flows, and nepheloid plumes. Most of the sands deposited in the Los Angeles basin were sourced from two fans: the Tarzana and Puente fans (Redin, 1991; Wright, 1991; Bilodeau et al., 2007; Figure 6). These thick, porous sands act as the carrier beds and reservoirs for the many oil fields in the Los Angeles basin while the fine-grained, organic-rich hemipelagic sediments source the petroleum systems in the Los Angeles basin (Yeats and Beall, 1991).

Major basin-filling units–the upper Topanga, Puente and Modelo Formations – form stratigraphic equivalents of the Monterey Formation in the subsurface of the Los Angeles basin and in the uplifted highland that surround it (Blake, 1991, Yeats and Beall, 1991; Figure 7). The lower to middle Miocene Topanga Group consists of coarse-grained sandstone interbedded with shale and siltstone, deposited at middle-bathyal to non-marine depths (Blake, 1991; Critelli et al., 1995). In the study area (the western portion of the basin), the Topanga Group was deposited in middle bathyal water depths (Blake, 1991). The Topanga Group is absent along the western shelf of the basin. In the

northern portion of the Los Angeles basin, the Modelo Formation unconformably overlies the Topanga Group (Blake, 1991).

In the northwestern portion of the basin, the Modelo Formation is age-equivalent to the Monterey Formation and is composed of two members consisting primarily of coarse-grained sandstones and interbedded silty shale (Blake, 1991). In the study area the Modelo Formation found in the subsurface has a higher concentration of sand that that described by Hoots (1931) for the Santa Monica Mountains. In the Santa Monica Mountains the Modelo Formation is upper Miocene in age and consists of two members. The lower member consists primarily of platey siliceous and argillaceous shale interbedded with some sandstone and conglomerate (Rumelhart and Ingersoll, 1997). The basal part of this member includes organic-rich, phosphatic shale and coarse clastics comprised of clasts from the underlying formations. The upper member of the Modelo Formation consists largely of soft, white diatomaceous shale, with varying amounts of interbedded sand depending on location that grade into a shaly-sandstone towards the west (Hoots, 1931; Rumelhart and Ingersoll, 1997). It is found in outcrop on both the north and south flanks of the eastern portion of the Santa Monica Mountains (Hoots, 1931).

In the central and southwestern portion of the subsurface Los Angeles basin, the Topanga Group is overlain by the Mohnian and Delmontian-stage Puente Formation (Blake, 1991). Compositionally, the Puente Formation is separated into three members: (1) a lower interbedded calcareous siltstone and sandstone, with localized organic-rich, phosphatic laminated and nodular shale in the western part of the basin, known as the

"Nodular Shale"; (2) a middle medium-to-coarse grained sandstone, interbedded with diatomaceous siltstone; and (3) an upper fine-to-coarse grained sandstone, interbedded with siliceous siltstone (Blake, 1991). Tovell (1942) reported outcrops of Nodular Shale in the Santa Monica Mountains, near Santa Ynez Canyon, Rustic Canyon and Stone Canyon, in the lower Modelo Formation. Though equivalent in age; the Puente Formation differs from the Monterey Formation found in Santa Barbara-Ventura, and Santa Maria basins in lithology, depositional environments, and tectonic deformation (Blake, 1991).

Monterey Formation-equivalent rocks are found in the Santa Monica Mountains, the Palos Verde Hills in Los Angeles County, and the Puente Hills and San Joaquin Hills in Orange County (Figure 5). These rocks are assigned to the Modelo, Puente, and Monterey plus upper portions of the Topanga in these areas, respectively. In the Palos Verdes Hills, the Valmonte Diatomite and Altamira Shale are considered members of the Monterey Formation with outcrops of Nodular-Shale-like facies at Lunada Bay, Altamira Canyon, White's Point and Point Fermin (Figure 9). In the San Joaquin Hills, outcrops of the Monterey Formation are widespread, and associated with the overlying partially siliceous Capistrano Formation and interfingered with the San Onofre Breccia near its base (Blake, 1991; Wright, 1991).

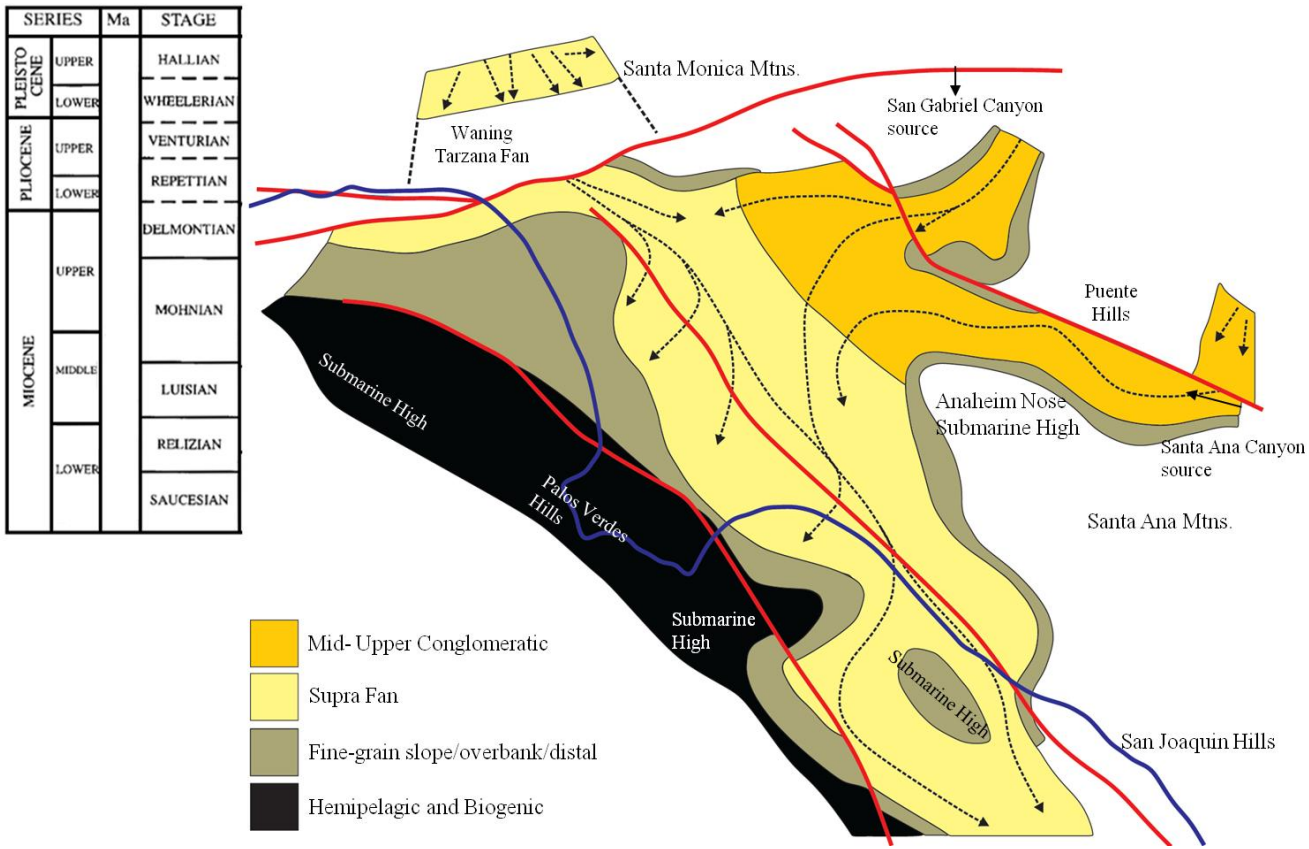

FIGURE 6. Major fan systems and their deposits in the Los Angeles basin diring Delmontian time, modified by Scott William Prior, drawn by Aaron Van Dolah, after Redin (1991). Time scale from Blake (1991).

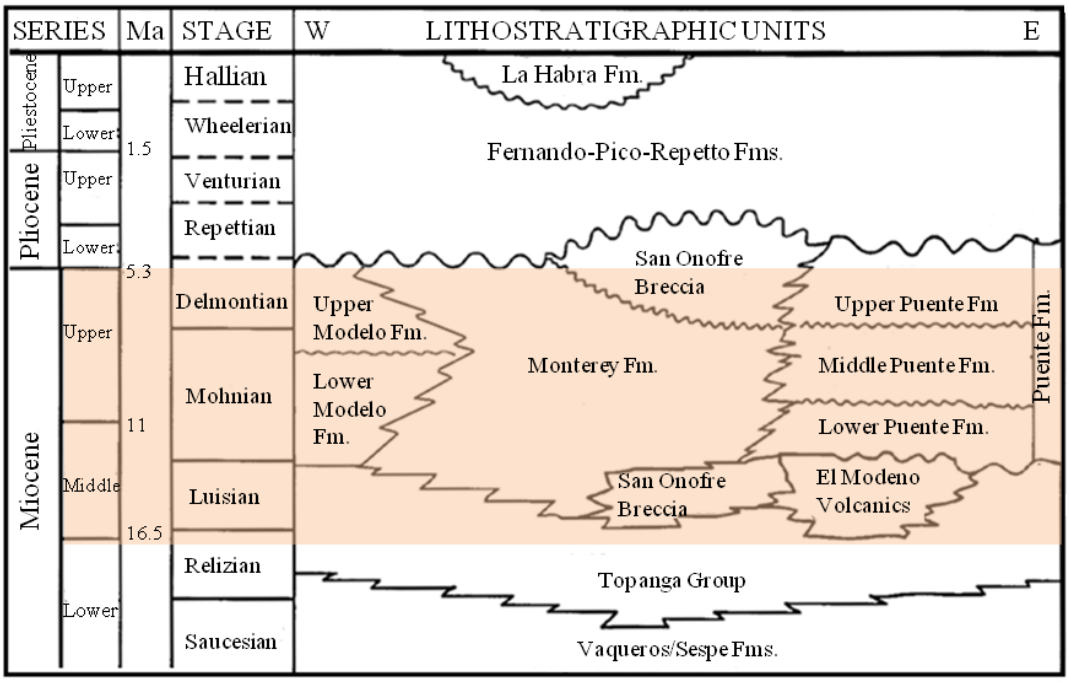

FIGURE 7. Stratigraphy of Los Angeles basin. After Rumelhart and Ingersoll (1997).

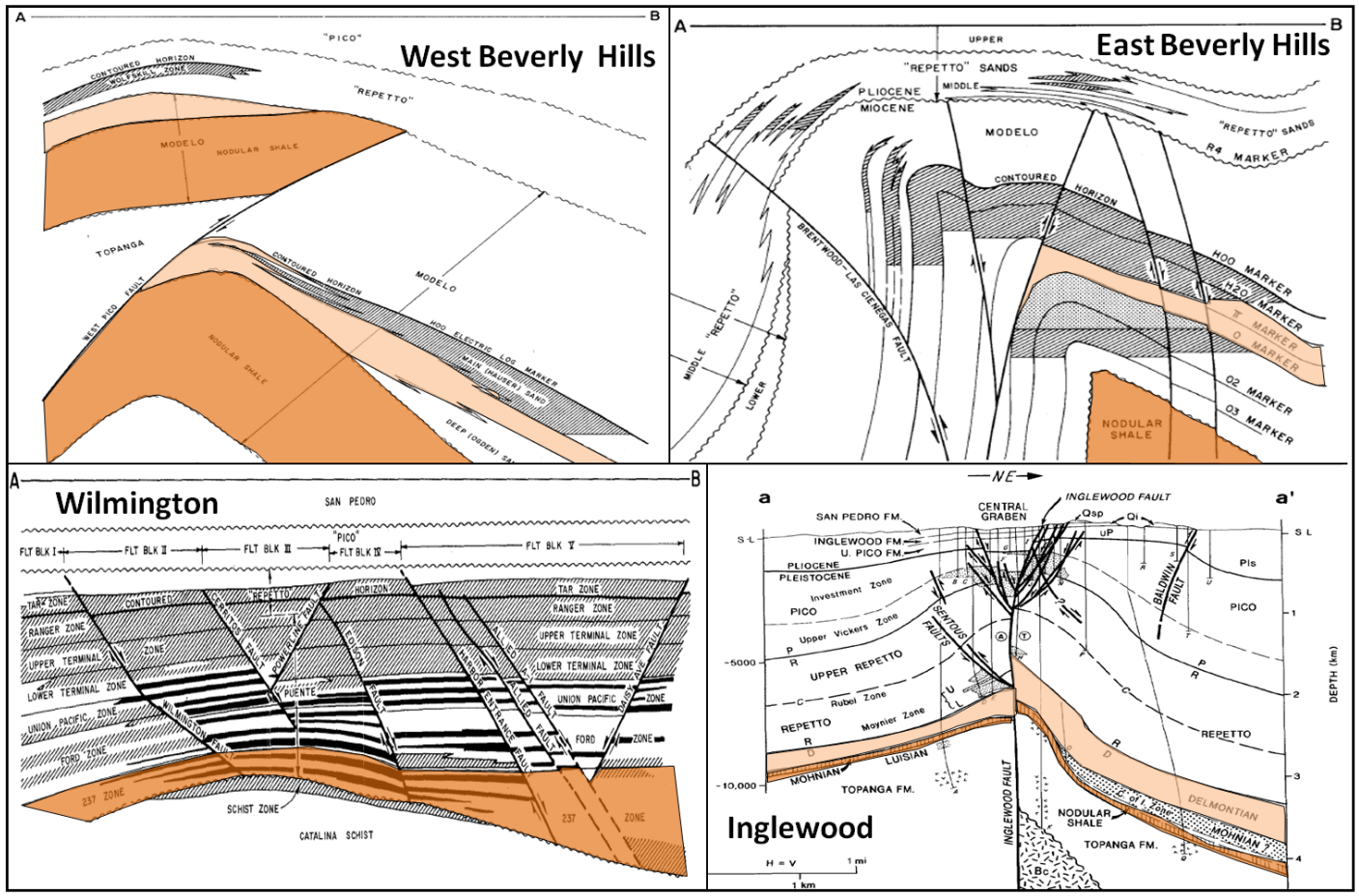

FIGURE 8. Structure and Monterey Formation-equivlant fine-grained facies in the Los Angeles basin. Based on literature and communication with respective oil companies. West Beverly Hills = A, East Beverly Hills-B, Wilmington = C, Inglewood = D, after DOGGR (1992).

Oil Field History

Five wells from four oil fields within the Los Angeles basin are examined in this study. Two wells from offshore Wilmington are used to demonstrate intra-field correlations, while the other three will demonstrate regional, basin-scale correlations in a roughly north-south transect along the western portion of the subsurface Los Angeles basin. Wells from the East and West Beverly Hills field, Inglewood, and offshore Wilmington oil field are described next.

East Beverly Hills

The East Beverly Hills field is eleven km from downtown Los Angeles concealed amongst neighborhoods and businesses. The western part of the Beverly Hills structure had been producing from Pliocene sands since the field was discovered in the early 1900s (Jacobson and Lindblom, 1987). In 1964, Occidental Petroleum drilled into the east flank of the West Beverly Hills structure, producing from upper Miocene sandstone stratigraphically equivalent to the Hauser sands (Jacobson and Lindblom, 1987). East Beverly Hills structure is an asymmetric anticline, oriented west-northwest with hydrocarbons accumulating in the crest as well as in stratigraphic pinchouts (Jacobson and Lindblom, 1977; Wright, 1991) (Figure 8).

The Modelo Formation is the Monterey Formation equivalent in the East Beverly Hills field. The organic-rich, Mohnian Nodular Shale is thought to be the proximal source most of the petroleum systems in the western Los Angeles basin (Walker et al., 1983). The deepest producing zone for East Beverly Hills is the Odgen zone, consisting of interbedded sandstone and shale, with a net to gross of 70 percent, and a thickness of

900 feet (Jacobson and Lindblom, 1987). The largest producing zone is the Hauser zone, a 600-feet- thick section of interbedded sandstone and shale with a net to gross of 85 percent. The shallowest Miocene producing zone is the Dunsmuir zone, a 400-to-500-feet thick section of interbedded sands and shales with a net to gross of 60 percent (Jacobson and Lindblom, 1987). The target of investigation for this study is the Nodular Shale and Odgen Zones.

West Beverly Hills

The West Beverly Hills field is eleven km from downtown Los Angeles, also concealed in an urban setting. The western portion of the field, now considered West Beverly Hills, lies under the city of Beverly Hills. W.W. Orcutt drilled the first well into the field, discovering oil in shallow Pliocene sands (Testa, 2007). The Modelo Formation is the Monterey Formation equivalent in the West Beverly Hills field. Early production was from shallow Pliocene Repetto sands while later exploration of the field yielded production from Miocene, Delmontian and Mohnian-stage sands. Middle to upper Miocene organic shales of the Nodular Shale source the petroleum system while anticlines and stratigraphic pinchouts trap the oil in the Beverly Hills field (Jacobson and Lindblom, 1987; Figure 4). Inter-and-intraformational shales act as seals in the West Beverly Hills petroleum system. These Mohnian and Delmonitan shales are the focus of the investigation for this field.

Inglewood

The Inglewood Oil field is at Baldwin Hills, thirteen km from downtown Los Angeles. The Baldwin Hills are the most pronounced topographic structure of the several

fields lying adjacent the right-lateral NIFZ, with a height of 300 feet above the surrounding area, and is highlighted in orange in Figure 3 (Testa, 2007). Initial production was from relatively shallow, Pliocene sands. Topographically, the Inglewood oil field consists of a domal structure, rising 91m above the surrounding plain (Testa, 2007). The major trap for the field is an elongated domal structure, trending northwest-southeast, 3.2 km long and 1.06 km wide, with displacement of 350 to 400 feet along the east flank and a smaller fold east of the fault (Testa, 2007). The upper zones of the field are influenced greatly by the NIFZ while the lower zones seem to be affected by the Sentous fault system, a south-verging thrust system (Elliot et al., 2009).

In the Inglewood field, the Puente Formation represents the Monterey Formation equivalent rocks. Locally, the Puente Formation consists of, from oldest to youngest, the Nodular Shale, the City of Inglewood zone, and the Bradna zone (Figure 5). The lower middle Miocene Sentous zone is the lowest producing zone at Inglewood, consisting of interbedded shale and sandstone and volcanic intrusives (Wright, 1987). The upper Miocene Nodular Shale is a very organic-rich shale with phosphate as nodules or laminations in shale or marlstone. The overlying upper Miocene City of Inglewood zone consists of interbedded sandstone and siltstone is a stratigraphic trap, pinching out up the southeast plunge of the Inglewood anticline (Wright, 1987). The upper Miocene Bradna zone consists of interbedded sandstone, siltstone and shale (Elliot et al., 2009). The Nodular Shale and Bradna zones are the primary targets of this study; however, samples are analyzed from the Sentous zone as well. The primary source for the Inglewood petroleum system is the organic rich Nodular Shale

Wilmington

The Wilmington field is thirty-two km south of downtown Los Angeles and was discovered in 1932 (Bartoush, 1937). It is the fourth largest oil field in the United States, in terms of cumulative production (Otott and Clarke, 1996). The Wilmington anticline is a broad, doubly plunging asymmetric fold cut by a series of normal and oblique normal faults on both the eastern and western plunges (Mayuga, 1970; Wright, 1991). The Wilmington Oil field lies along the Torrance-Wilmington structural trend (Clarke, 1987). The structural high lies onshore, near the Long Beach Harbor. Seismic exploration indicated that the onshore structure extended offshore to the southeast for nearly six km (Otott and Clarke, 1996). Offshore development began in the late 1960's, extending the length of the field to of 21 km (Wright, 1991). Growth of the Wilmington anticline is associated with the THUMS-Huntington Beach fault (Truex, 1974; Wright, 1991).

In Wilmington field, the Puente Formation represents the Monterey Formation equivalent rocks. Locally, from oldest to youngest, the Puente is divided into the, Ford, Union Pacific, Lower Terminal, Upper Terminal, and Lower Ranger Zones (Figure 8; Otott and Clarke, 1996). The 237 Zone is middle to upper Miocene and consists of a lower dark brown-black, organic-rich shale that contains phosphatic nodules near the base of the section (Norton and Otott, 1996). The lower section of the 237 zone also becomes increasingly siliceous and calcareous with depth (Truex, 1974). The upper section of the 237 Zone consists of interbedded fine-to-medium grained, poorly sorted sandstone and The Union Pacific and Ford zones are turbidite deposits and consist of

interbedded sandstone and shale (Norton and Otott, 1996). The 237 zone and other fine-grained deposits of the Puente Formation are the main targets for this study

The main source rock for the Wilmington field is the Black Shale Member of the 237 Zone, equivalent to the Nodular Shale and lithologically similar to the middle phosphatic member of Pisciotto and Garrison's nomenclature. Upper Miocene and lower Pliocene coarse clastics deposited by turbidites, fractured basement and siliceous shale are reservoirs for the Wilmington field. Anticlinal traps and associated structures formed in the latest Miocene and early to middle Pliocene time, permitting accumulation of hydrocarbons (Wright, 1991). Late Pliocene and Quaternary fine-grained sediments act as the seal for the Wilmington petroleum system.

CHAPTER 3

METHODS

Sample Selection and Preparation

The focus of this study is the fine-grained hemipelagic sediments, which were carefully handpicked from cuttings to remove drilling additives and unwanted lithologies, including sediments larger than very-fine silt, 0.0625 mm. Mudlogs were used as a first pass to identify shaley intervals with Monterey Formation-type sediments. Image, electrical, and nuclear logs helped confirm the selected intervals for analysis. Image logs were used to identify unfaulted intervals and in wells. Sample intervals varied from 10 ft. to 40 ft. A riffle splitter was used to remove any preferential sorting from the sample bags, half of the sample was sieved through a series of sieves for analysis, preserving the remaining half for future work. Samples were passed through 2.00 mm, 1.00 mm, and 0.500 mm sieves. Special care was taken to exclude cavings from upsection. Sediments at 1.00 mm sieve size were used for analysis. Sand, sandstone and siltstone cuttings, and drilling additives were manually removed by hand from the cuttings under a binochular microscope. Picked samples were cross-checked to maintain consistency of the carefully selected of samples. The remaining fine-grained fraction was washed twice by sonication and dried. The samples were powdered with a corundum mortar and pestle and passed through a 0.063 mm sieve prior to analyses.

Techniques

X-Ray Diffraction (XRD)

A Rigaku MiniFlex XRD spectrometer and PANalytical X'Pert Highscore Plus software were used for qualitative and semi-quantitative analysis. Thirteen minerals were identified as well as silica phases: quartz, opal-CT, plagioclase, orthoclase, muscovite, biotite, chlorite, calcite, dolomite, carbonate-fluorapatite, hydroxyapatite, pyrite, and barite. The Reitveld Refinement method was used to quantify the thirteen minerals identified in the cuttings. Results had less than 5 percent error when calibrated with known multi-component standards. This technique worked well for the most common minerals expected in the Monterey Formation. One limitation of the technique was the inability to identify and quantify the amount of clays in the cuttings (Moore and Reynolds, 1997). Clay minerals have a high variability in measured XRD peak intensity owing to mixed layering and varying chemical composition and their tendency to become oriented during sample preparation (Moore and Reynolds, 1997; Srodon et al., 2001).

Fourier Transform Infrared Spectroscopy (FTIR)

A Bruker Alpha Diamond Attenuated Total Reflection (ATR) device was used to measure sample spectra for FTIR. Bruker's Opus software was used for data interpretation, and Infometrix, Inc. Pirouette software was used for multivariate analysis. FTIR analyses was also used to quantify the relative weight abundance of expected minerals in the cuttings. Where XRD had limitations, FTIR excelled. Rather than measuring thediffraction related to crystal lattice, FTIR measures the amount of infrared energy absorbed by vibration of the various atomic bonds and radicals in mineral in the

rock (Smith, 2011). Once the spectra were collected, a calibration model was constructed. Standards were created using sixteen Monterey-type minerals: quartz, opal-CT, albite, orthoclase, muscovite, biotite, chlorite, calcite, dolomite, barite, pyrite, hydroxyapatite, carbonate-fluorapatite, illite, smectite, and montmorillonite. These minerals were also used to create a cross-validation model for data analysis. Of the sixteen Monterey-type components, quartz, calcite, dolomite, barite, illite, and montmorillonite were validated with correlation coefficient (R^2) values greater than 80 percent. Owing to limitations using XRD, the results from FTIR were used to determine the clay-to-quartz ratio in the samples. Knowing the amount of quartz in the sample (XRD), the ratio of measured and combined and illite and montmorillonite were divided by total quartz (FTIR). This ratio was then multiplied by the known total quartz (XRD) and then normalized to account for unknown clay-mineral abundance.

X-Ray Fluorescence

A PANalytical Axios Wavelength Dispersive XRF spectrometer was used for quantitative analysis of the major oxides in the samples. Samples were sent to Activation Laboratories Ltd. (ActLabs), Ontario, Canada for analysis. ActLab analyzed 0.5 g equivalent sample sizes. Twelve oxides were measured using a Panalytical Axios Advanced wavelength dispersive XRF: Al_20_3, Cao, Cr_2O_3, Fe_2O_3, K_2O, MgO, MnO, Na_2O, P_2O_5, SiO_2, TiO_2, V_2O_5. According to their website, the intensities were measured and calculated using the International Standard G-16 of Dr. K. Norrish of CSIRO, Australia (ActLab.com).

Proxies

Proxies are used to identify sedimentary components that characterize different lithostratigraphic facies. Feldspars and phyllosilicates (XRD) are a proxy for detritus (sediment less than 0.0625 mm), opal-CT (XRD) is a proxy for biogenic and diagenetic silica. Unlike many of the oxides measured with XRF, P_2O_5 contributes primarily to phosphate, thus providing the best way to identify intervals of enriched phosphate. Calcite and dolomite (XRD) are a proxy for carbonates.

Mudlogs

Mudlogs were used to supplement identified compositional zones as well as extend or condense a zone if needed. If sample intervals were too broad, the lithology and comments tracks were used to fill in the missing interval. It is noted if mudlogs were used to refine compositional zones.

Limitations

The primary goal of this investigation is to determine stratigraphic trends and lateral correlations in the geochemical and mineralogical composition of the rocks. Much of the Monterey Formation is thin-bedded with a great deal of vertical stratigraphic variation. Cuttings were used because they are representative of mechanically averaged samples from thick intervals. In addition to removing cuttings with detrital grains larger than 0.0625 mm, readily apparent cavings from up-section were also removed. Sample depths are based on measured depth in feet for the mudlog, and were not corrected for correlation to electrical or nuclear logs. The sample intervals varied from 10 to 40 ft in the five wells and cuttings are probably not equally representative of the entire

the five wells and cuttings are probably not equally representative of the entire stratigraphic interval. Fine-grained sediment, such as the hemipelagic sediment studied here, is often crushed by drilling and lost in the process of collecting the cuttings; thus, some intervals had very low sample weight that affected the number of analyses/sample. Differentiating detrital silica from biogenic and diagenetic silica was a challenge. Opal-CT was identified using XRD techniques, however detrital and diagenetic quartz could not be separated using XRD. Faults and unconformities are unresolvable with the sample interval and resolution of the data.

CHAPTER 4

RESULTS

Data Description

A total of 125 samples were analyzed from five wells using XRD, XRF, and FTIR (Table 1). XRD and XRF data are given in weight percent (e.g. percent quartz) versus measured depth in feet. Actual well names are not used. Mineralogical abundances (XRD and FTIR) and major oxides (XRF) are presented in Figures 9 (XRD), 10 (FTIR), and 11 (XRF), respectively. Proxies for Monterey Formation-type components are presented for each well in Figures 12 through 16. Data in Figure 9 were derived and corrected for clay from FTIR data. See Appendices A, B, and C for data tables for XRD, FTIR, and XRF measurements.

TABLE 1. Table Showing Well Name, Location, Number of Samples, and Depth Intervals.

Well Name	Location	Number of Samples	Sample Depth (MD)
East Beverly Hills A	East Beverly Hills	12	9400’-10100’
West Beverly Hills B	West Beverly Hills	45	3480’-8070’
Inglewood C	Inglewood	23	7190’-8340’
Wilmington D	Wilmington	17	9090’-10750’
Wilmington E	Wilmington	17	9120’-10320’

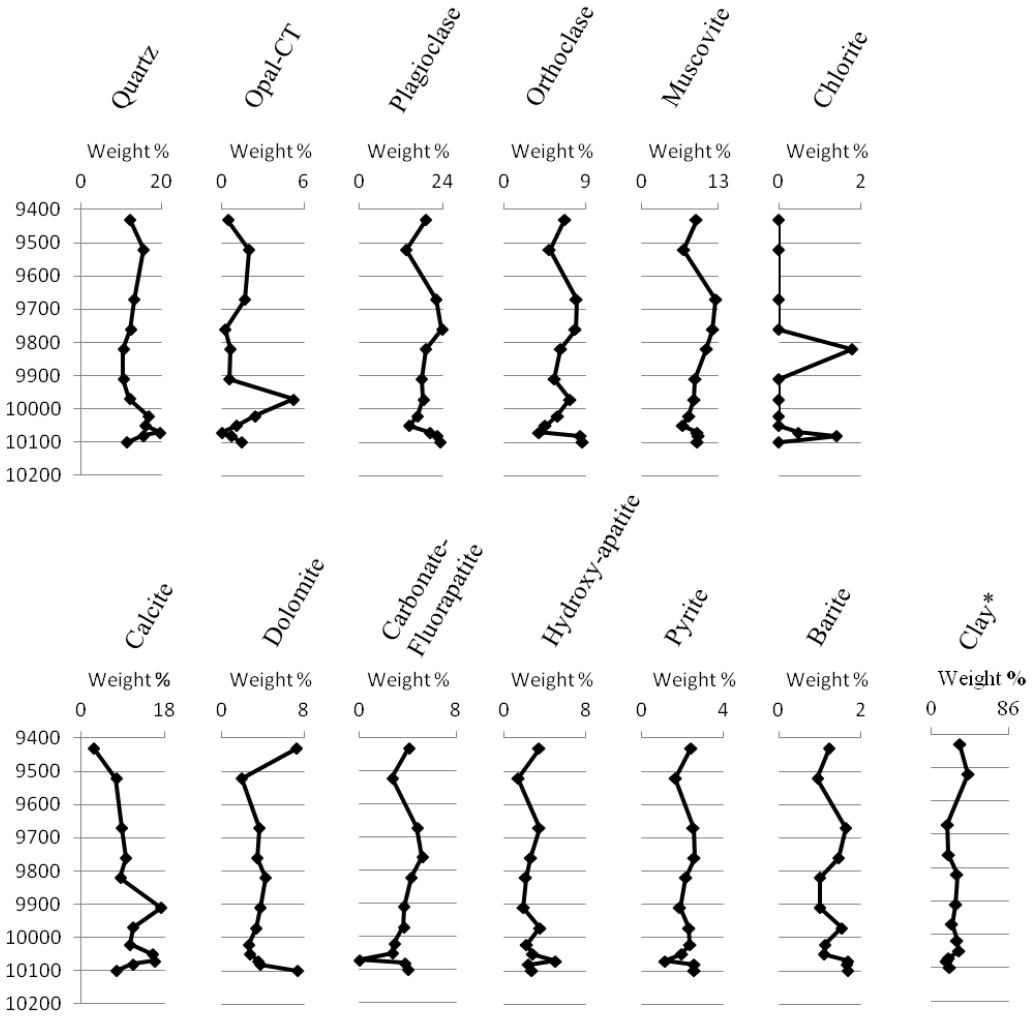

FIGURE 9. Mineralogical abundances in cuttings from East Beverly Hills A, measured by XRD. *Derived from FTIR analyses.

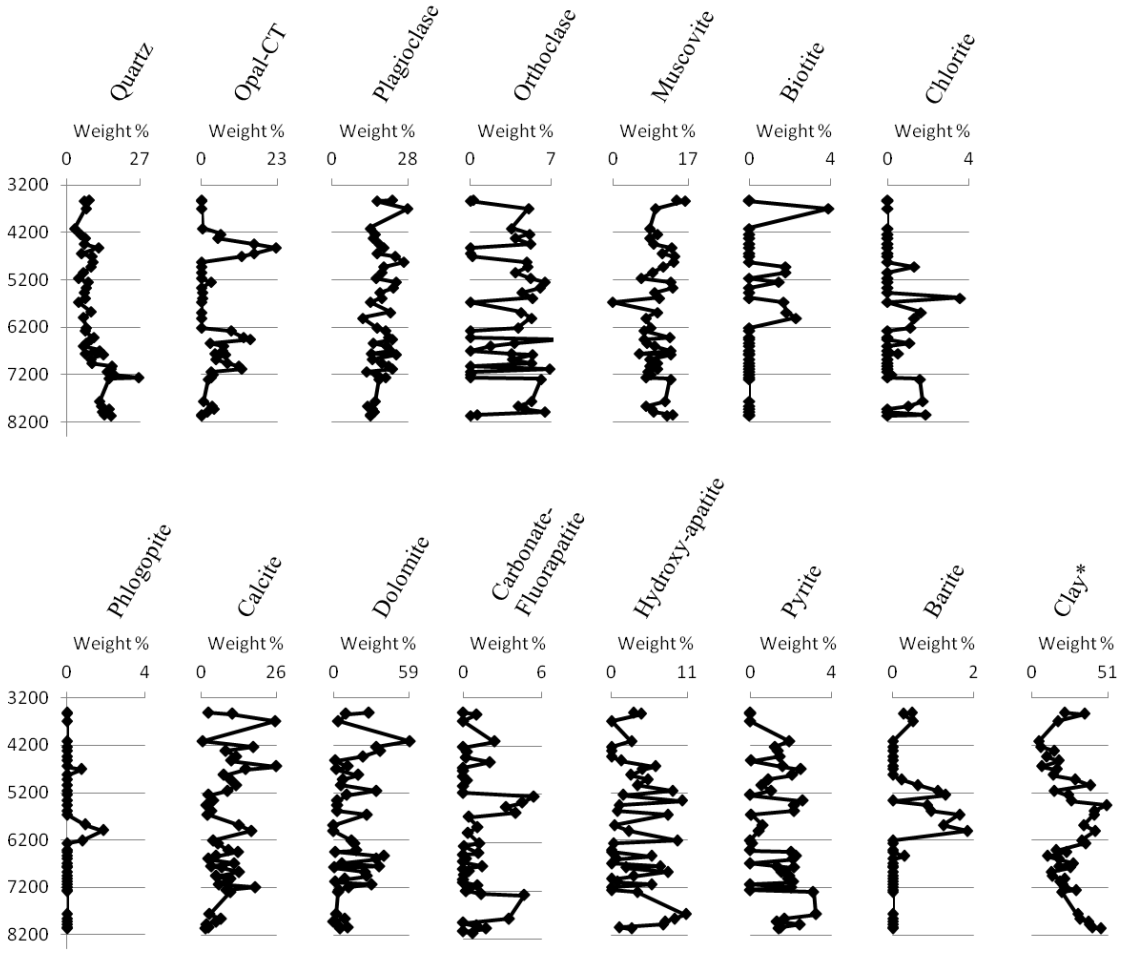

FIGURE 10. Mineralogical abundances in cuttings from West Beverly Hills well B, measured by XRD. *Derived from FTIR analyses.

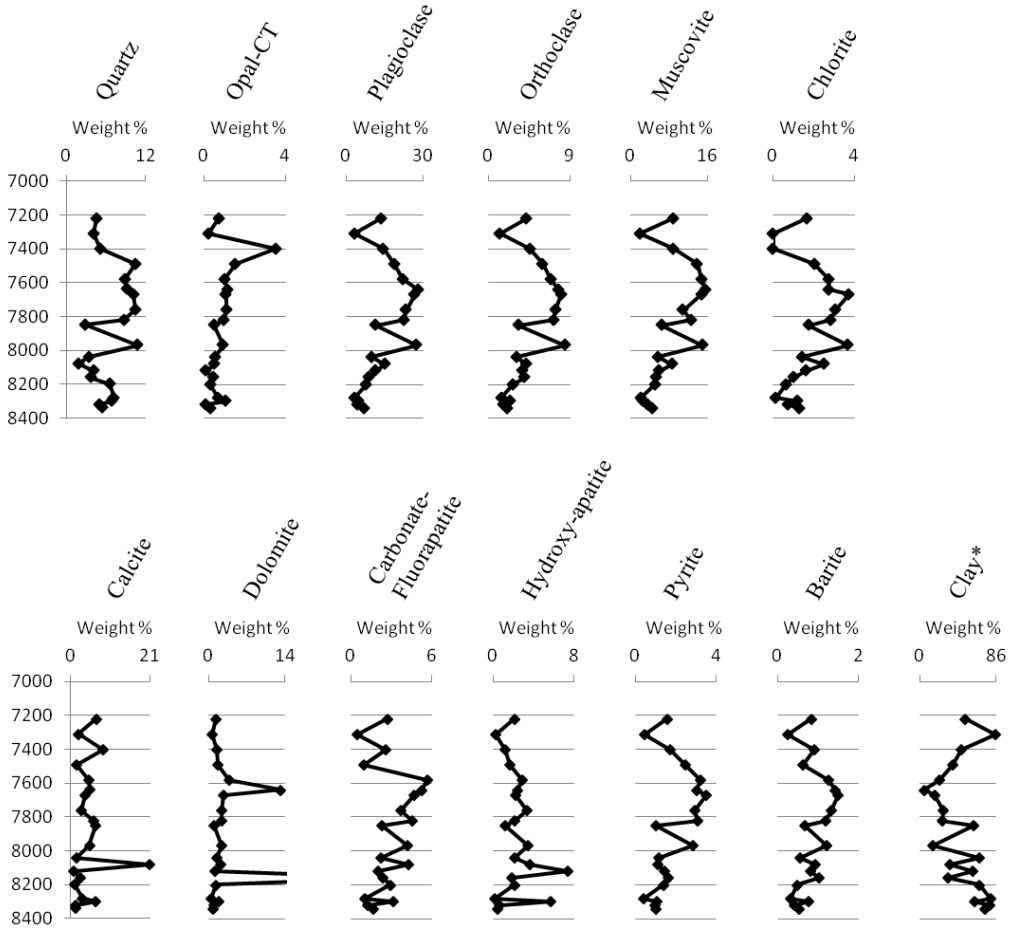

FIGURE 11. Mineralogical abundances in cuttings from Wilmington well C, measured by XRD. *Derived from FTIR analyses.

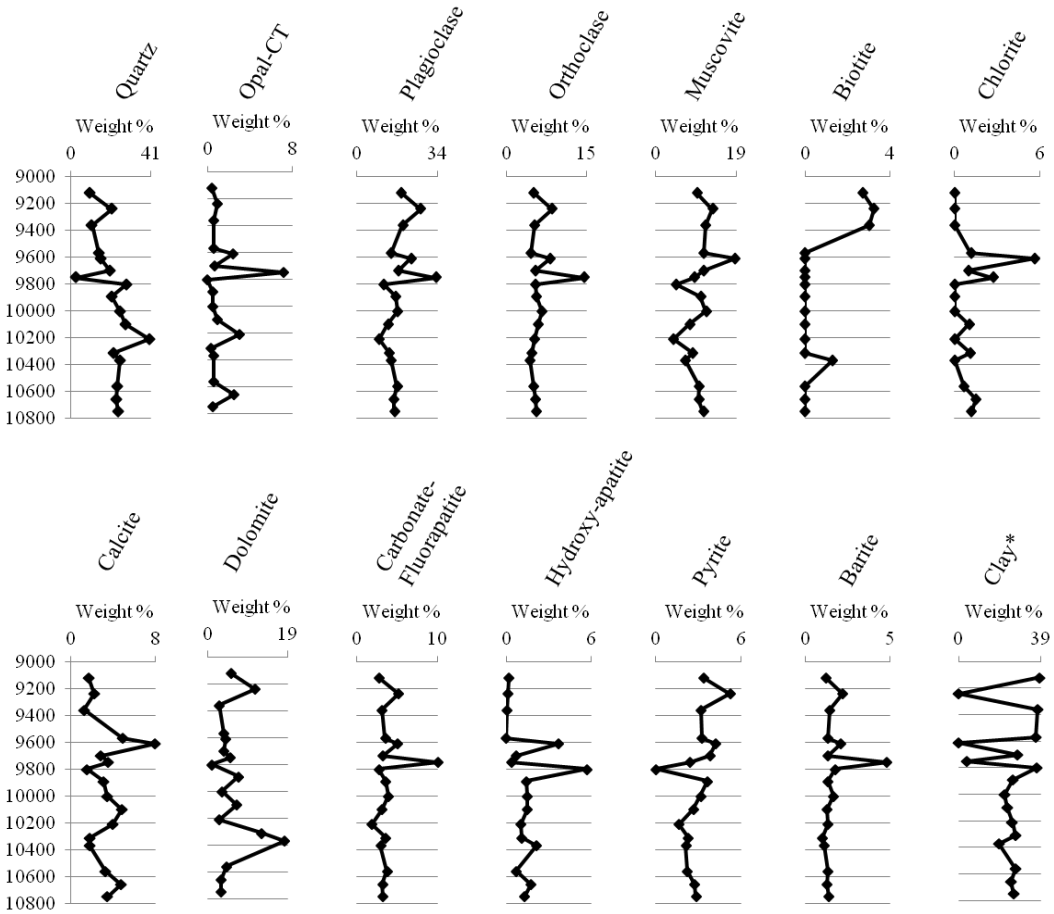

FIGURE 12. Mineralogical abundances in cuttings from Wilmington well D, measured by XRD. *Derived from FTIR analyses.

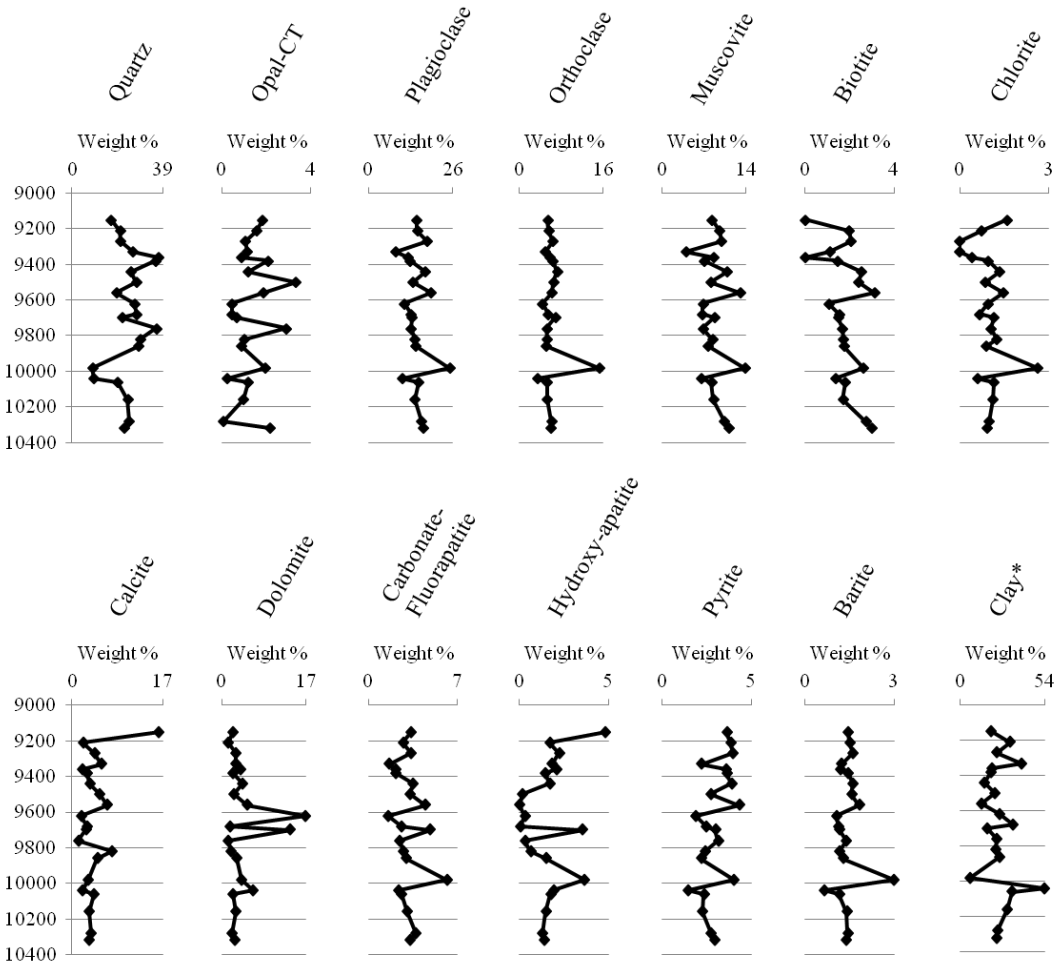

FIGURE 13. Mineralogical abundances in cuttings from Wilmington well E, measured by XRD. *Derived from FTIR analyses.

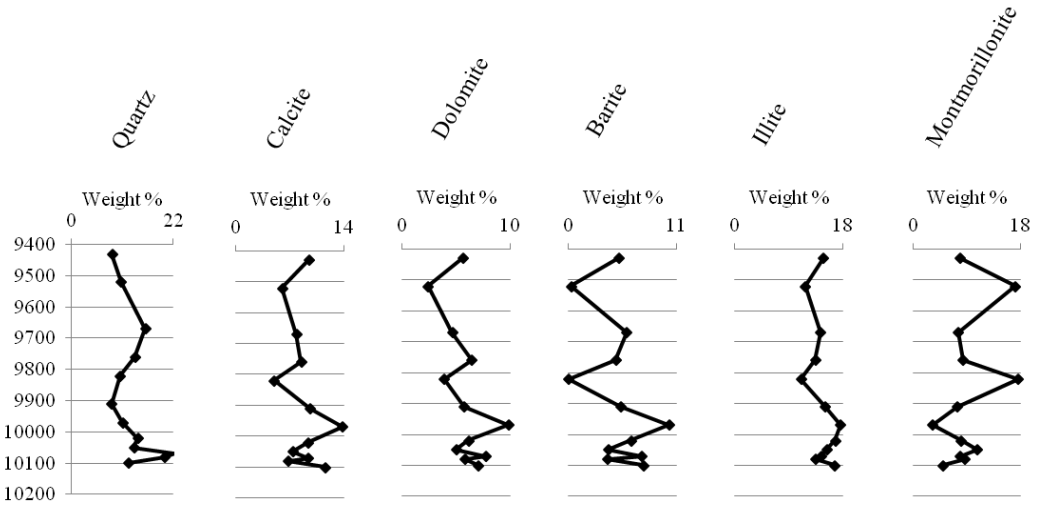

FIGURE 14. Mineralogical abundances in cuttings from West Beverly Hills well A, measured by FTIR.

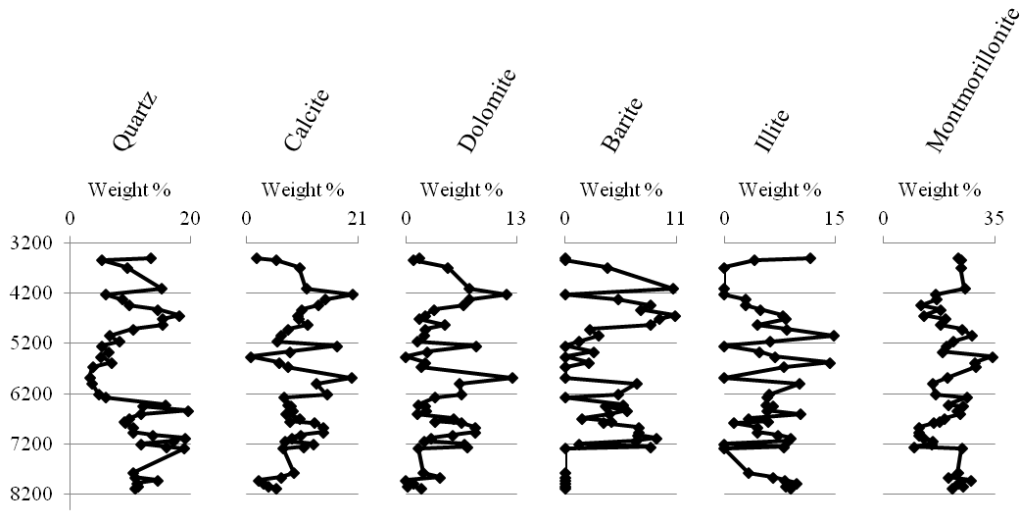

FIGURE 15. Mineralogical abundances in cuttings from East Beverly Hills well B, measured by FTIR.

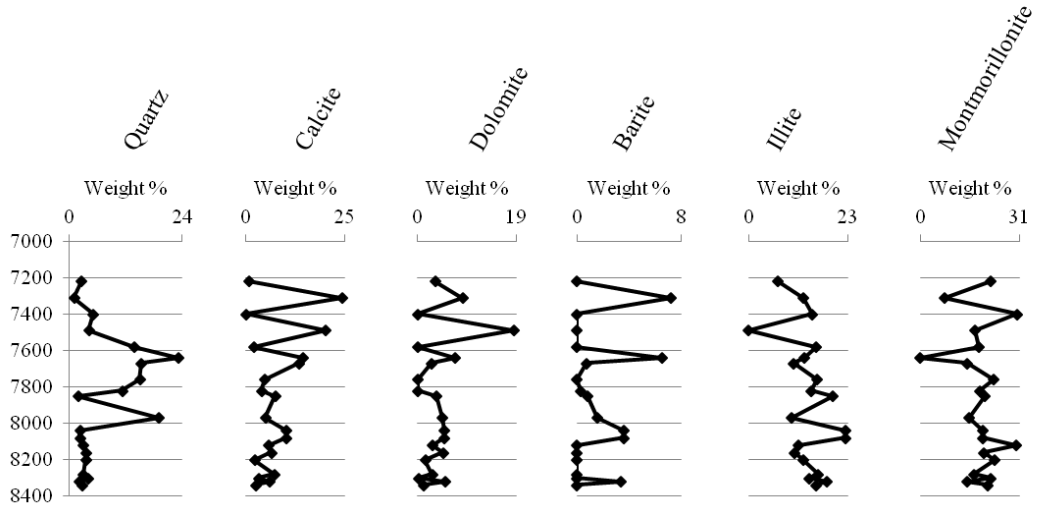

FIGURE 16. Mineralogical abundances in cuttings from Inglewood well C, measured by FTIR.

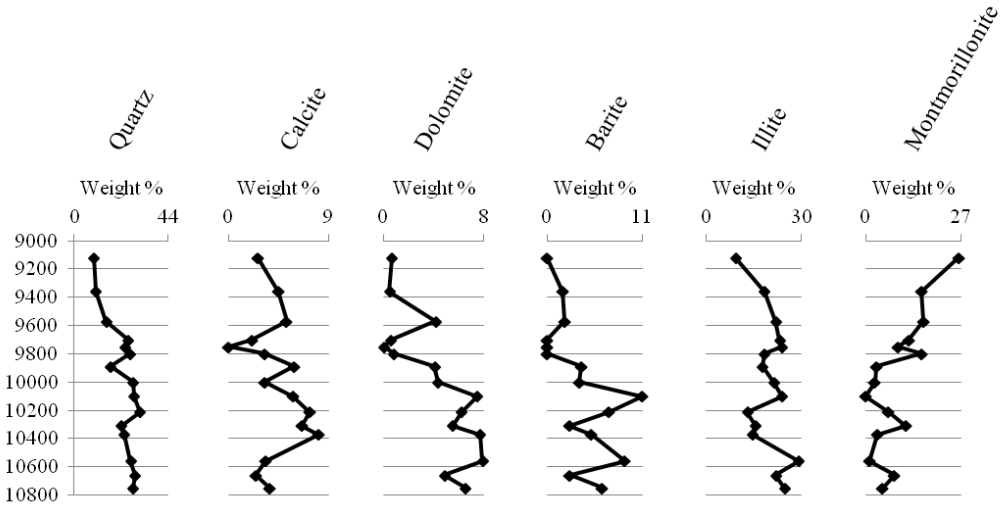

FIGURE 17. Mineralogical abundances in cuttings from Wilmington well D, measured by FTIR.

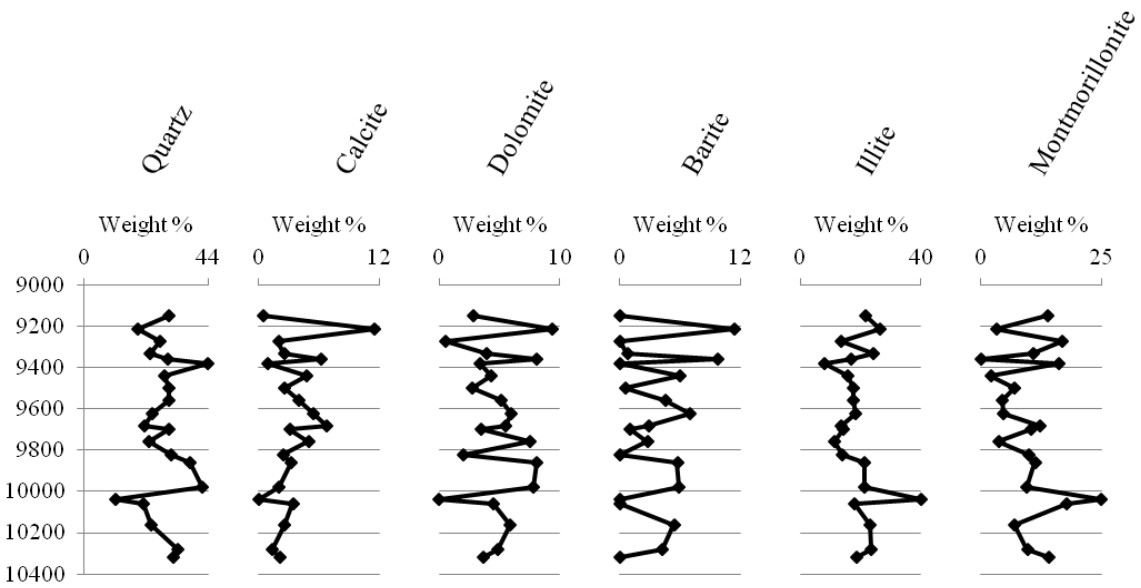

FIGURE18. Mineralogical abundances in cuttings from Wilmington well E, measured by FTIR.

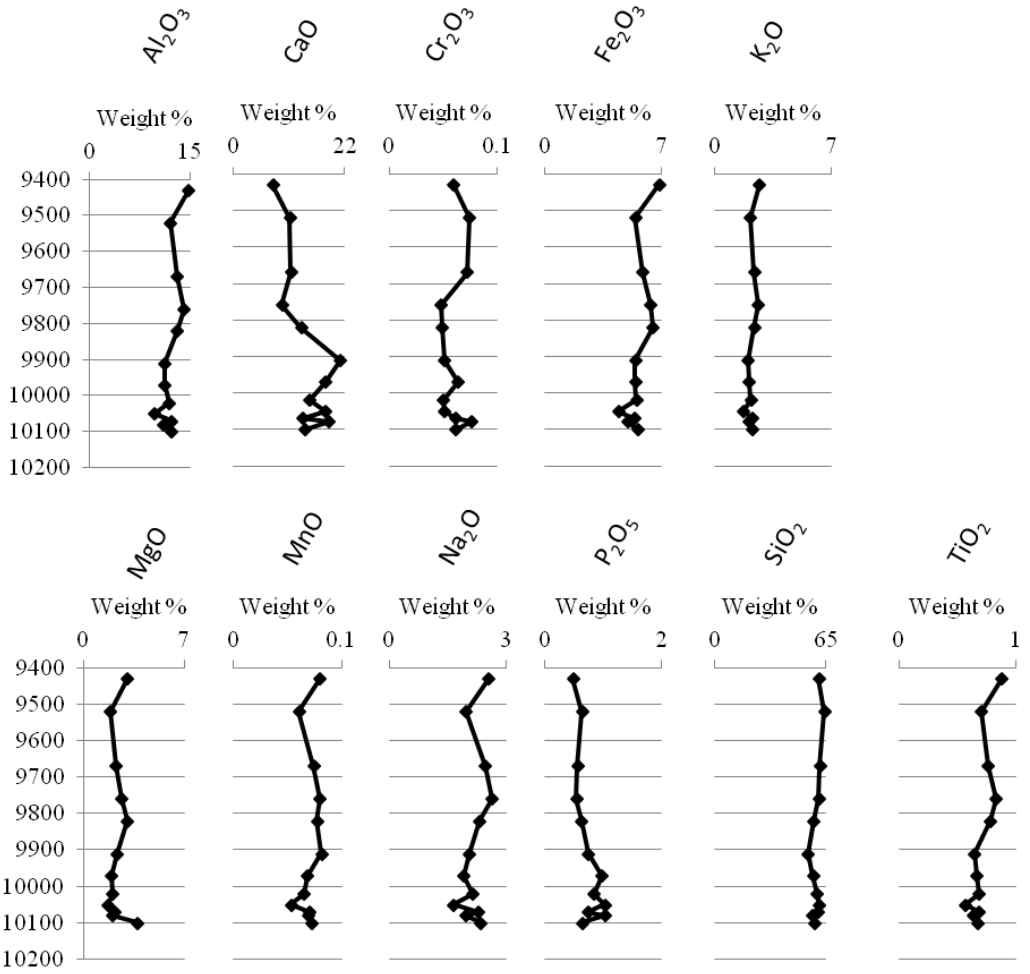

FIGURE 19. Major oxides in cuttings from East Beverly Hills well A, measured by XRF.

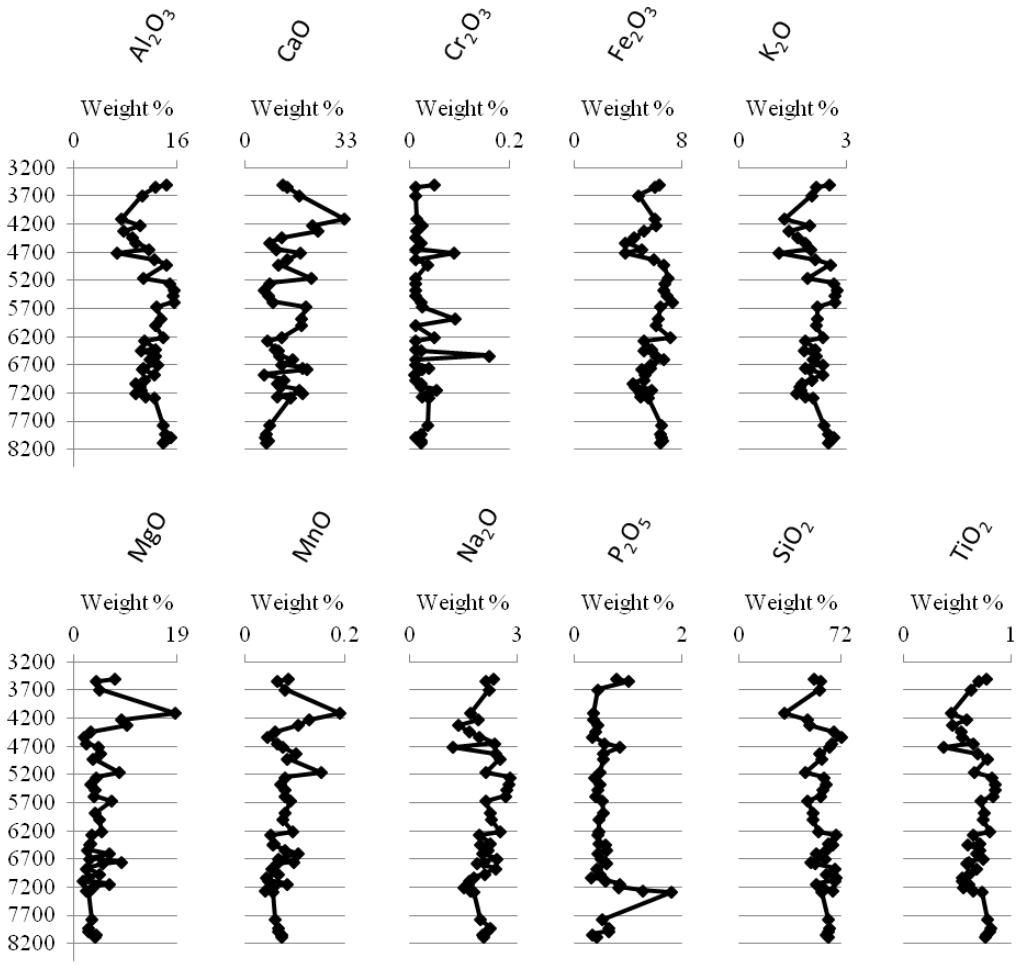

FIGURE20. Major oxides in cuttings from West Beverly Hills well B, measured by XRF.

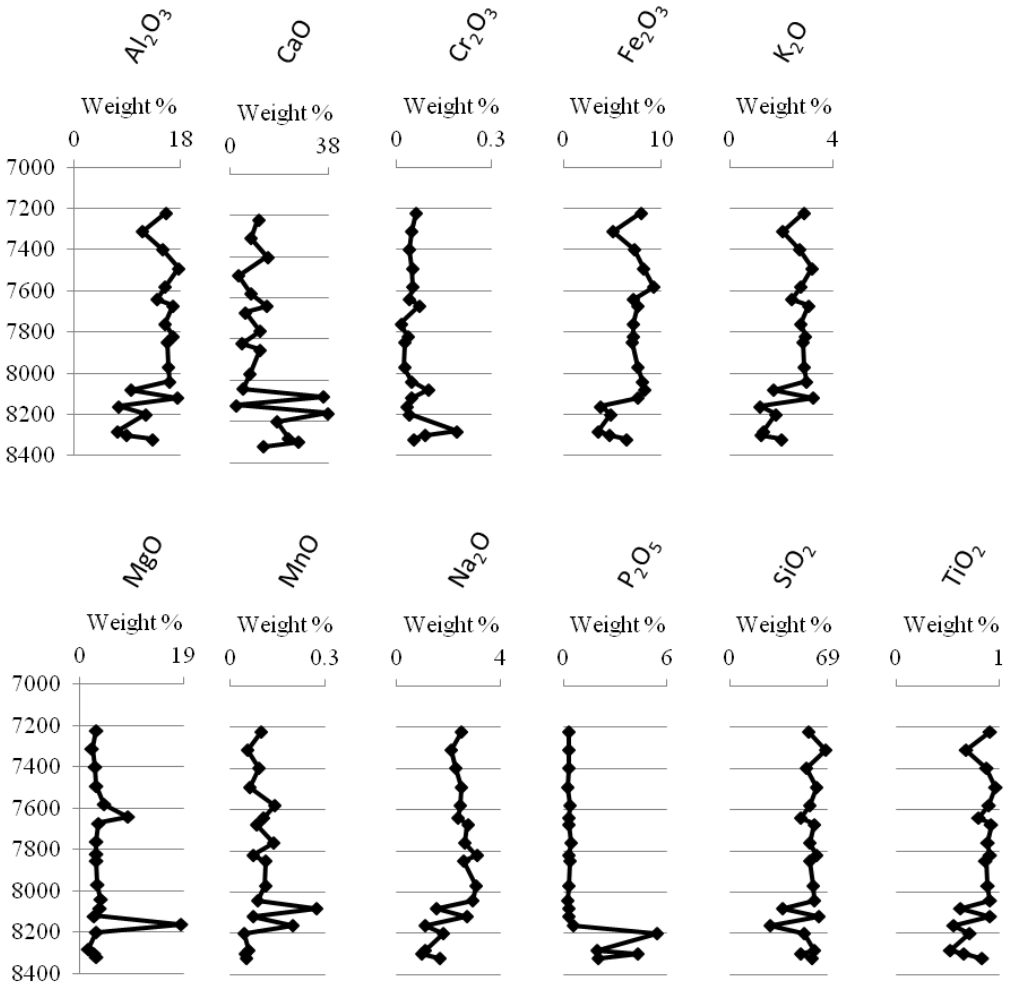

FIGURE 21. Major oxides in cuttings from Inglewood well C, measured by XRF.

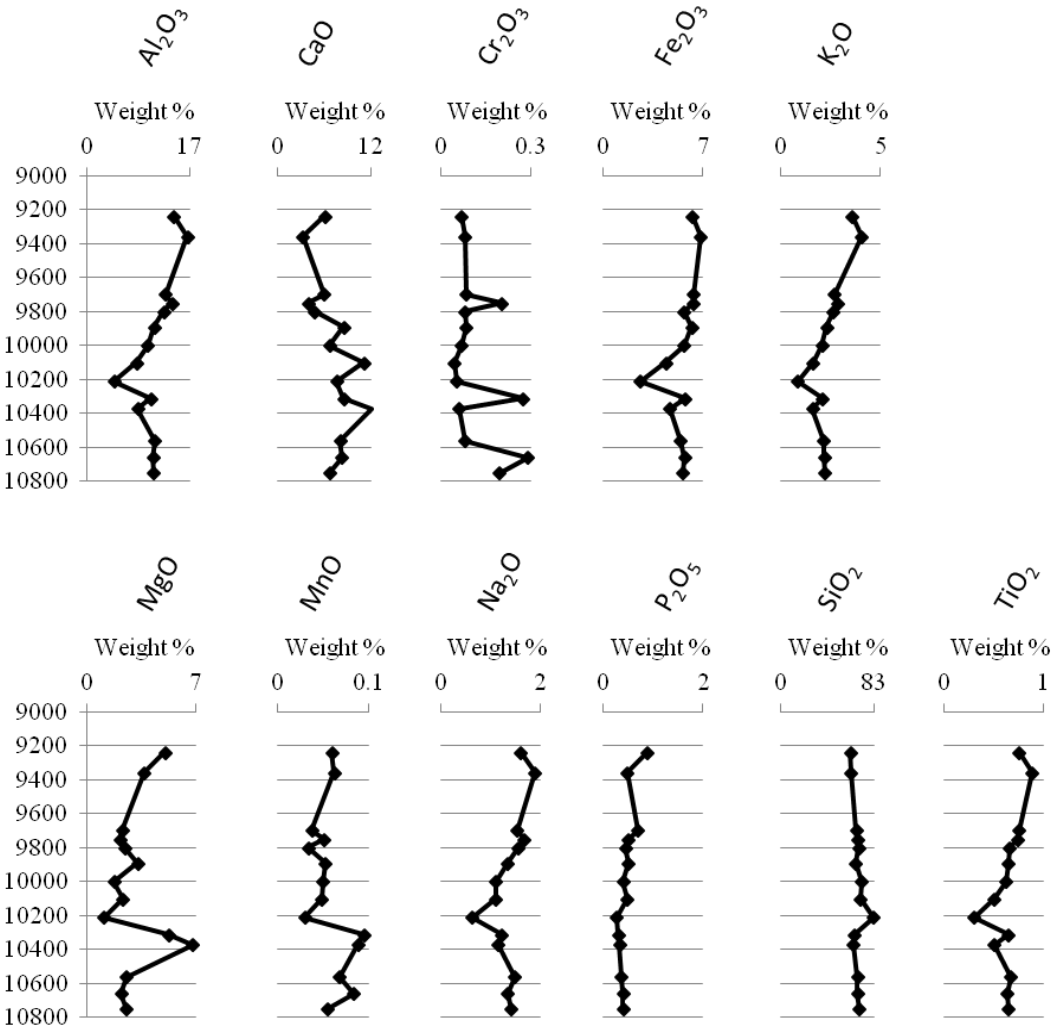

FIGURE 22. Major oxides in cuttings from Wilmington well D, measured by XRF.

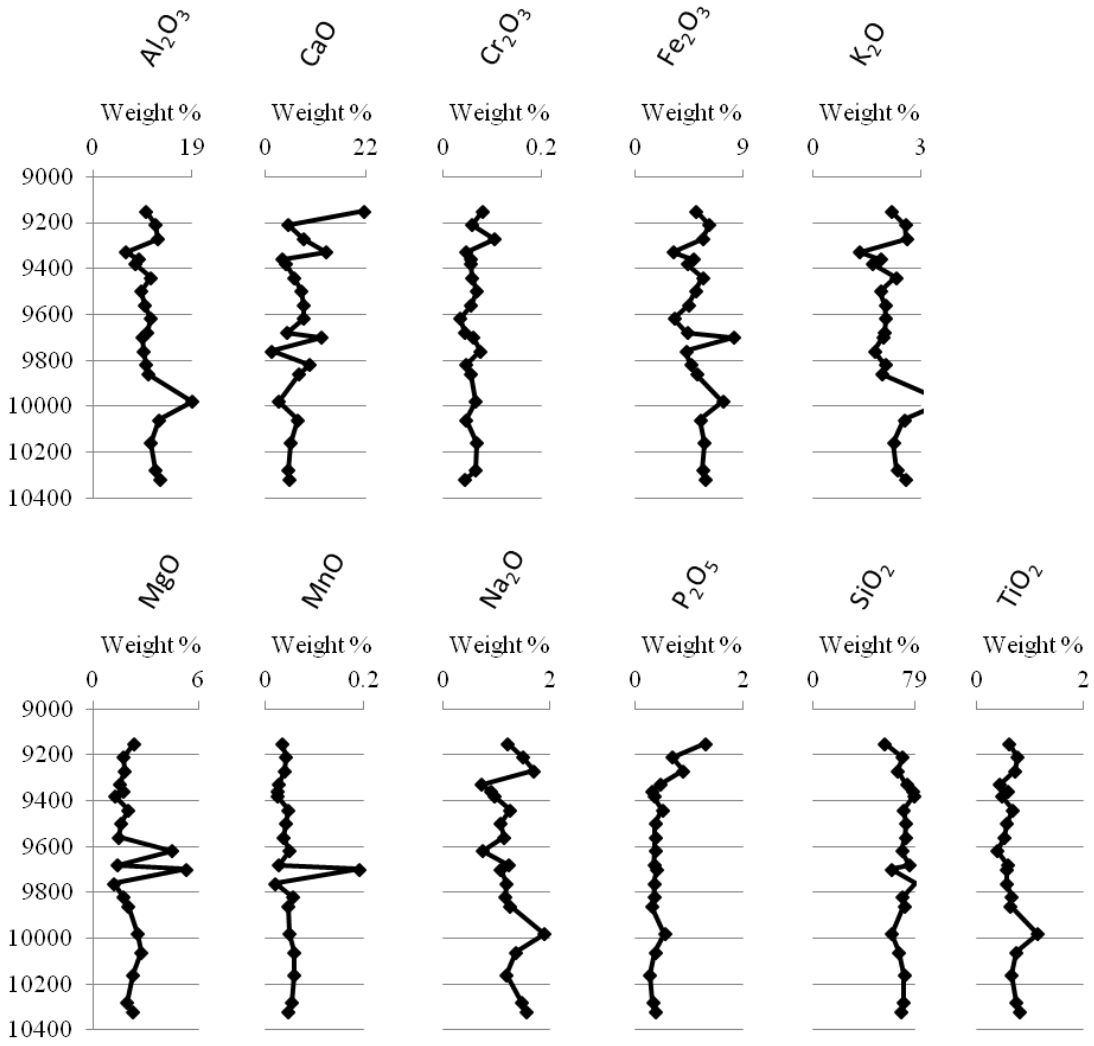

FIGURE 23. Major oxides in cuttings from Wilmington well E, measured by XRF.

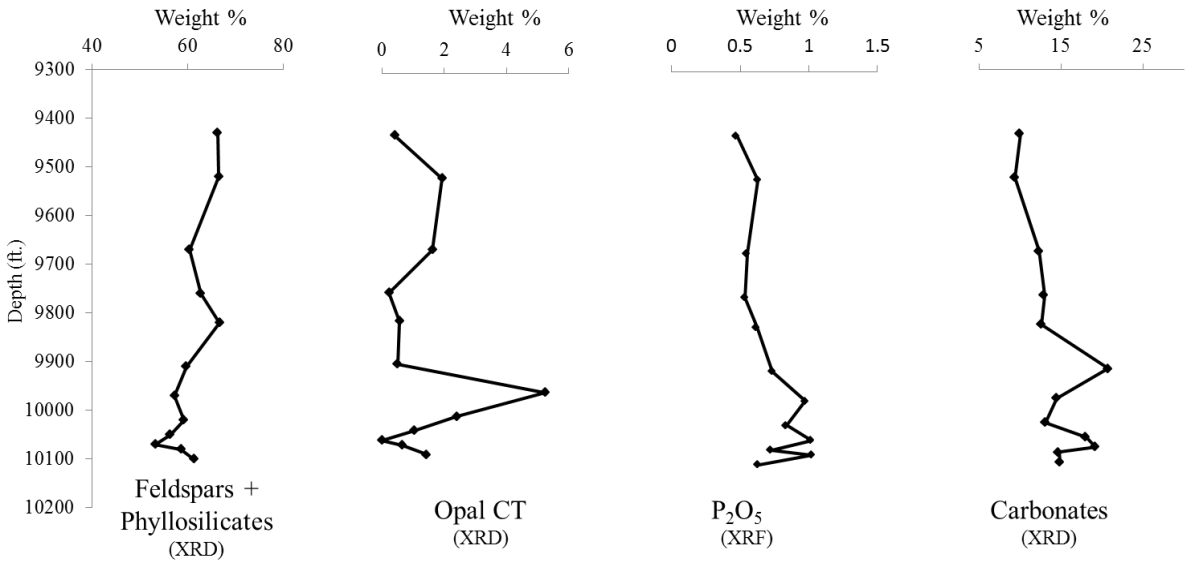

FIGURE 24. Proxies for Monterey Formation-type components for East Beverly Hills well A.

East Beverly Hills Well A

Twelve samples from East Beverly Hills well A were sampled from 9400' to 10100' MD (Table 1). Mineralogical abundances in cuttings from East Beverly Hills well A are presented in Figure 9 and 14, and the major oxides are presented in Figure 19. Proxies for Monterey Formation-type components are presented in Figure 24. Detritus is the main component of the individual fine-grained samples analyzed for East Beverly Hills well A, with the detrital component ranging between 53 to 66 wt. %. Measured opal-CT ranges from 0 to 5.2 wt. %, phosphate ranges from 0.4 to 1 wt. %, and carbonates range from 9 to 20.8 wt. %.

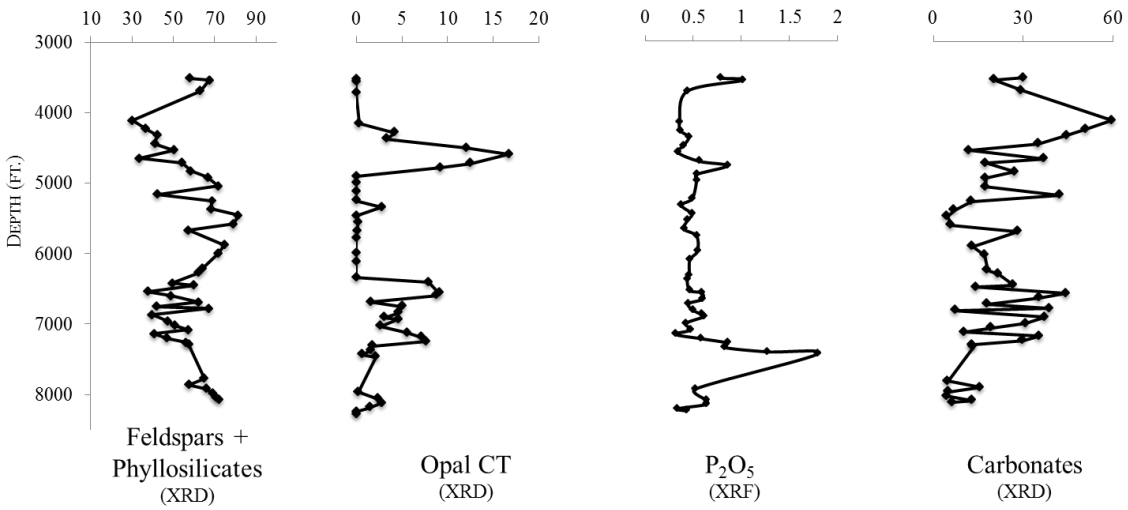

FIGURE 25. Proxies for Monterey Formation-type components for West Beverly Hills well B.

West Beverly Hills Well B

Forty-five samples from West Beverly Hills well B were sampled from 3480' to 8070' MD (Table 1). Mineralogical abundances in cuttings from West Beverly Hills well B are presented in Figure 10 and 115, and the major oxides are presented in Figure 20. Proxies for Monterey Formation-type components are presented in Figure 25. Detritus is the main component of the individual fine-grained samples analyzed for West Beverly Hills well B, with the detrital component ranging 30 to 81 wt. %. Measured opal-CT ranges from 0 to 16.7 wt. %, phosphate ranges from 0.3 to 1.8 wt %, and carbonates range from 4.5 to 59.6 wt. %.

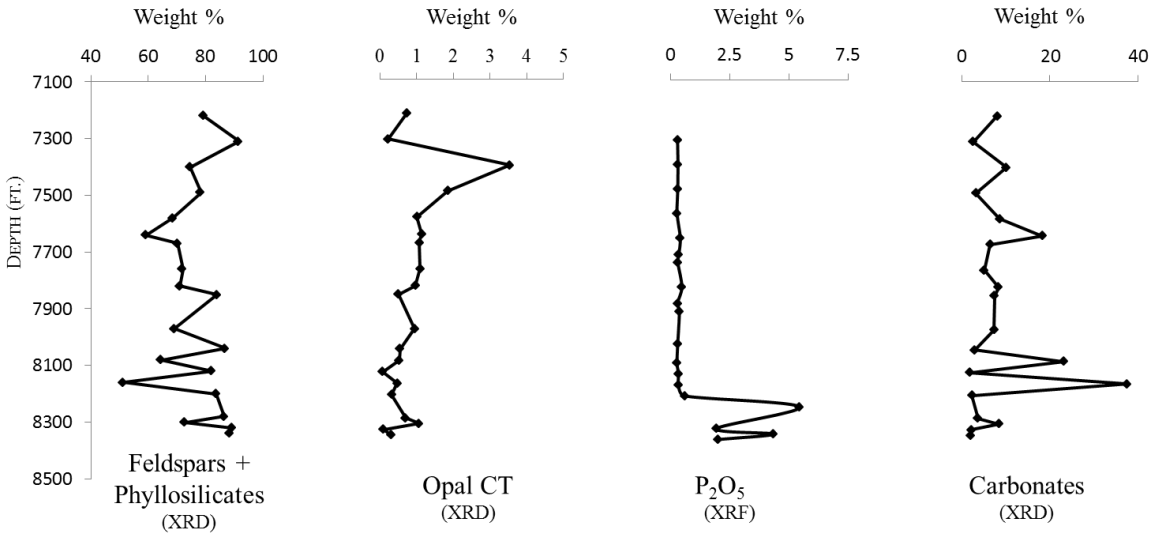

FIGURE 26. Proxies for Monterey Formation-type components for Inglewood well C.

Inglewood Well C

Forty-five samples from Inglewood well C were sampled from 7190’ to 8340’ MD (Table 1). Mineralogical abundances in cuttings from Inglewood well C are presented in Figure 11 and 16, and the major oxides are presented in Figure 21. Proxies for Monterey Formation-type components are presented in Figure 26. Detritus is the main component of the individual fine-grained sample analyzed for Inglewood well C, with the detrital component ranging between 45 to 90 wt. %. Measured opal-CT ranges from 0.1 to 3.5 wt. %, phosphate ranges from 0.3 to 5.4 wt. %, and carbonates range from 2.1 to 37.5 wt. %.

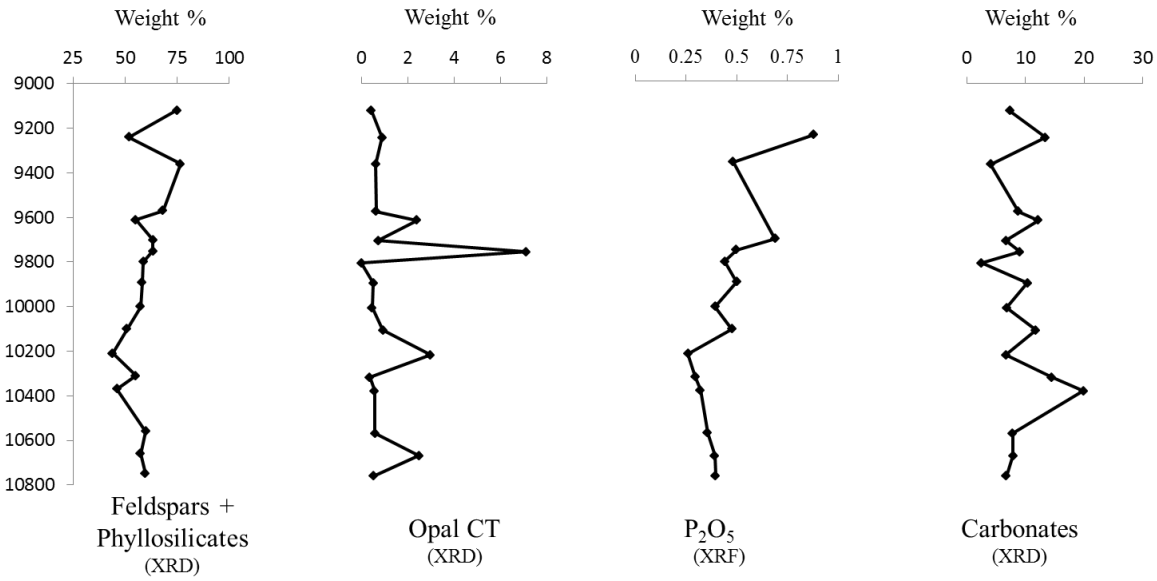

FIGURE 27. Proxies for Monterey Formation-type components for Wilmington well D.

Wilmington Well D

Seventeen samples from Wilmington well D were sampled from 9090’ to 10750’ MD (Table 1). Mineralogical abundances in cuttings from Wilmington well D are presented in Figure 12 and 117, and the major oxides are presented in Figure 22. Proxies for Monterey Formation-type components are presented in Figure 27. Detritus is the main component of the individual fine-grained samples analyzed for Wilmington well D, with the detrital component ranging 45 to 75 wt. %. Measured opal-CT ranges from 0.1 to 3.5 wt. %, phosphate ranges from 0.3 to 5.4 wt. %, and carbonates range from 2.1 to 37.5 wt. %.

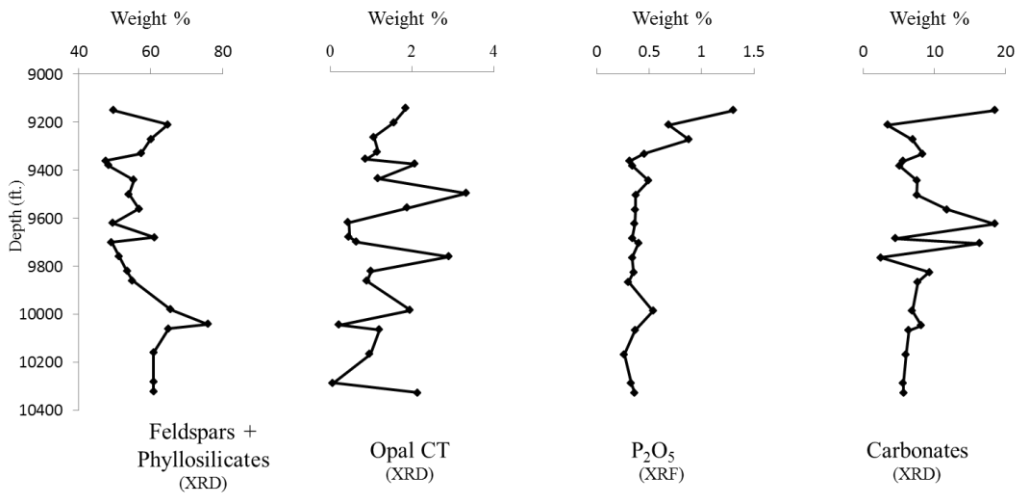

FIGURE 28. Proxies for Monterey Formation-type components for Wilmington well E.

Wilmington Well E

Seventeen samples from Wilmington well E were sampled from 9120’ to 10320’ MD (Table 1). Mineralogical abundances in cuttings from Wilmington well E are presented in Figure 13 and 18, and the major oxides are presented in Figure 23. Proxies for Monterey Formation-type components are presented in Figure 28. Detritus is the main component of the individual fine-grained samples analyzed for Wilmington well E, with the detrital content ranging 50 to 80 wt. %. Measured opal-CT ranges from 0.1 to 3.5 wt. %, phosphate ranges from 0.3 to 5.4 wt. %, and carbonates range from 2.1 to 37.5 wt. %.

CHAPTER 5

DISCUSSION

Geochemical and mineralogical data from five wells in the Los Angeles basin suggest that fine-grained facies of Monterey Formation-equivalent rocks share compositional similarities to successions described in previous studies of other Neogene sedimentary basins in California, in spite being vastly more diluted by siliciclastic sediment containing abundant aluminosilicates. Sedimentary components consistent with Monterey-Formation sediments in other basins, including opal-CT- and possibly quartz-phase siliceous mudstone, porcelanite and chert, organic-rich phosphatic shales, and carbonates (including dolomite and calcite), are found within the fine-grained rocks of the Los Angeles basin.

Sedimentary Components

Previous Work

For her PhD dissertation, Isaacs (1980), developed equations for calculating the primary sedimentary components of Monterey Formation-type rocks from XRF-derived geochemical composition (Table 2) that have been widely used and cited. Al_20_3, CaO, K_2O, MgO, Na_2O, P_2O_5, SiO_2, were used to estimate the amount of aluminosilicates, total detritus, detrital quartz, biogenic and diagenetic silica, apatite, dolomite, and calcite in the samples. In a number of studies (1980, 1981, 1989, 1990, 1991, 1992, 1993), she applied this geochemical method to characterize changes in the sedimentary components of

different members of the Monterey and Sisquoc formations in the Santa Barbara and Santa Maria basins. However, Isaacs' equations were created for the Santa Barbara area, which has a much lower and possibly mineralogically different detrital content than the inboard Los Angeles basin, raising the possibility that her equations would not be suitable in more detrital-rich successions that may contain a mineralogically distinct suite of clastic sediments.

Application of Sedimentary Component Equations

For this study, Isaacs' methods were initially followed and XRF-measured major oxides were corrected for loss on ignition (LOI), normalized, and then analyzed using Isaacs' equations on an organic-carbon-free basis. Sedimentary components in this study that were calculated do not agree well with values quantified with XRD and many samples have pre-normalized sums of components totaling between 150-200%. Calculated sedimentary components are found in Appendices D, and in Figures 16 to 20. Clearly, many sedimentary components, especially calcite and dolomite, are over- or incorrectly estimated with the published equations. Isaacs' equations assume an invariant composition of detrital mineral that may vary in total abundance, but not in their proportions. This allowed her to use a simple multiplier of Al_2O_3 as a proxy for aluminosilicates, total detritus, and to calculate the amount of detrital quartz.

TABLE 2. Isaacs' (1980) Equations to Convert Elemental Abundances to Abundances of Sedimentary Components. Equations were Derived from Isaacs' Work in the Western Santa Barbara Coastal Area.

Sedimentary Component	Equations
Detritus	$5.6 \times Al_2O_3$
Aluminosilicates	$4.2 \times Al_2O_3$
Detrital quartz	Aluminosilicates ÷ 3
Silica	$SiO_2-(3.5 \times Al_2O_3)$
Apatite	$[P_2O_5-(0.032 \times Al_2O_3)] \div 0.424$
Dolomite	$[MgO-(0.11 \times Al_2O_3)] \div 0.219$
Calcite	$[CaO-(0.08 \times Al_2O_3)-(0.555 \times \text{apatite})-(0.304 \times \text{dolomite})] \div 0.56$

Though the equations should be reliable for most Monterey Formation strata in distal, hemipelagic depositional settings, Isaacs' suggests explanations to why there may be variation in the determination of Monterey Formation sedimentary components (Isaacs, 1981). The amount of aluminosilicates material may be underestimated where mica and chlorite are abundant, which this study shows is the case for the Los Angeles basin. Negative values reflect errors in the conversion parameters, as a result of partitioning too much CaO, MgO, and P_2O_5 into aluminosilicates (Isaacs, 1989) whereas inadequate assignment of CaO would lead to overestimates of carbonates. Furthermore, the percent of Al_2O_3 varies considerably between different common aluminosilicate

minerals (Table 4), so different ratios of these minerals than found in the Santa Barbara coastal area will yield distinct multipliers to derive total aluminosilicates and total detritus from Al_2O_3.

Isaacs' equations were developed for the Santa Barbara-Ventura basin, which generally contains very little detritus with only slight compositional variation. She determined an average composition of 61% mixed-layer illite-montmorillonite, 20 % plagioclase feldspar, 7 % K-feldspar, and 11% (undifferentiated) mica (Isaacs, 1980). Weight percent of the mineral components of the aluminosilicate fraction for Isaacs' standards are compared with the five Los Angeles basin wells from this study in Table 3. To determine the proportion of mineral components in the detrital fraction of the LA basin, clay (illite and montmorillonite), plagioclase, orthoclase, and mica (muscovite, biotite, chlorite, and phlogopite) abundances from each well sample were normalized and averaged. This comparison shows reveals a gross difference in mineralogic composition of the detrital fraction between the two basins. Average clay (illite-montmorilionite) value for Santa Barbara basin (SBB) is 61%, whereas the average for the Los Angeles basin (LAB, this study) is 45 % (39.7 to 59.6%). Average plagioclase value in SBB is 20%, the average for LAB is 28% (20.0 to 33.7 %). Average orthoclase in SBB is 7%, but 9% in LAB (6.0 to 10.8 %). Isaacs found an average of 11% mica, whereas the average for the LAB wells is 18%, with values ranging 14.1 to 20.0 %. With the exception of Inglewood well C, all of the wells have less clay than Isaacs' average.

TABLE 3. Averaged Percentages of Detrital Minerals, Clay, Plagioclase, Orthoclase, and Mica from Study Areas

Well/Area	Clay	Plagioclase	K-feldspar	Mica	Total
A	41.8	31.5	10.7	16.3	100.2
B	40.7	33.7	5.9	19.7	100
C	59.6	20	6.3	14.1	100
D	39.7	29.7	10.8	19.8	100
E	43.2	26.1	10.7	20	100
LA Basin	45	28	9	18	100

TABLE 4. Averaged Percentages for Detrital Minerals, Clay, Plagioclase, Orthoclase, and Mica for the Santa Barbara basin, Isaacs (1980)

Area	Clay	Plagioclase	K-feldspar	Mica	Total
SB Basin	61	20	7	11	99

Although the abundance of major mineral groups can be compared as discussed above, published data does not permit comparison of specific minerals within some of those groups — such as plagioclase feldspars or micas — that have a large range of Al_2O_3 compositions (Table 4). Different proportions of minerals within a group would potentially have a significant impact on the Al_2O_3 multiplier for total aluminosilicates or detritus. For example, Isaacs' does not specify what type of mica was calculated, so an average of 17 % Al_2O_3 was used as a multiplier (Table 4), however, this study of the Los Angeles basin finds a predominance of muscovite with more than twice as large % Al_2O_3 (38.4 %).

XRF-calculated values for calcite and dolomite in the LAB samples were clearly overestimated when compared to XRD values; their values are presented in Appendix D, Tables 16 to 20. Because these carbonate abundances are primarily calculated from CaO wt. %, this overestimation indicates that excess calcium exists in other mineral phases. The most likely explanation is that there is proportionately more calcium-plagioclase in the LA basin aluminosilicate fraction than in Isaacs' samples from the Santa Barbara coast. As discussed in Rummelhart and Ingersoll (1997), the sandstone of the Modelo Formation in the Santa Monica Mountains contain a high proportion of plagioclase derived from plutonic complexes, now uplifted in the San Gabriel Mountains. The Modelo-age Ca-plagioclase-rich anorthosite complex now in the western San Gabriel Mountains and a Na-plagioclase-rich plutonic complex now in the central and eastern San Gabriel Mountains (Rummelhart and Ingersoll, 1997), with the Los Angeles basin fans being derived primarily from the central and eastern sources.

Although these are not the most Ca-plagioclase-rich sediments, they still contain significant Ca that should not be assigned to the carbonate minerals, as largely done in Isaacs' formulae.

TABLE 5. Mineral Composition Fractions of Al_2O_3 in Weight Percent.

Mineral	% Al_2O_3
Quartz	0
Albite	20.4
Anorthite	35.8
Orthoclase	18.3
Biotite	11.8
Muscovite	38.4
Phlopopite	12.2
Chlorite	17.1
Montmorillonite	18.6
Illite	17
Mixed-layer illite-smectite	23

Differentiation of the amount of detrital vs. biogenic/diagenetic silica is a challenge, as XRD does not distinguish between diagenetic and detrital quartz. Isaacs' equations for sedimentary components did not resolve this either. Isaacs determined detrital quartz to be equal to 33% of the weight of the aluminosilicates in the SBB samples (Isaacs, 1980). Rumelhart and Ingersoll (1997) estimate that that there is approximately an equal amount of detrital quartz to total feldspars in the lower Modelo Formation and about half as much detrital quartz as total feldspars in the sand-sized

fraction of the middle and upper Modelo Formation in the Santa Monica Mountains and Eastern Ventura basin. In this study, total feldspars account for 35 to 40 % of the aluminosilicates, using Rumelhart and Ingersoll's estimates, detrital quartz could account for between 20 and 35% of the total aluminosilicate fraction – a somewhat smaller fraction than would be calculated with the SBB-based equations. This relationship, too, is consistent with a greater decrease in geologically unstable feldspars (particularly the Ca-rich plagioclases) in sediments of the more distal, outboard basins such as Santa Maria and Santa Barbara.

Samples from Isaacs' study show very little compositional variation, and as a result the amounts of Ca, Na, and K in the aluminosilicate fraction are relatively proportionate and were not useful variables when these equations were developed. Consequently, she could more simply rely primarily on the Al_2O_3 measurement to calculate total aluminosilicates and to partition Ca between different mineral groups. However, feldspars and phyllosilicates (detritus) are the main component of the samples analyzed in the Los Angeles basin where muscovite mica, chlorite and plagioclase (including Ca-rich) are abundant. Although outside of the scope of this thesis, it appears feasible to develop Isaacs-type geochemical formulae for sedimentary components that are more suitable to this proximal basin setting. Thus, in future development of formulae for the Los Angeles basin, it is expected that CaO, Na_2O and K_2O would be important to properly calculate the detrital (aluminosilicates and detrital quartz), and authigenic/biogenic (apatite, calcite and dolomite) components. Similarly, different geochemical equations for sedimentary components would likely have to be developed

for other depositional basins with distinct provenances and mineralogic composition of the fine-grained fraction, such as, perhaps, the San Joaquin or Cuyama basins.

Compositional Zones

Because of the different detrital abundance and mineralogic composition of detritus in the Los Angeles basin, Isaacs' geochemical equations for sedimentary components cannot be applied without considerable caution and uncertainty. Therefore, for the purpose of identifying compositional zones in the fine-grained deposits of the Los Angeles basin, a limited set of geochemical and mineralogic components are selected to as representative of important Monterey-Formation-type components, including: detritus (feldspars + micas + clays), originally biogenic silica (opal-CT), authigenesis in a carbonaceous sediment (P_2O_5), and biogenic and diagenetic carbonate (dolomite + calcite). These proxies for key sedimentary components are evaluated for stratigraphic occurrence and lateral correlation in the following sections. Because of the predominant detrital content, most of the absolute values of biogenic and diagenetic proxies are much lower than what characterizes similar compositional zones in the outboard basins. Consequently, this discussion focuses on identifying intervals with relative increases in the abundances of the important proxies, rather than specifying specific threshold levels of abundance for identification. Nonetheless, it should be realized that a 30' interval of drill cuttings with only 10 wt. % opal-CT could represent a cumulative 3' of pure opal-CT chert, 6' of porcelanite, or more than 10' of siliceous/porcelaneous shale. And that these lithologies may be distributed as thin beds and laminations throughout the interval or may be concentrated in fewer distinct thick beds. Figures showing 2 or 3 side-by-side

colors in the same horizon represent stratigraphic intervals containing interstratified proxy components at a notable level, and closely spaced superjacent horizontal bars indicate separate stratigraphic zones of different proxies.

Geochemical, mineralogic and mudlog data from East Beverly Hills well A permits identification of three compositional zones: a lower siliceous-phosphatic-calcareous zone, a middle calcareous zone and an upper siliceous zone, despite the majority of the sampled intervals being dominated by detritus (55 to 66 wt. %) (Figure 29). Two intervals are identified as siliceous, 9900' to 10100' MD (measured depth in well) and 9520' to 9720' MD, with values ranging 0 to 5.2 wt. % and 1.6 to 1.9 wt. % opal-CT, respectively. Two intervals have been identified as calcareous, 9900' to 10100' MD and 9720 to 9890' MD, with values ranging 13.1 to19.2 wt. % and 12 to 13 wt. % total carbonate, respectively. One interval has been identified as phosphatic, 9900' to 10100' MD, with values ranging 0.7 to 1.0 wt. % P_2O_5. Mudlog lithology descriptions of porcelaneous, dolomitic or phosphatic intervals support the limits of the identified zones and refined the limits of the three zones, even where measured XRD values do not strongly reflect the siliceous or calcareous nature of the intervals.

Geochemical, mineralogic and mudlog data from West Beverly Hills well B help identify four compositional zones: a lowermost phosphatic zone, lower siliceous-calcareous zone, middle calcareous zone, and an uppermost siliceous-calcareous zone (Figure 30). Samples from West Beverly Hills well B are the most siliceous of the wells studied. Two intervals have been identified as siliceous, 6210' to 7290' MD and 4110' to 4710' MD, with values ranging 2.1 to 14.7 wt. % and 5.0 to 22.6 wt. % opal-CT,

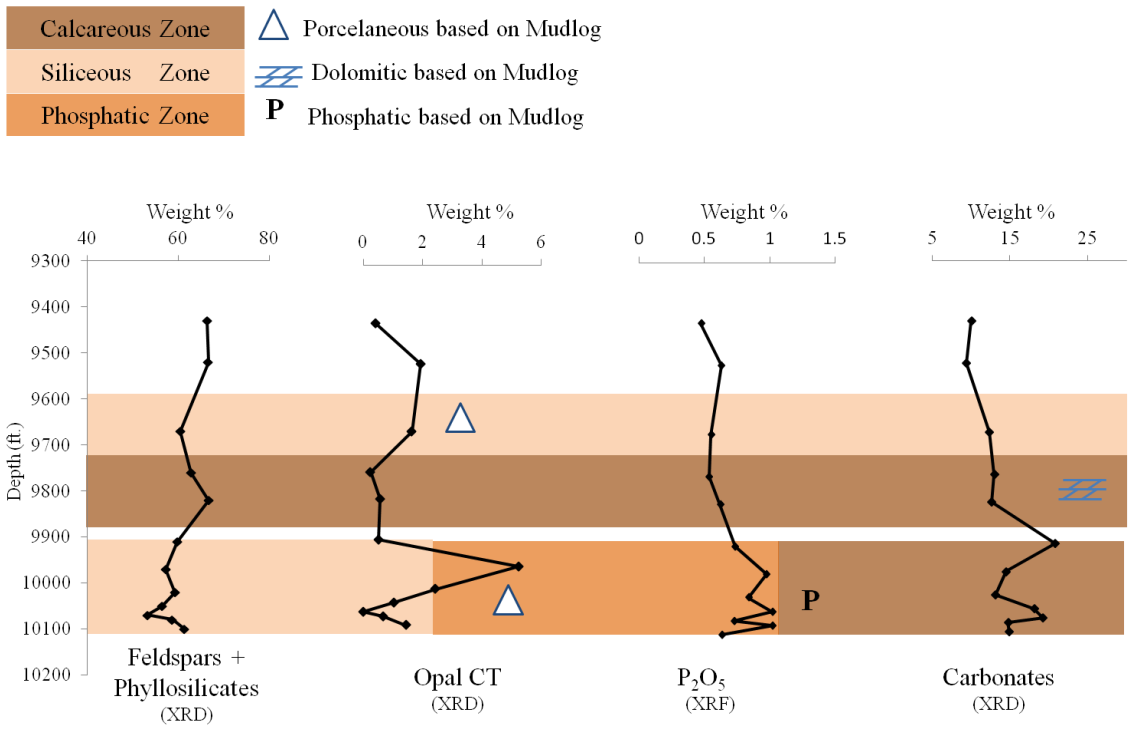

FIGURE 29. Compositional zonations for East Beverly Hills well A. Light Orange = Siliceous Zone, medium orange = Phosphatic Zone, and brown = Calcareous Zone. Symbols represent correlation with the mudlog.

respectively. Three intervals are identified as calcareous, 6210’ to 7290’ MD, 5580’ to 6210’ MD, and 4110’ to 4710’ MD, with values ranging 7.4 to 44.3 wt. %, 6.0 to 28.2 wt. %, and 12.0 to 59.6 wt. % carbonate, respectively. One interval is identified as a phosphatic zone, 7110’ to 7300’ MD, with values ranging 0.8 to 1.8 wt. % P_2O_5. Lithology descriptions of porcelaneous shale, chert, phosphatic, and dolomitic intervals in the mudlog support the limits of the identified zones.

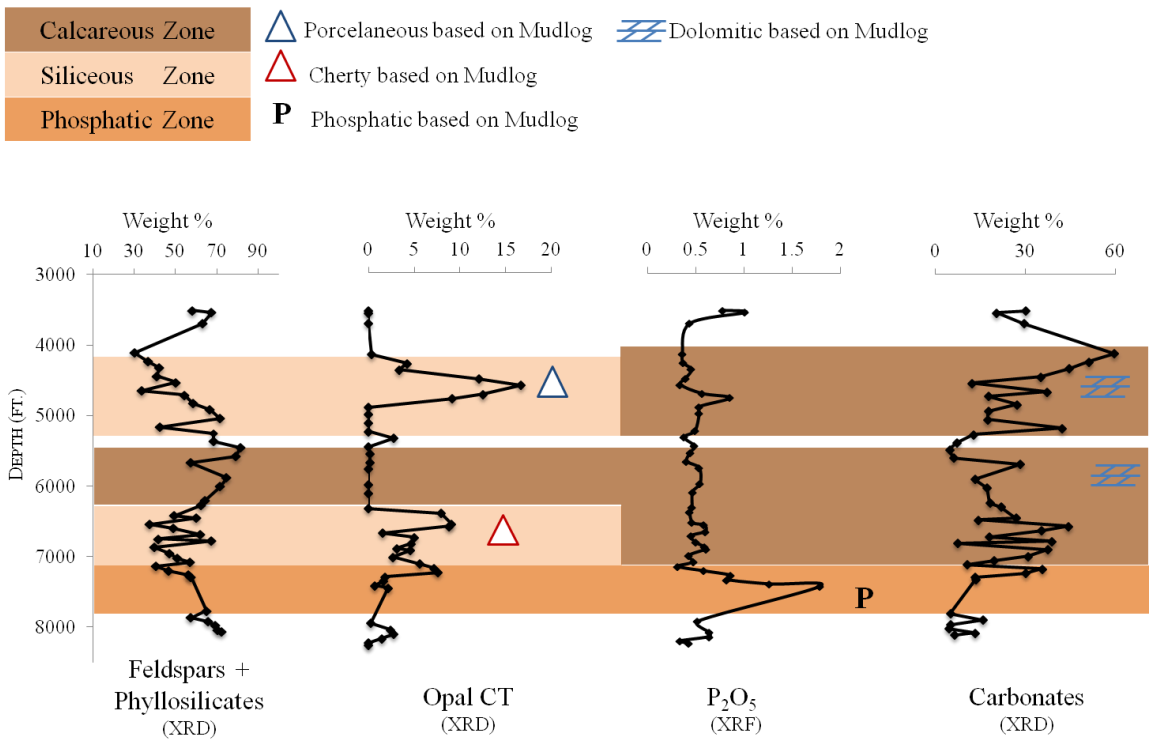

FIGURE 30. Compositional zonations for West Beverly Hills well B. Light Orange = Siliceous Zone, medium orange = Phosphatic Zone, and brown = Calcareous Zone. Symbols represent correlation with the mudlog.

Geochemical, mineralogical, and mudlog data from Inglewood well C permit identification of four compositional zones: a lowermost phosphatic zone, lower calcareous zone, middle calcareous zone, and an uppermost siliceous zone (Figure 31). One interval is identified as siliceous, 7340’ to 7600’ MD, with values ranging 1.0 to 3.5 wt. % opal-CT. Two intervals have been identified as calcareous zones, 8090’ to 8160’ MD and 7610’ to 7640’ MD, with values ranging 23.1 to 37.5 wt. % and 6.4 to 18.2 wt. % total carbonate, respectively. One interval is identified as a phosphatic zone, 8180’ to 8320’ MD, with values ranging 1.4 to 5.4 wt. % P_2O_5.

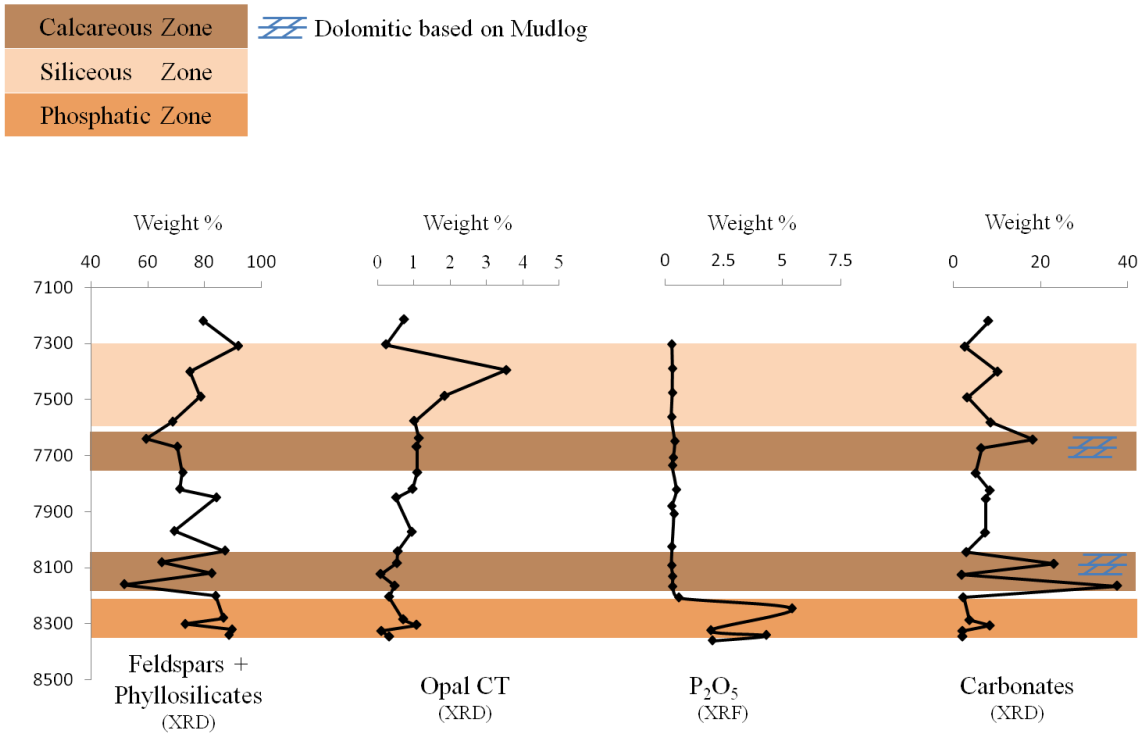

FIGURE 31. Compositional zonations for Inglewood well C. Light Orange = Siliceous Zone, medium orange = Phosphatic Zone, and brown = Calcareous Zone. Symbols represent correlation with the mudlog.

Mudlog lithology descriptions of dolomitic intervals support the limits of the identified zones.

Geochemical, mineralogic and mudlog data from Wilmington well D permit identification of five compositional zones: a lowermost siliceous zone, a lower calcareous zone, a middle siliceous zone, an upper siliceous-phosphatic-calcareous zone, and an uppermost phosphatic-calcareous zone (Figure 32).

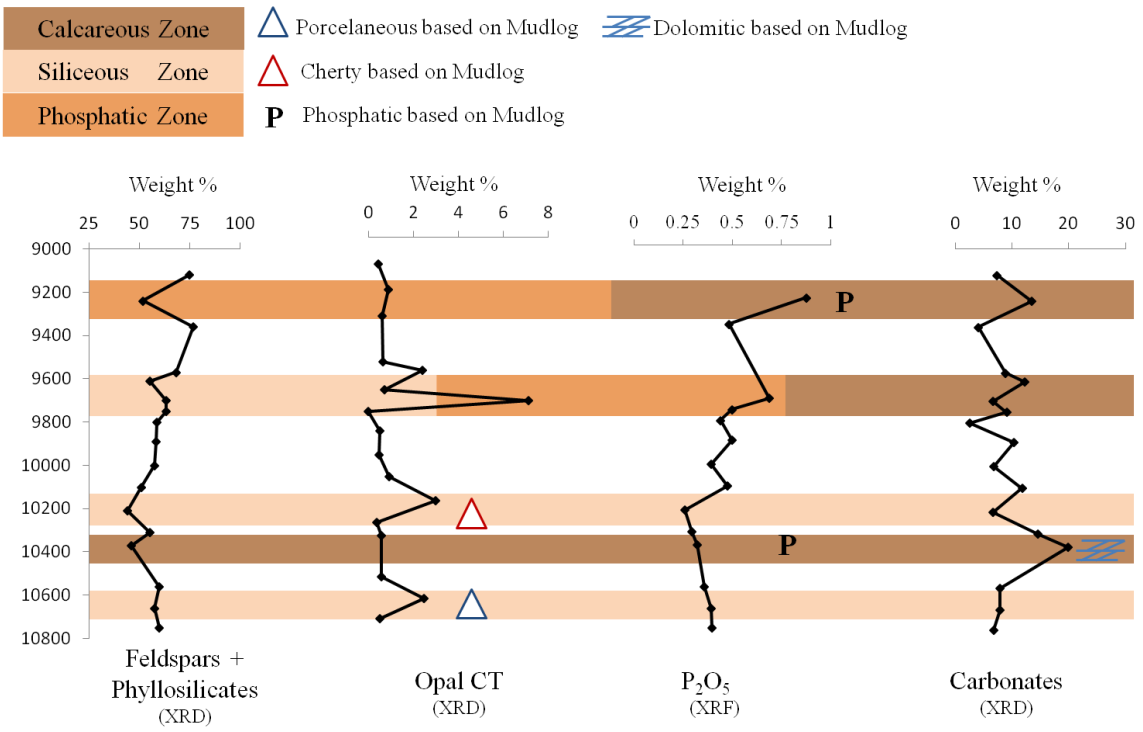

FIGURE 32. Compositional zonations for Wilmington well D. Light Orange = Siliceous Zone, medium orange = Phosphatic Zone, and brown = Calcareous Zone. Symbols represent correlation with the mudlog.

Three intervals are identified as siliceous, 10600’ to 10700’ MD, 10100’ to 10250’ MD, and 9610’ to 9780’ MD, with values ranging 0.5 to 2.5 wt. %, 0.9 to 3.0 wt. %, and 0.6 to 7.1 wt. % opal-CT, respectively. Three intervals are calcareous, 10310’ to 10560’ MD, 9610’ to 9780’ MD, and 9190’ to 9240’ MD, ranging from 7.8 to 20.0 wt. %, 6.7 to 12.2 wt. %, and 7.3 to 13.4 wt. % total carbonate, respectively. Two intervals are phosphatic, 9610’ to 9780’ MD and 9190’ to 9240’ MD, with 0.5 to 0.7 wt. % and 0.9 wt. % P_2O_5. Mudlog lithology descriptions of porcelaneous, chert, phosphatic and dolomitic intervals support the limits of the identified zones.

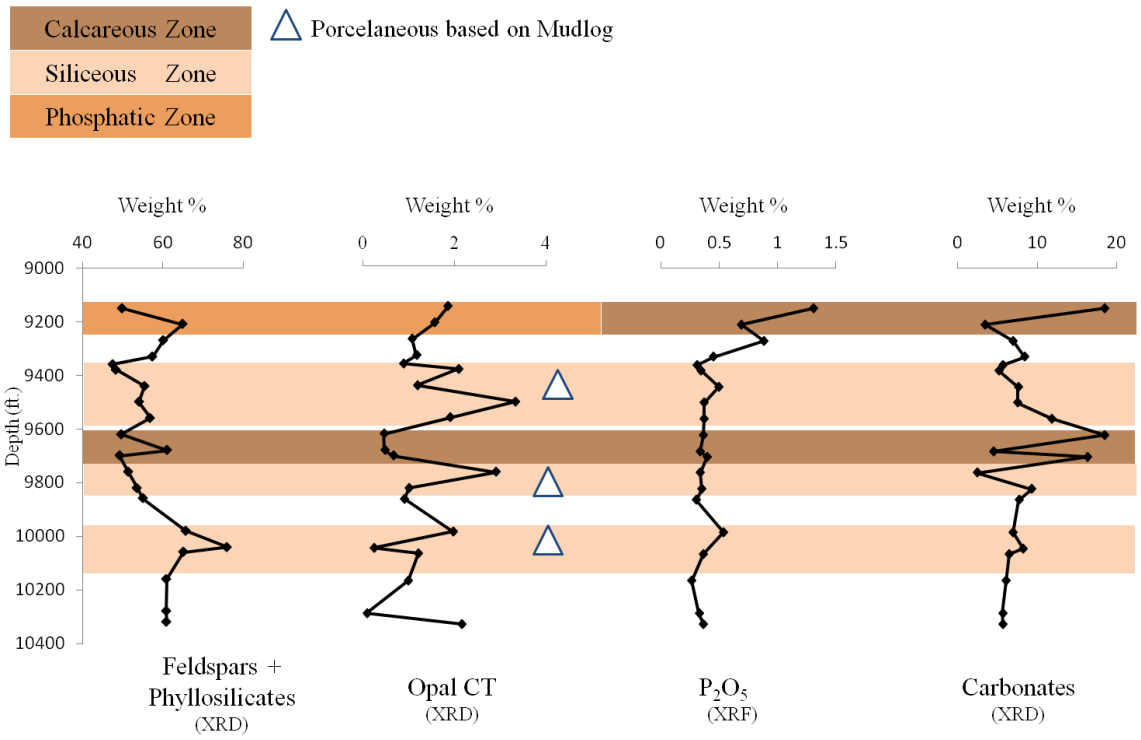

FIGURE 33. Compositional zonations for Wilmington well E. Light Orange = Siliceous Zone, medium orange = Phosphatic Zone, and brown = Calcareous Zone. Symbols represent correlation with the mudlog.

Geochemical, mineralogic, and mudlog data from Wilmington well E help identify five compositional zones: two lower siliceous zones, middle calcareous zone, upper siliceous zone, and an uppermost phosphatic-calcareous zone (Figure 33). Three intervals are siliceous, 9980’ to 10160’ MD, 9760’ to 9820’ MD, and 9380’ to 9560’ MD, with values ranging 0.2 to 1.9 wt. %, 1.0 to 3.0 wt. %, and 1.2 to 3.3 wt. % opal-CT, respectively. Two intervals are calcareous, 9620’ to 9700’ MD and 9150’ to 9270’ MD, with values ranging 4.5 to 18.5 wt. % and 3.4 to 18.5 wt. % total carbonate, respectively.

One interval is phosphatic, 9150' to 9270' MD, ranging from 0.6 to 1.3 wt. % P_2O_5. Mudlog lithology descriptions of porcelaneous intervals support the limits of the identified zones.

A simplified schematic of the identified compositional zones is shown in Figure 34. Despite the overall abundance of fine-grained detritus, two different compositional successions can be recognized in the biogenic/diagenetic proxies. The first seen in wells A, B, and C, consists of a lower phosphatic facies that may be interbedded with siliceous and/or calcareous components, a middle calcareous facies, that may have siliceous components, and an upper siliceous facies, that also, may be in part calcareous. The second pattern is seen in wells D and E, and consists of alternating zones of siliceous and calcareous facies in the lower sections, and an upper phosphatic facies that has both siliceous and calcareous components.

The Monterey Formation is most widely known for its siliceous sediments. All wells have intervals enriched in opal-CT that are associated with chert present in the cuttings and reported on the mudlog, providing evidence for diagenetic (originally biogenic) silica in the basin. Of the wells studied, samples from West Beverly Hills well B have the greatest abundance of diagenetic silica, up to 20 wt. % opal-CT in some intervals. Diagenetic quartz could not be distinctly identified, as discussed above. Crossover of density and porosity logs in West Beverly Hills B's well log supports the presence of low-grain-density material such as opal-A or opal-CT (Reid and McIntyre, 2001) in the siliceous zone (Figure 35). XRD confirms it to be opal-CT. The uppermost siliceous zone in wells A and B could be correlative with siliceous intervals in the upper

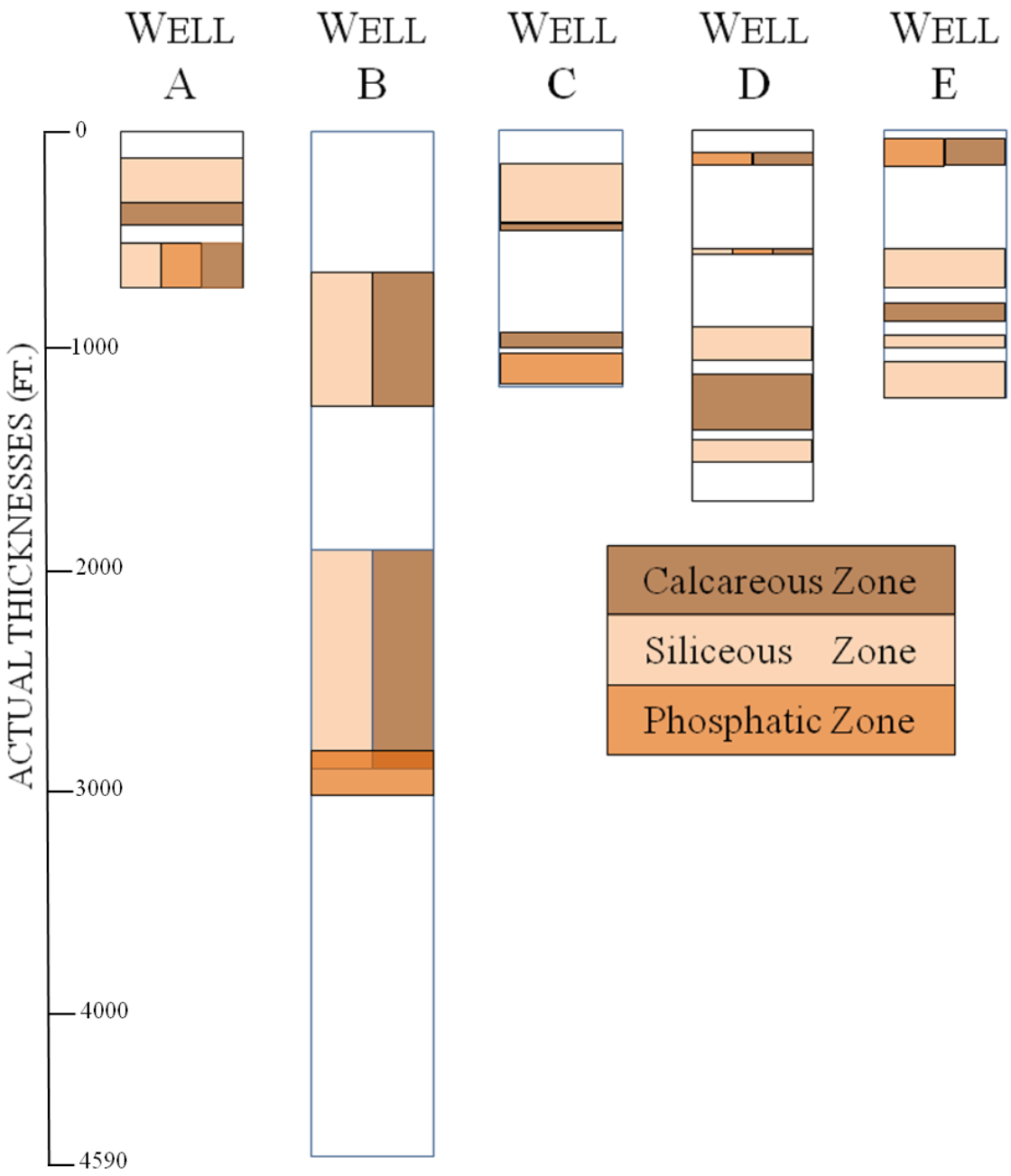

FIGURE 34. Comparison of compositional zonations for all five wells.

Mohnian to Delmontian Modelo Formation, described as diatomaceous, platey-siliceous, or cherty shales (Hoots, 1931), but it is unclear which interval they are best correlated with. If correlative with the upper member of the upper Mohnian-Delmontian Modelo, it should be largely lacking in carbonate, as is the case in well A. But if representative of the Mohnian lower member, it may include associated calcareous components, as occurs in well B. The uppermost siliceous zone in wells A and B are also consistent with the Delmontian uppermost member of the Puente Formation, described as fine-to-course sandstone, interbedded with siliceous siltstone (Blake, 1991). The alternating siliceous and calcareous zones in the lower succession, found in wells D and E are similar to Truex's descriptions of the lowermost section of the 237 Zone. These sediments are described as silty shale becoming increasingly calcareous and cherty with depth (Truex, 1974). These zones may be equivalent to the Luisian porcelaneous- calcareous shales of the middle Altamira Shale in Palos Verde (Woodring et al., 1946). P_2O_5 contributes primarily to phosphate in authigenic carbonate-fluorapatite and biogenic hydroxyapatite, thus providing the best way to identify intervals of enriched phosphate.

In the Los Angeles basin, carbonates make up the second largest component in the samples. Every well has several calcareous zones throughout the sampled interval The calcareous zones in wells C, D, and E are consistent with the basal member of the Puente Formation. The lowermost member of the Puente Formation is described as partially calcareous, but there is little mention of carbonate content otherwise (Durham and Yerkes, 1964; Blake, 1991). The zones identified in this study are more calcareous

than what has been previously described for the equivalent Modelo and Puente formations.

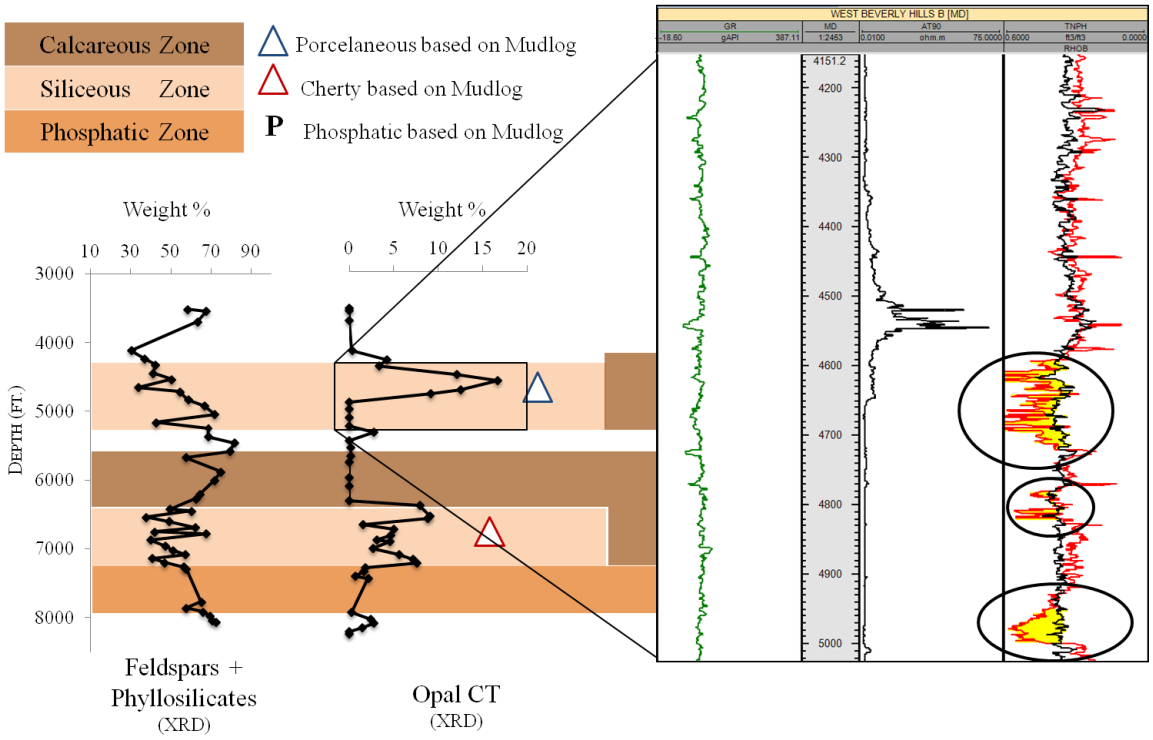

FIGURE 35. Density-porosity crossover on West Beverly Hills well B's log corresponds with the high measured amounts of opal-CT. Density-porosity crossover can indicate opal-A or opal-CT, both of which have low density and high porosity.

All five wells had enriched intervals of phosphate that correlated with well logs. The phosphatic zones in wells A and B are assigned by previous workers to the basal Modelo Formation. The phosphatic zones in wells C, D, and E are generally assigned to the lower Puente Formation. The phosphatic member, locally known as the Nodular Shale, is a "hot shale" with very distinct log characteristics, such high gamma ray, high

resistivity, low density and slow sonic velocity (Redin, 1999). Despite the resolution and distribution of the sample intervals, this high-gamma-ray, high-resistivity phosphatic member is picked on all five well's logs.

Biostratigraphy of the Los Angeles Basin

The chronostratigraphic resolution of the data is not very high. No proprietary data was released for the wells studied in this thesis. Publically available biostratigraphy data is sparse and chiefly based on the California benthic foraminiferal stages of Kleinpell (1931) and Wissler (1943, 1958), and on Blake's (1991) stratigraphic summary for the Los Angeles basin. Although generally abundant and commonly used across California, benthic foraminiferal stages have distinct limitations for precise chronostratigraphic correlation. One limitation is that stage boundaries can be diachronous and some assemblages more representative of environmental conditions than age (Crouch and Bukry, 1979). Another problem is that some of the stages can be quite long, for example, the key Mohnian stage runs from 13.6 to 7.1 Ma — 6.5 million years duration in the updated chronostratigraphic framework of Barron and Isaacs (2001). Further subdivision of such long stages is possible with integration of other dating techniques, but other biostratigraphic data is not available for the wells in this study.

The age of the phosphatic zone, found in both successions is somewhat unsettled. Truex (1974) reports that the "black shale" within the 237 Zone (Nodular Shale and lithostratigraphic equivalent to the phosphatic zone in other basins) in the Wilmington oil field is of Luisian age, based on a single paleontology report from the oil field, but it is unclear from what part of the stratigraphic section the determination was made. Like

Troxel (1954), Truex interpreted the black shale in Wilmington to be correlative with the Altamira Shale member of the Monterey Formation of Palos Verde peninsula. The Altamira Shale ranges from middle Miocene Luisian in the lower member to early Mohnian in the upper member (Woodring et al., 1946). The Altamira Shale is, in turn, overlain by the other siliceous Monterey members – the Valmonte Diatomite and Malaga Mudstone of Mohnian through Delmontian ages. Blake (1991) classified the Nodular Shale as Mohnian. Elliot et al. (2009) refer to the Nodular Shale as middle Miocene, lowermost Mohnian stage. So across the LA basin, the phosphatic facies may be as old as upper Luisian or more commonly of the slightly younger lower Mohnian stage.

The alternating siliceous and calcareous zones in the lower succession are likely of middle Miocene Luisian stage. Wilmington type logs from DOGGR (1992) have an unconformity between Cretaceous or older Catalina Schist and the upper Miocene 237 Zone. Samples deeper than the identified phosphatic zone in wells D and E are of some of the missing rocks. Blake (1991) shows an unconformity between the Luisian Schist Conglomerate and Luisian Topanga Formation which may include the lowermost 237 zone black shale.

Monterey Formation-Equivalent Rocks in Other Basins

Compositional zones containing Monterey Formation-type components identified in other California basins are also found in the Los Angeles basin. While the same general sequence described by Pisciotto and Garrison (1981) — lower calcareous, middle phosphatic, and upper siliceous — are not found, there is actually considerable finer variation documented in the Coast Range basins, including the 4-part stratigraphic

zonation of MacKinnon (1989) in the Santa Maria basin, the 5-part zonation of Isaacs (1980, 1983) in the Santa Barbara basin. Some of these have intrabasinal variation, especially in the middle portion of the Monterey (Hornafius, 1991). Nonetheless, there is some similarity to these successions in the five wells from the Los Angeles basin studied for this thesis. According to the Division of Oil, Gas, and Geothermal Resources (DOGGR, 1992) the Monterey Formation-equivalent rocks of the Modelo and Puente Formation are chiefly upper Miocene, largely of the Mohnian to Delmontian benthic foraminiferal stage (Blake, 1991). Ages of Monterey Formation-equivalent rocks in many of California's Neogene sedimentary basins are shown in Table 5. Many of the facies of the Monterey Formation are time-transgressive (Pisciotto and Garrison 1981), which is evident from Table 5, or laterally variable, even within a single basin (Hornafius, 1991). The lower calcareous zone of Pisciotto and Garrison is older in many of the other basins — Saucesian in the Santa Maria and Salinas basins. In the Los Angeles basin upper and middle calcareous zones are Mohnian and lower calcareous zones are Luisian stage. The oldest phosphatic zone is found in the Coast Ranges is Relizian age, the youngest phosphatic zone — Mohnian — is found in the Los Angeles, San Joaquin, Santa Barbara-Ventura and Salinas basins. The oldest siliceous zone is Saucesian in age in the Coast Ranges. Based on the data in Table 5, the Monterey Formation-equivalent rocks in the Los Angeles basin are most similar in age to zones in the Santa Barbara-Ventura basin.

The successions identified in the Los Angeles basin bear resemblance to Isaacs' compositional zones in the Santa Barbara area. Isaacs' generalized facies for the

Monterey Formation in Santa Barbara (originally defined in 1980, renamed in 1983) is presented in Figure 36, and consists of a lower calcareous-siliceous member, carbonaceous marl member, transitional marl-siliceous member, upper calcareous-siliceous, and a clayey-siliceous member. The alternating siliceous-calcareous zones in wells D and E are likely equivalent to the lower calcareous-siliceous member in the Santa Barbara-Ventura basin. The phosphatic zone in all five wells across the Los Angeles basin is likely equivalent to the carbonaceous marl or transitional marl-siliceous members in the Santa Barbara-Ventura basins. The calcareous-siliceous zones in wells A, B, and C are stratigraphically positioned to possibly be equivalent to the transitional marl-siliceous member or upper calcareous-siliceous member in the Santa Barbara-Ventura basin. The uppermost siliceous zone in wells A and C in the Los Angeles basin is stratigraphically consistent with being equivalent to the clayey-siliceous member of the Santa Barbara-Ventura basin. While acknowledging the uncertainties created by lack of precise dating, potentially time-transgressive nature of facies, and the real possibilities of unidentified compositional zones washed out by abundant sand deposition, the similar succession compositional zones within the same gross time frame, suggest that the intercalated fine-grained facies of the uppermost middle through upper Miocene LA basin record the same compositional zonation as the Monterey Formation rocks in the Santa Barbara-Ventura basin as documented by Isaacs (1980, 1981, 1983).

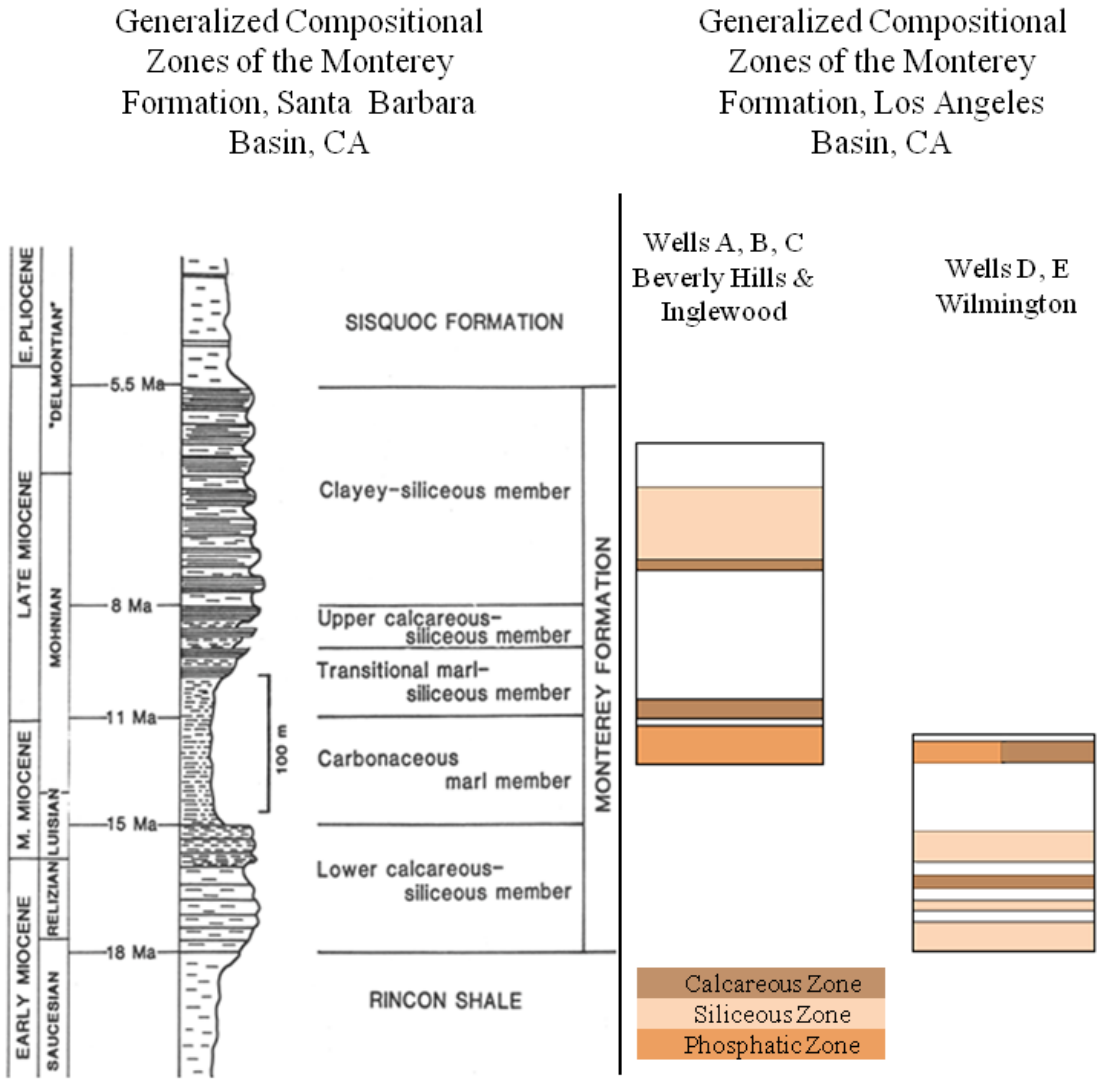

FIGURE 36. Compositional zones for the Santa Barbara basin and Los Angeles basins, modified from Isaacs (1980, 1983).

Table 6. Ages of Monterey Formation-Equivalent Sedimentary Rocks in Various California Sedimentary Basins. SMM=Santa Monica Mountains

	Benthic Foraminiferal Stages (Kleinpell, 1931)					
Basin	Saucesian	Relizian	Luisian	Mohnian	Delmontian	Author
Coast Ranges	calcareous, siliceous facies	calcareous, phosphatic, siliceous facies	calcareous, phosphatic, siliceous facies	phosphatic, siliceous facies	Siliceous facies	Pisciotto and Garrison (1981)
Western Los Angeles	Vaqueros (SMM)	Schist Conglomerate/ Topanga Fm.	Topanga Fm.	Lower Puente calcareous-phosphatic facies, Modelo Fm.	Upper Puente Fm. siliceous facies Upper Modelo Fm.	Hoots (1931) and Blake (1991)
San Joaquin	Temblor Fm.	Gould	Devilwater	McDonald/Antelope		Graham and Williams (1985)
Santa Barbara-Ventura		lower calcareous-siliceous facies	carbonaceous-marl facies	carbon-marl (lower), transition (lower), upper calc-siliceous (middle), clayey-siliceous (upper)	clayey-siliceous facies	Isaacs (1980,1981)
Santa Maria	Pt. Sal Fm. calcareous facies	Pt. Sal Fm. calcareous facies	phosphatic facies	upper calcareous-siliceous, clayey-siliceous facies	clayey-siliceous facies	Woodring and Bramlette (1950) and McKinnon (1989)
Salinas	Sandholdt Member calcareous facies	Sandholdt Member calcareous facies	Sandholdt Member calcareous-phosphatic facies	Hames Member phosphatic-siliceous facies	Hames Member siliceous facies, Butte Member diatomaceous facies	Duram (1974)

Controls of Significance of the Compositional Zones

Results of this study can be used to test three different hypotheses for hemipelagic compositional zonation along the California margin associated with deposition of the Monterey Formation. The first is that the compositional zones are a reflection of broad scale, oceanographic conditions that can be seen in multiple basins along the California Margin. The second option is that the compositional zones identified here are locally driven. The third is that the different facies are part of a prograding margin, as suggested by Isaacs (2001).

The first hypothesis is that the compositional zones in the Los Angeles basin were controlled by oceanographic, California margin-wide events. Previous work by Ingle (1981), Barron (1986) and Biddle (1991) suggested that controls on deposition of Monterey Formation-equivalent rocks operated on a large-scale and are not related to the formation of any single basin or basin type. These account for the widespread occurrence of siliceous/diatomaceous sediment across the Pacific Rim and the broad occurrence of a more calcareous lower section overlain by a siliceous upper section related to the transition from the warm middle Miocene highstand to development of increased upwelling and lowered sea level in association with growth of the Antarctic ice sheet in the late Miocene (Barron, 1986). Table 5 demonstrates the many similarities between the various Neogene sedimentary basins. In a broad sense, the two overlying successions of compositional zones in Monterey Formation-equivalent sedimentary rocks in the Los Angeles basin are consistent with the patterns identified in the other basins. This finding provides some support that oceanographic conditions were significant enough that they

had a broad impact on the margin and even left their signal in the clastic-dominated LA basin. Nonetheless, the amount of variation within the different Monterey Formation-equivalent successions does suggest that there was some local control on the compositional zones that are preserved.

A second hypothesis is that the compositional zones in the Los Angeles basin were controlled by local events. Two successions have been identified in the Monterey Formation-equivalent rocks in the Los Angeles basin. The lower succession found in the offshore Wilmington oil field consists of alternating calcareous and siliceous zones overlain by a phosphatic zone that has calcareous and siliceous components. The upper succession found in the northwestern portion of the Los Angeles basin consists of a phosphatic zone that locally has calcareous and siliceous components, overlain by a middle calcareous zone, overlain by a siliceous zone that locally has calcareous components. Correlation of the zones between wells or of the stratigraphic position of the two sequences is uncertain, however the proposed correlations and succession is consistent with all of the available data. The lower siliceous-calcareous zones are not identified in wells A, B, and C — these wells ended drilling in or below the phosphatic zone and do not have deeper samples, where the zones encountered in wells D and E would be expected. The upper siliceous zones are not present in wells D and E. The phosphatic zone in these wells is overlain by a thick turbiditic sandstone units, and it is likely that the younger fine-grained siliceous sediments found in wells A, B, and C were not preserved in wells D and E. These conclusions find relatively similar hemipelagic deposits where they can be correlated, suggesting a minimal influence of local variation

in oceanographic conditions on the composition of the fine-grained rocks, not to be confused with the vast importance of local deposition on the distribution and accumulation of the intercalated coarse-grained facies.

A third hypothesis is that the compositional zones in the Los Angeles basin are related to their position as part of a greater prograding margin. Isaacs (2001) proposed that, rather than being deposited in isolated, silled basins, the Monterey Formation-equivalent rocks were deposited along slopes of broad irregular depressions along an open continental margin, much like the current diatomaceous margin of southwest Africa. In a prograding margin, lithofacies would generally progress seaward from clay and diatomaceous sediments related to nearshore upwelling and deposited on the margin slope to increasing calcareous sediments related to slow pelagic deposition, with water depth and bathymetry being the main controls of facies variation (Isaacs, 2001). In deep waters, the calcareous sediment would accumulate slowly, but as water depth shallowed, the thickness of the siliceous zone would increase as a result of up-section shoaling (Isaacs, 2001). If this were the case for a broad margin that spanned the currently defined basins, the equivalent compositional zones in the Los Angeles basin should be older than an outboard basin like Santa Barbara. However, data in Table 5 suggest that compositional zones in Los Angeles basin and Santa Barbara basin are quite similar. The expected stratigraphic succession in a prograding margin consists of a lower calcareous zone representing slow deep water deposition, overlain by a thicker siliceous zone representing rapid slope deposits. Although calcareous zones are overlain by siliceous zones, they also overlie and underlie the primary phosphatic Nodular Shale unit. Results

from this investigation do not provide support for the prograding margin model of compositional lithofacies.

Significance of Findings

Four compositional zones have been identified in two overlapping successions in the Monterey-equivalent strata of the Los Angeles basin. The lowermost zone consists of alternating siliceous and calcareous facies and is only seen in wells D and E from the Wilmington field. This zone is overlain by a phosphatic facies that has both siliceous and calcareous components that is present across all fields. This zone is overlain by a middle calcareous facies (that may have siliceous components) and an uppermost siliceous facies (that may be in part calcareous) in wells A, B and C of the Inglewood and East and West Beverly Hills fields. This sequence of zones is consistent with compositional stratigraphy found in other Neogene sedimentary basin along the California margin (Table 5). Results of this study suggest that the zones identified in the Los Angeles basin are most similar to compositional zones found it the Santa Barbara-Ventura basin (Figure 36).

Despite the overwhelming amount of detritus in the basin, distinct hemipelagic signals reflecting oceanographic conditions can be identified by careful removal of coarse-grained sand, sandstone, and siltstone with grains larger than 0.0625 mm. Calculation of sedimentary components with the equations of Isaacs (1980) created for the Santa Barbara basin was inaccurate due to the distinct mineralogic composition of detritus in the Los Angeles basin that in turn is largely due to its proximal position and chemically immature sediments.

Methods and techniques described in this investigation can be applied to other studies involving mixed fine- and coarse-grained rocks. There is much to learn about the fine-grained sediments, especially in detrital rich basins. The chemical signature of these zones can be used as a tool for correlation both in field as well as across fields. Though not included in this study, analyses of biomarkers and trace elements can also be used to assist in well correlation. Specific compositional character can be discerned on well logs in supplement to chemical and mineralogic analysis: organic-rich, phosphatic intervals can be identified on well logs its characteristic high gamma ray, high resistivity, low density and slow sonic velocity. Opal-A and opal-CT can also be identified on well logs due to their low density and high porosity, which can be seen as crossover between the density and porosity curves.

CHAPTER 6

CONCLUSIONS

This study compositionally characterizes the hemipelagic facies of the Monterey Formation-equivalent rocks in the Los Angeles basin. Using chemostratigraphic techniques, four compositional zones were identified in five wells in a roughly north-south transect through four oil fields in the western portion of the Los Angeles basin. Although the basin has been studied extensively, little work has been done on the fine-grained portion. The Los Angeles basin is one of the innermost Neogene sedimentary basins along the California Margin, and accumulated a more detrital-rich and coarser-grained sediment fill than better-studied outboard basins. In spite of the high detrital content, inorganic geochemical and mineralogical data from five wells in the Los Angeles basin indicate:

1. Four compositional zones in the Los Angeles basin exist within middle to upper Miocene fine-grained facies: a lower alternating siliceous and calcareous zone, a phosphatic zone with calcareous and siliceous components, a calcareous zone, and an uppermost siliceous zone, locally with calcareous components.

2. The Luisian to lower Mohnian hemipelagic succession is preserved and identifiable in the southwestern basin (Wilmington field), whereas the lower Mohnian to Delmontian hemipelagic succession is identifiable in the western and northern basin (Inglewood, East- and West Beverly Hills fields).

3. Compositional zones identified in other California basins are similar to zones present in the Los Angeles basin, with particular similarity to the Santa Barbara coastal area.

4. The fine-grained detrital fraction in the proximal Los Angeles basin is especially rich in muscovite, chlorite, and plagioclase feldspars compared to the outboard basins, such as Santa Barbara.

5. The mineralogic composition of the detrital fraction in the Los Angeles basin is incompatible with Isaacs' (1980) equations for sedimentary components. Large abundances of Ca-feldspar and phyllosilicates (muscovite and chlorite) in the detrital fraction adversely affect ratios and multipliers of Isaacs' equations. Adjusting the equations to account for increased amounts of Ca-feldspar and phyllosilicates will allow the development of equations accurately to estimate Monterey Formation-type sedimentary components from major oxides measured by XRF.

6. Correlation of intercalated fine-grained facies in a sand-dominated succession on a chemical and mineralogic basis is possible between and within fields, even when sand-bodies are distinct and uncorrelatable.

CHAPTER 7

RECOMMENDATIONS FOR FUTURE WORK

This study has set the groundwork for chemostratigraphic studies in the Los Angeles basin. A coarse sample selection of five wells permitted a broad overview of the degree of compositional variation and the presence of stratigraphic trends within the Monterey Formation-equivalent sedimentary rocks of the Los Angeles basin. Recommendations for future work include:

1. The development of Isaacs-type equations to calculate sedimentary components for the Monterey Formation-equivalent rocks in the Los Angeles basin, using major/minor oxides. The high detrital content and difference in mineralogic compositional from Santa Barbara basin means that new formulae will need to be developed. Abundances of calcium feldspar may explain overestimates of calcite and dolomite, and abundances of muscovite will shift the ratio of Al_2O_3 to total aluminosilicates. K_2O, Na_2O and TiO_2 may need to be factored into the corrections, unlike Isaacs' equations for Santa Barbara where Al_2O_3 was the primary variable used for detritus. Corrected equations will help differentiate detrital, biogenic, and diagenetic silica, critically important constituents of Monterey-type sedimentary rocks.

2. FTIR has the potential to radically change the way fine-grained rocks are analyzed. While FTIR cannot replace the mineralogical identification that XRD provides, the conveniences of FTIR can accelerate the analysis process. Other than powdering the sample, there is little to no sample preparation, nor is the sample destroyed in the process.

The machine is small and portable and measurements are made in less than a minute. If the remaining ten Monterey Formation-type components were to be validated with acceptable R^2 values, then FTIR could be used for bulk quantitative analysis. In order to complete this process, the twenty Monterey Formation-type standards will need to re-made, within the detection limit of the Alpha Diamond ATR (0.05 percent of the sample). Spectra for the standards would be collected and used to rebuild the calibration model in Pirouette or similar multivariate analysis statistical software.

3. This study is the first of this kind in the Los Angeles basin. It provides information on five wells in four fields and a limited stratigraphic resolution. However, the Los Angeles basin is structurally and stratigraphically complex and economically important. Techniques described in this paper should be applied to other wells and outcrop section in the Los Angeles basin to establish a basin-wide compositional stratigraphy, identifying vertical as well as lateral patterns and trends. These can be used, not only for correlation, but to better understand the distribution of hemipelagic sediments through the basin.

APPENDICES

APPENDIX A

X-RAY DIFFRACTION DATA TABLES

TABLE 1. Semi-quantitative Mineralogical Abundances Measured by XRD, in % by Weight for East Beverly Hills well A, *Derived from FTIR analyses

Depth	Quartz	Opal-CT	Plagio-clase	Ortho-clase	Musco-vite	Chlorite	Calcite	Dolo-mite	Carbonate-fluorapatite	Hydroxy-apatite	Pyrite	Barite	Clay*
9430	12.2	0.4	19.0	6.7	9.4	0.0	2.8	7.3	4.1	3.4	2.4	1.2	31.2
9520	15.5	1.9	13.3	5.0	7.1	0.0	7.5	1.9	2.7	1.4	1.6	0.9	41.1
9670	13.2	1.6	21.8	7.9	12.6	0.0	8.7	3.6	4.7	3.4	2.5	1.6	18.1
9760	12.3	0.2	23.5	7.8	12.0	0.0	9.6	3.4	5.2	2.6	2.6	1.5	19.5
9820	10.6	0.6	18.9	6.2	11.1	1.8	8.4	4.2	4.3	2.1	2.1	1.0	28.7
9910	10.5	0.5	17.7	5.5	9.1	0.0	17.0	3.8	3.7	1.9	1.9	1.0	27.4
9970	12.1	5.2	18.2	7.2	8.9	0.0	11.2	3.3	3.6	3.5	2.3	1.5	22.9
10020	16.7	2.4	16.5	5.8	8.0	0.0	10.5	2.6	2.8	2.2	2.3	1.1	28.8
10050	16.0	1.0	14.1	4.6	6.9	0.0	15.4	2.7	2.7	2.8	1.9	1.1	30.7
10070	19.6	0.0	20.0	3.8	9.4	0.5	15.7	3.6	0.0	5.0	1.1	1.7	19.7
10080	15.5	0.7	22.1	8.4	9.7	1.4	11.0	3.8	3.8	2.4	2.6	1.7	17.1
10100	11.4	1.4	23.0	8.6	9.5	0.0	7.5	7.4	4.0	2.7	2.6	1.7	20.1

TABLE 2. Semi-quantitative Mineralogical Abundances Measured by XRD, in % by Weight for West Beverly Hills well B, *Derived from FTIR analyses

Depth	Quartz	Opal-CT	Plagio-clase	Ortho-clase	Musco-vite	Biotite	Chlorite	Phlogo-pite	Calcite	Dolo-mite	Carbonate-fluorapatite	Hydroxy-apatite	Pyrite	Barite	Clay*
3510	8.2	0	22.0	0.2	14.4	0	0	0	2.4	27.6	0	3.2	0	0.5	21.4
3540	6.5	0	16.3	0	16.3	0	0	0	10.6	9.8	1.0	4.3	0	0.3	34.9
3690	6.9	0	27.8	5.0	9.6	3.9	0	0	25.5	3.9	0	0	0	0.5	17.0
4110	2.8	0.3	13.9	3.5	8.2	0	0	0	0.7	58.9	2.4	2.9	1.9	0	4.6
4230	5.0	5.9	15.8	5.1	10.1	0	0	0	17.8	33.3	0	0	1.2	0	5.8
4320	6.6	4.9	15.2	3.8	8.3	0	0	0	8.5	36.2	0.3	0	1.4	0	15.0
4440	6.3	16.0	17.3	5.2	9.2	0	0	0	12.1	22.9	0.2	0	1.5	0	9.4
4530	11.6	22.6	19.1	0.0	13.1	0	0	0	10.5	1.6	2.1	1.4	0.1	0	18.1
4650	5.4	15.9	16.4	0.0	11.1	0	0	0	25.9	11.3	0	6.3	1.6	0	6.1
4710	9.0	12.2	23.3	0.2	13.8	0	0	0.8	15.3	2.3	0	4.4	2.5	0	16.4
4830	9.5	0.0	26.3	4.8	13.6	0	0	0	7.9	19.3	0	2.8	2.1	0	13.7
4920	9.0	0.0	19.0	5.0	11.2	1.8	1.3	0	10.1	7.6	0.3	5.2	0.9	0.2	28.6
5040	6.1	0.0	18.3	3.9	8.9	1.8	0.0	0	11.9	5.6	0	3.7	0.6	0.6	38.9
5160	4.3	0.0	16.1	5.2	6.4	0	0	0	9.2	33.0	0	8.8	1.0	1.1	14.8
5250	7.7	2.7	23.6	6.5	13.0	1.4	0	0	2.7	10.0	5.4	1.7	0	1.3	24.1
5370	7.2	0.1	22.6	6.0	13.5	0	0	0	4.3	2.7	4.5	10.2	2.6	0	26.4
5460	6.3	0.2	17.7	4.5	9.3	0	0	0	2.0	2.8	3.3	1.2	2.2	0.9	50.0
5580	6.7	0.1	18.4	5.4	10.3	0	3.6	0	3.4	2.6	4.0	0.8	2.2	0.9	41.6
5670	4.2	0	14.1	0	0	1.7	0	0	2.3	25.9	0.4	8.2	0.1	1.6	41.5
5880	8.8	0	21.5	4.4	10.1	1.8	1.6	0.9	13.0	0.1	1.1	0.3	0.6	1.2	34.5
6000	6.1	0	11.1	5.2	7.4	2.3	1.3	1.8	17.1	0	0.4	2.5	0.4	1.8	42.5
6210	7.0	0	16.4	4.1	8.6	0	1.1	0.8	4.1	14.0	1.2	9.5	0	0	33.1
6270	6.6	8.8	19.8	0	7.0	0	0	0	5.9	15.9	0.1	0.3	0.1	0	35.6
6420	9.8	12.7	20.8	0	12.8	0	0	0	9.4	17.3	1.2	0	0	0	16.0
6540	6.9	2.6	15.0	3.8	7.6	0	1.1	0	5.0	39.3	0.2	5.8	2.3	0.3	10.2
6600	6.2	6.6	20.0	1.7	9.3	0	0	0	2.5	33.0	0	0.7	2.1	0	18.0
6690	12.1	6.4	21.4	0.0	12.9	0	0	0	11.5	6.4	1.4	0	0	0	27.8
6750	6.8	4.1	14.2	3.5	6.0	0	0.5	0	3.5	35.2	0	7.0	1.3	0	17.7
6780	13.4	7.1	23.6	5.4	13.1	0	0	0	7.0	0.5	0.5	2.0	2.2	0	25.3

TABLE 2. Continued

Depth	Quartz	Opal-CT	Plagio-clase	Ortho-clase	Musco-vite	Biotite	Chlorite	Phlog-opite	Calcite	Dolo-mite	Carbonate-fluorapatite	Hydroxy-apatite	Pyrite	Barite	Clay
6870	8.7	4.3	14.8	3.7	8.4	0	0	0	13.1	24.3	0.1	8.1	1.6	0	13.0
6960	9.1	7.8	18.4	5.2	10.0	0	0	0	5.1	25.8	0	3.1	1.9	0	13.6
7020	16.6	11.3	20.8	0	8.3	0	0	0	10.2	9.1	0	0	1.9	0	21.8
7080	16.3	12.1	22.1	6.9	10.0	0	0	0	9.2	1.3	1.1	0.8	2.1	0	18.2
7140	14.7	2.9	12.5	0	7.8	0	0	0	6.1	29.4	0.5	5.8	0	0	20.3
7200	17.4	3.4	16.5	0	8.5	0	0.2	0	18.7	11.4	0.2	0	2.0	0	21.7
7260	26.6	2.7	19.6	0	7.4	0	0	0	8.7	4.4	1.3	0	0	0	29.2
7290	15.5	2.1	17.2	6.1	12.9	0	1.6	0	10.0	3.4	4.7	3.7	3.1	0	19.7
7770	12.0	0.6	15.7	5.3	11.7	0	1.7	0	2.8	2.1	3.5	10.8	3.3	0	30.6
7860	12.7	3.2	13.0	4.1	7.5	0	1.0	0	6.7	9.0	0	9.0	1.7	0	31.9
7920	15.4	3.6	14.7	4.7	8.8	0	0	0	5.1	0	1.0	7.7	1.3	0	37.7
7980	13.0	1.6	15.4	6.4	9.1	0	0	0	2.0	2.5	1.7	7.4	2.5	0	38.4
8040	13.7	0	14.0	0.5	13.5	0	1.9	0	2.5	10.6	0	1.1	1.5	0	40.6
8070	16.3	0	14.1	0	12.2	0	0	0	1.6	4.8	0.7	2.9	1.4	0	46.1

TABLE 3. Semi-quantitative Mineralogical Abundances Measured by XRD, in % by Weight for Inglewood well C, *Derived from FTIR analyses

Depth	Quartz	Opal-CT	Plagio-clase	Ortho-clase	Musco-vite	Chlorite	Calcite	Dolo-mite	Carbonate-fluorapatite	Hydroxy-apatite	Pyrite	Barite	Clay*
7220	4.6	0.7	13.8	4.2	8.9	1.7	6.7	1.3	2.7	2.1	1.6	0.8	50.9
7310	4.2	0.2	3.3	1.3	1.9	0	1.9	0.7	0.5	0.2	0.5	0.3	85.0
7400	5.2	3.5	14.6	4.6	9.0	0	8.6	1.6	2.6	1.2	1.7	0.9	46.6
7490	10.5	1.9	18.8	6.0	14.0	2.0	1.5	1.7	1.0	1.7	2.5	0.6	37.6
7580	8.8	1.0	22.3	6.9	14.8	2.7	4.8	3.8	5.6	2.9	3.2	1.2	21.9
7640	9.2	1.1	28.3	7.7	15.6	2.8	5.0	13.2	5.2	2.4	3.0	1.4	5.0
7670	10.2	1.1	26.9	8.1	14.8	3.7	3.7	2.7	4.7	2.2	3.5	1.5	16.8
7760	10.4	1.1	23.6	7.4	11.0	3.1	2.7	2.4	3.7	3.4	2.9	1.3	27.0
7820	8.7	1.0	22.7	7.2	12.6	2.8	5.9	2.5	4.5	2.2	3.0	1.2	25.7
7850	2.9	0.5	11.6	3.3	6.5	1.8	6.5	1.0	2.3	1.2	1.0	0.7	60.9
7970	10.8	0.9	27.6	8.5	15.0	3.7	4.9	2.5	4.2	3.4	2.8	1.2	14.4
8040	3.5	0.5	9.9	3.1	5.7	1.4	1.4	1.5	2.2	2.1	1.2	0.5	66.8
8080	1.8	0.5	15.1	4.1	8.7	2.5	20.9	2.2	4.3	3.6	1.1	0.9	34.2
8120	4.2	0.1	11.6	3.7	6.0	1.6	0.7	1.1	2.0	7.3	1.4	0.8	59.4
8160	3.7	0.5	8.9	4.0	5.3	1.0	2.5	35.0	2.4	1.8	1.6	1.0	32.3
8200	6.6	0.3	7.9	2.7	5.1	0.6	0.9	1.4	2.9	2.1	1.4	0.5	67.5
8280	7.2	0.7	3.3	1.5	2.1	0.1	3.1	0.6	1.1	0.1	0.4	0.3	79.6
8300	6.9	1.1	4.9	2.4	2.6	1.2	6.6	1.9	3.2	5.6	1.1	0.8	61.9
8320	5.0	0.1	4.3	1.6	3.5	0.7	1.2	1.0	1.3	0.6	1.0	0.4	79.3
8340	5.5	0.3	7.0	2.1	4.6	1.3	1.3	0.8	1.6	0.4	1.0	0.5	73.4

TABLE 4. Semi-quantitative Mineralogical Abundances Measured by XRD, in % by Weight for Wilmington well D, *Derived from FTIR analyses

Depth	Quartz	Opal-CT	Plagio-clase	Ortho-clase	Musco-vite	Biotite	Chlorite	Calcite	Dolo-mite	Carbonate-fluorapatite	Hydroxy-apatite	Pyrite	Barite	Clay*
9120	9.8	0.4	18.7	5.2	9.7	2.7	0	1.7	5.6	2.8	0.2	3.4	1.2	38.6
9240	21.1	0.9	26.9	8.5	13.3	3.2	0	2.2	11.2	5.1	0.1	5.2	2.2	0
9360	10.9	0.6	19.2	5.2	11.7	3.0	0	1.2	2.8	3.1	0.1	3.2	1.4	37.5
9570	14.3	0.6	14.4	4.6	11.3	0	1.1	4.9	3.9	3.5	0.0	3.2	1.3	36.7
9610	15.3	2.4	22.7	8.2	18.7	0	5.6	7.9	4.3	5.0	3.7	4.2	2.1	0
9700	20.2	0.7	17.5	5.5	11.3	0	0.9	2.9	3.8	3.2	0.7	3.8	1.4	28.2
9750	2.8	7.1	33.3	14.6	9.0	0	2.7	3.6	5.5	10.0	0.4	2.4	4.8	3.9
9800	28.6	0.0	11.2	5.5	4.8	0	0	1.5	1.0	2.7	5.7	0	1.8	37.2
9890	20.9	0.5	16.4	5.6	10.5	0	0	3.0	7.3	3.6	1.4	3.6	1.3	25.7
10000	25.1	0.5	17.1	6.7	11.8	0	0	3.4	3.4	3.9	1.5	3.1	1.6	21.7
10100	28.0	0.9	13.0	5.9	7.9	0	1.0	4.8	6.9	3.1	1.5	2.6	1.3	23.1
10210	40.3	3.0	9.3	5.3	4.1	0	0	3.9	2.8	1.9	1.0	1.6	1.3	25.4
10310	22.0	0.4	13.7	4.7	8.7	0	1.1	1.8	12.7	3.5	1.1	2.3	1.0	26.9
10370	25.1	0.6	14.4	4.4	7.0	1.3	0	1.8	18.1	2.9	2.1	2.1	1.1	19.1
10560	23.7	0.6	16.9	5.1	10.2	0	0.7	3.3	4.5	3.7	0.7	2.2	1.3	27.0
10660	23.3	2.5	15.5	5.5	10.2	0	1.5	4.7	3.2	3.2	1.7	2.7	1.3	24.8
10750	24.2	0.5	15.7	5.6	11.2	0	1.2	3.5	3.3	3.2	1.3	2.8	1.4	26.2

TABLE 5. Semi-quantitative Mineralogical Abundances Measured by XRD, in % by Weight for Wilmington well E, *Derived from FTIR analyses

Depth	Quartz	Opal-CT	Plagio-clase	Ortho-clase	Musco-vite	Biotite	Chlorite	Calcite	Dolo-mite	Carbonate-fluorapatite	Hydroxy-apatite	Pyrite	Barite	Clay*
9150	16.6	1.9	14.9	5.4	8.3	0	1.6	16.2	2.3	3.4	4.8	3.6	1.4	19.6
9210	20.4	1.6	15.1	5.5	9.5	2.0	0.7	2.0	1.4	2.7	1.7	3.8	1.5	32.0
9270	20.7	1.1	18.2	6.3	9.8	2.1	0	4.1	2.8	3.4	2.2	4.0	1.6	23.7
9330	26.1	1.2	8.5	4.9	3.9	1.1	0	5.4	2.9	1.7	1.8	2.2	1.2	39.0
9360	37.0	0.9	12.2	5.8	8.6	0	0.4	1.9	3.7	2.1	2.1	3.6	1.2	20.5
9380	35.8	2.1	12.8	6.3	6.9	1.4	1.0	2.8	2.3	2.2	1.4	3.6	1.4	19.9
9440	25.2	1.2	17.8	7.2	10.8	2.5	1.3	3.3	4.3	3.5	1.7	3.9	1.6	15.8
9500	27.5	3.3	13.9	6.4	8.0	2.4	0.9	5.1	2.4	3.3	0.2	2.7	1.6	22.4
9560	18.9	1.9	19.3	6.2	12.9	3.1	1.5	6.5	5.3	4.5	0	4.3	1.8	13.9
9620	26.6	0.4	11.1	4.4	6.7	1.0	1.0	1.6	16.9	1.6	0.3	1.9	1.0	25.4
9680	27.6	0.5	13.3	5.4	6.7	1.5	0.7	2.9	1.7	2.6	0.1	2.5	1.1	33.5
9700	21.3	0.7	13.5	6.8	8.7	1.5	1.2	2.6	13.8	4.9	3.5	3.0	1.2	17.5
9760	36.1	2.9	13.2	5.2	6.7	1.7	1.1	1.1	1.3	2.4	0.3	3.1	1.4	23.4
9820	29.1	1.0	14.4	5.3	8.4	1.7	1.2	7.4	1.9	2.8	0.6	2.4	1.2	22.6
9860	28.4	0.9	14.7	5.1	7.7	1.7	0.9	4.7	3.0	3.0	1.5	2.2	1.3	24.9
9980	8.7	2.0	25.1	15.1	13.7	2.6	2.6	3.0	3.9	6.2	3.6	4.0	3.0	6.4
10040	9.2	0.2	10.6	3.4	6.5	1.3	0.6	1.9	6.3	2.4	1.9	1.4	0.7	53.5
10060	19.5	1.2	15.5	5.3	8.2	1.8	1.1	4.1	2.3	2.6	1.7	2.3	1.1	33.1
10160	23.9	1.0	14.5	5.3	8.5	1.7	1.1	3.2	2.9	3.1	1.5	2.2	1.4	29.9
10280	24.3	0.1	16.5	6.1	10.3	2.7	1.0	3.6	2.0	3.7	1.3	2.7	1.4	24.2
10320	22.2	2.2	16.9	5.9	11.0	3.0	0.9	3.1	2.6	3.3	1.4	2.9	1.4	23.1

APPENDIX B

FOURIER TRANSFORM INFRARED DATA TABLES

TABLE 6. Mineralogical Abundances Measured by FTIR, in % by Weight for East Beverly Hills Well A

Depth	Quartz	Calcite	Dolomite	Barite	Illite	Montmorillonite
9430	8.8	9.4	5.6	5.1	14.7	7.9
9520	10.8	6.0	2.4	0.3	11.7	17.0
9670	16.0	7.9	4.6	5.9	14.3	7.5
9760	13.7	8.4	6.5	4.8	13.4	8.4
9820	10.6	4.9	3.9	0.0	11.1	17.6
9910	8.7	9.6	5.8	5.4	15.1	7.5
9970	11.1	13.8	9.8	10.2	17.7	3.3
10020	14.4	9.4	6.1	6.4	16.7	8.1
10050	13.6	7.3	5.0	4.0	15.3	10.7
10070	22.3	9.4	7.7	7.5	14.4	7.9
10080	20.1	6.8	5.8	4.0	13.5	8.7
10100	12.3	11.6	7.0	7.6	16.6	5.0

TABLE 7. Mineralogical Abundances Measured by FTIR, in % by Weight for West Beverly Hills Well B

Depth	Quartz	Calcite	Dolomite	Barite	Illite	Montmorillonite
3510	13.4	1.9	1.6	0	11.7	23.3
3540	5.3	5.6	0.9	0	4.0	24.4
3690	9.4	10.0	4.9	4.1	0	24.2
4110	15.2	11.2	7.4	10.7	0	25.5
4230	6.0	20.0	11.7	0	0	16.4
4320	8.6	14.9	7.4	5.3	3.0	16.6
4440	9.9	13.4	6.8	8.5	2.8	11.8
4530	14.5	10.4	3.4	7.4	4.9	17.9
4650	18.2	9.7	2.2	10.9	7.9	12.7
4710	15.3	9.8	1.6	9.3	8.3	19.5
4830	15.4	11.4	4.6	8.5	4.4	17.9
4920	10.4	7.7	2.2	2.4	8.4	24.7
5040	6.6	6.5	2.2	3.3	14.8	27.8
5160	8.2	5.8	1.4	1.3	6.2	21.7
5250	5.3	17.0	8.2	0	0	19.7
5370	6.3	8.1	2.5	2.8	4.8	18.5
5460	5.1	0.7	0	0	6.9	34.1
5580	6.9	6.1	2.3	2.3	14.2	28.7
5670	3.7	7.7	1.8	0	8.0	28.8
5880	3.3	19.7	12.5	0	0	19.8
6000	3.7	13.2	6.2	7.0	10.2	15.4
6210	4.8	15.1	6.5	5.2	6.1	16.4
6270	5.9	7.0	3.4	0.0	5.8	26.1
6420	15.8	7.8	1.5	5.7	5.7	20.2
6450	12.2	8.3	2.3	3.9	6.5	24.8
6540	19.6	8.6	2.4	6.1	5.8	23.0
6600	11.7	7.4	1.4	4.3	10.3	23.9
6690	9.8	10.0	5.6	1.7	3.3	19.2
6750	9.0	8.1	3.4	4.6	5.9	17.5
6780	9.1	12.7	6.5	3.7	1.3	15.7
6870	10.5	14.5	8.1	7.2	4.5	11.1
6960	10.5	14.5	8.1	7.2	4.5	11.1
7020	13.8	10.1	5.5	7.2	7.2	11.0
7080	19.1	8.4	2.9	9.0	8.9	12.5
7140	17.2	7.3	2.1	6.9	8.6	15.3
7200	11.7	12.6	6.9	1.4	0	15.1
7260	15.9	10.7	7.2	8.4	8.0	9.5
7290	19.0	6.9	1.5	0	0.0	24.6
7770	10.4	8.9	2.1	0	3.2	23.4
7860	10.8	6.4	4.0	0	6.6	20.3
7920	14.6	2.2	0	0	8.2	27.5
7980	11.2	3.1	0.9	0	9.8	23.3
8040	11.2	4.1	0.2	0	8.3	24.9
8070	10.8	5.6	1.8	0	9.0	21.7

TABLE 8. Mineralogical Abundances Measured by FTIR, in % by Weight for Inglewood Well C

Depth	Quartz	Calcite	Dolomite	Barite	Illite	Montmorillonite
7220	2.6	0.8	3.3	0	6.8	21.9
7310	1.0	24.1	8.6	7.3	12.6	7.8
7400	5.0	0	0	0	14.8	30.3
7490	4.1	20.1	18.3	0	0	17.1
7580	13.8	1.9	0	0	15.7	18.5
7640	23.1	14.4	7.2	6.6	13.0	0
7670	15.2	13.4	2.7	0.7	10.5	14.5
7760	15.0	4.8	0	0	15.8	22.9
7820	11.2	3.8	0	0.3	14.5	18.6
7850	1.9	7.4	3.6	0.9	19.4	20.3
7970	18.9	4.9	4.7	1.6	9.9	15.3
8040	2.2	10.1	5.1	3.6	22.6	19.7
8080	2.2	10.1	5.1	3.6	22.6	19.7
8120	2.9	5.7	2.8	0	11.6	30.1
8160	3.5	6.3	4.8	0	10.6	19.9
8200	3.5	2.1	1.4	0	12.7	23.4
8280	3.0	7.1	2.8	0	16.1	17.0
8300	4.0	3.2	0.2	0	14.0	22.0
8320	2.1	5.8	5.2	3.3	18.2	14.7
8340	2.8	2.5	1.2	0	15.6	21.2

TABLE 9. Mineralogical Abundances Measured by FTIR, in % by Weight for Wilmington Well D

Depth	Quartz	Clacite	Dolomite	Barite	Illite	Montmorillonite
9120	9.0	2.6	0.6	0	9.2	26.4
9360	9.9	4.5	0.4	1.8	18.3	15.9
9570	14.8	5.2	4.1	2.0	21.9	16.3
9700	25.2	2.1	0.6	0	23.1	12.2
9750	23.7	0.0	0	0	23.8	9.1
9800	26.2	3.2	0.8	0	18.3	15.8
9890	16.8	5.9	4.0	4.0	17.6	3.0
10000	27.6	3.2	4.3	3.7	21.3	2.6
10100	27.9	5.8	7.5	11.0	23.9	0
10210	30.6	7.3	6.2	7.1	12.8	6.5
10310	22.0	6.6	5.5	2.6	15.5	11.4
10370	23.4	8.1	7.7	5.1	14.6	3.2
10560	26.4	3.3	7.9	9.0	29.1	0.9
10660	28.2	2.5	4.8	2.7	21.9	8.2
10750	27.3	3.6	6.5	6.4	24.7	4.8

TABLE 10. Mineralogical Abundances Measured by FTIR, in % by Weight for Wilmington Well E

Depth	Quartz	Calcite	Dolomite	Barite	Illite	Montmorillonite
9150	29.8	0.4	2.9	0	21.6	13.7
9210	19.0	11.5	9.4	11.3	26.5	3.2
9270	26.7	2.0	0.6	0	13.8	16.8
9330	23.5	2.5	4.0	0.7	24.4	10.7
9360	29.7	6.2	8.1	9.7	16.8	0.0
9380	43.7	0.9	3.4	0	8.1	16.2
9440	28.3	4.8	4.3	6.0	15.8	2.0
9500	29.9	2.5	2.8	0.5	17.5	6.9
9560	29.9	4.0	5.2	4.5	17.7	4.4
9620	24.2	5.4	6.0	7.0	18.4	4.6
9680	21.2	6.8	5.5	2.9	13.5	12.3
9700	29.9	3.1	3.5	1.0	14.3	10.3
9760	22.9	4.9	7.5	2.7	11.3	3.6
9820	30.7	2.4	2.0	0	13.8	10.0
9860	37.3	3.2	8.1	5.7	21.5	11.2
9980	41.8	2.0	7.8	5.9	21.3	9.5
10040	11.2	0	0	0	40.0	24.9
10060	21.2	3.4	4.5	0	18.1	17.8
10160	23.9	2.5	5.9	5.4	23.0	7.0
10280	33.3	1.3	4.9	4.2	23.6	9.6
10320	31.5	2.0	3.7	0	18.7	14.0

APPENDIX C

X-RAY FLUORESENCE DATA TABLES

TABLE 11. Major Oxides Measured by XRF, in % by Weight for East Beverly Hills Well A

Depth	Al_2O_3	CaO	Cr_2O_3	Fe_2O_3	K_2O	MgO	MnO	Na_2O	P_2O_5	SiO_2	TiO_2
9430	14.8	7.8	0.1	6.8	2.7	3.1	0.1	2.6	0.5	60.8	0.9
9520	12.0	11.1	0.1	5.4	2.1	1.9	0.1	2.0	0.6	64.0	0.7
9670	13.0	11.3	0.1	5.8	2.4	2.2	0.1	2.5	0.5	61.2	0.8
9760	14.2	9.6	0.0	6.3	2.6	2.6	0.1	2.6	0.5	60.6	0.8
9820	13.2	13.4	0.0	6.4	2.4	3.0	0.1	2.3	0.6	57.7	0.8
9910	11.3	21.1	0.1	5.4	2.0	2.4	0.1	2.1	0.7	54.3	0.6
9970	11.2	18.2	0.1	5.4	2.0	1.9	0.1	1.9	1.0	57.5	0.7
10020	11.9	15.1	0.1	5.5	2.2	2.0	0.1	2.1	0.8	59.5	0.7
10050	9.7	18.2	0.1	4.4	1.7	1.7	0.1	1.7	1.0	60.9	0.6
10070	12.3	13.7	0.1	5.3	2.2	2.2	0.1	2.3	0.7	60.3	0.7
10080	11.1	18.9	0.1	4.9	2.0	2.0	0.1	2.0	1.0	57.2	0.6
10100	12.2	14.2	0.1	5.5	2.2	3.7	0.1	2.3	0.6	58.3	0.7

TABLE 12. Major Oxides Measured by XRF, in % Weight for West Beverly Hills Well B

Depth	Al_2O_3	CaO	Cr_2O_3	Fe_2O_3	K_2O	MgO	MnO	Na_2O	P_2O_5	SiO_2	TiO_2
3510	14.3	12.3	0.1	6.3	2.5	7.5	0.1	2.3	0.8	53.1	0.8
3540	12.7	13.6	0	6.0	2.2	4.0	0.1	2.1	1.0	57.7	0.7
3690	10.6	17.5	0	4.8	2.0	4.7	0.1	2.2	0.4	56.9	0.6
4110	7.3	32.0	0	6.0	1.3	18.6	0.2	1.7	0.4	32.1	0.4
4230	10.2	21.6	0	6.1	2.0	8.7	0.1	1.9	0.4	48.4	0.6
4320	7.8	23.5	0	5.1	1.4	9.7	0.1	1.4	0.5	50.2	0.5
4440	9.1	12.0	0	4.4	1.6	3.1	0.1	1.7	0.4	67.0	0.5
4530	9.6	8.2	0	3.8	1.8	1.8	0	1.9	0.3	71.9	0.5
4650	11.6	10.3	0	5.0	2.0	2.3	0.1	2.4	0.6	65.2	0.6
4710	6.6	17.9	0.1	3.8	1.1	4.6	0.1	1.2	0.9	63.4	0.4
4830	12.5	13.8	0	5.9	2.1	4.9	0.1	2.4	0.5	57.1	0.7
4920	14.4	10.7	0	6.6	2.6	3.5	0.1	2.5	0.5	58.2	0.8
5160	10.8	21.6	0	6.9	1.9	8.4	0.2	2.1	0.5	46.9	0.7
5250	14.9	8.0	0	6.7	2.6	4.1	0.1	2.8	0.4	59.6	0.8
5370	15.6	6.4	0	6.7	2.7	3.1	0.1	2.7	0.5	61.3	0.9
5460	15.3	7.7	0	6.9	2.7	3.9	0.1	2.7	0.4	59.4	0.9
5580	15.5	9.1	0	7.3	2.7	3.6	0.1	2.7	0.4	57.8	0.8
5670	12.9	19.7	0	6.4	2.2	6.9	0.1	2.1	0.5	48.4	0.7
5880	13.5	18.3	0.1	6.2	2.2	3.9	0.1	2.2	0.5	52.1	0.7
6000	12.7	18.3	0	6.1	2.1	4.6	0.1	2.3	0.5	52.5	0.7
6210	13.9	12.0	0.1	7.1	2.3	5.0	0.1	2.5	0.5	55.7	0.8
6270	10.9	7.3	0	5.2	1.9	3.2	0.1	1.9	0.4	68.5	0.6
6420	12.7	9.8	0	5.7	2.1	3.0	0.1	2.2	0.5	63.1	0.7
6450	10.4	10.9	0	5.2	1.8	2.8	0.1	2.0	0.6	65.7	0.6
6540	12.6	11.4	0.2	6.0	2.1	2.5	0.1	2.2	0.6	61.6	0.7
6600	11.7	15.6	0	6.6	2.1	6.6	0.1	2.0	0.4	54.2	0.7
6690	13.0	11.9	0	5.6	2.3	2.9	0.1	2.4	0.5	60.4	0.7
6750	10.8	18.6	0	5.7	1.9	8.7	0.1	2.1	0.6	50.9	0.6
6780	10.5	20.0	0	5.0	2.0	5.3	0.1	1.9	0.6	54.0	0.6
6870	12.4	6.2	0	5.3	2.3	2.2	0.1	2.4	0.4	67.9	0.7
6960	10.9	12.5	0	5.2	2.0	4.7	0.1	2.1	0.5	61.4	0.6
7020	9.5	10.6	0	4.3	1.8	2.6	0	1.8	0.3	68.4	0.5
7080	10.3	11.6	0	4.5	1.7	1.7	0	1.7	0.6	67.2	0.5
7140	10.4	17.6	0.1	5.7	1.7	6.5	0.1	1.6	0.9	54.7	0.6
7200	9.6	18.6	0	4.9	1.6	3.4	0.1	1.5	0.8	58.8	0.6
7260	11.1	10.4	0	4.9	1.8	2.2	0	1.7	1.3	65.7	0.6
7290	12.5	14.8	0	5.5	2.1	2.7	0.1	1.8	1.8	58.0	0.7
7770	13.8	8.0	0	6.4	2.4	3.3	0.1	2.0	0.5	62.6	0.8
7920	14.2	6.9	0	6.4	2.5	2.7	0.1	2.2	0.6	63.5	0.8
7980	15.1	6.7	0	6.5	2.6	2.7	0.1	2.2	0.6	62.8	0.8
8040	14.2	7.7	0	6.5	2.5	4.1	0.1	2.0	0.3	61.6	0.8
8070	13.9	7.1	0	6.4	2.5	3.9	0.1	2.0	0.4	62.9	0.8

TABLE 13. Major Oxides Measured by XRF, in % by Weight for Inglewood Well C

Depth	Al_2O_3	CaO	Cr_2O_3	Fe_2O_3	K_2O	MgO	MnO	Na_2O	P_2O_5	SiO_2	TiO_2
7220	15.6	10.8	0.1	8.0	2.9	3.0	0.1	2.5	0.3	55.8	0.9
7310	11.5	7.9	0	5.1	2.0	2.2	0.1	2.1	0.3	68.1	0.7
7400	15.0	14.3	0	7.3	2.7	2.7	0.1	2.3	0.3	54.3	0.9
7490	17.7	2.9	0	8.2	3.2	2.9	0.1	2.5	0.3	61.3	1.0
7580	15.4	7.8	0	9.3	2.8	4.4	0.1	2.4	0.4	56.4	0.9
7640	14.0	14.1	0	7.2	2.4	8.8	0.1	2.3	0.4	49.8	0.8
7670	16.7	5.6	0.1	7.7	3.1	3.4	0.1	2.7	0.3	59.5	0.9
7760	15.3	11.4	0	7.2	2.7	3.0	0.1	2.6	0.5	56.2	0.9
7820	16.7	4.4	0	7.1	2.9	3.0	0.1	3.1	0.3	61.5	0.9
7850	15.7	11.3	0	7.1	2.8	2.9	0.1	2.6	0.4	56.2	0.9
7970	16.0	7.3	0	7.6	2.9	3.1	0.1	3.0	0.3	58.8	0.9
8040	16.2	4.9	0	8.0	3.0	3.8	0.1	2.9	0.3	59.8	0.9
8080	9.6	36.2	0.1	8.3	1.7	3.5	0.3	1.5	0.3	37.7	0.6
8120	17.5	2.1	0	7.7	3.2	2.6	0.1	2.7	0.3	62.7	0.9
8160	7.5	37.9	0	3.8	1.2	18.6	0.2	1.1	0.6	28.5	0.6
8200	12.1	17.9	0	4.9	1.8	2.9	0	1.8	5.4	52.4	0.7
8280	7.3	22.3	0.2	3.6	1.3	1.5	0.1	1.1	1.9	60.0	0.5
8300	8.9	26.4	0.1	4.7	1.2	2.6	0	1.0	4.3	50.0	0.7
8320	13.2	12.6	0.1	6.4	2.0	2.9	0.1	1.6	2.0	58.2	0.8

TABLE 14. Major Oxides Measured by XRF, in % by Weight for Wilmington Well D

Depth	Al_2O_3	CaO	Cr_2O_3	Fe_2O_3	K_2O	MgO	MnO	Na_2O	P_2O_5	SiO_2	TiO_2
9240	14.4	6.0	0.1	6.2	3.6	5.0	0.1	1.6	0.9	61.4	0.8
9360	16.6	3.2	0.1	6.8	4.1	3.6	0.1	1.9	0.5	62.2	0.9
9700	13.0	6.0	0.1	6.3	2.7	2.2	0	1.5	0.7	66.7	0.8
9750	14.0	3.9	0.2	6.3	2.8	2.1	0.1	1.7	0.5	67.6	0.7
9800	12.7	4.7	0.1	5.7	2.6	2.4	0	1.6	0.4	69.1	0.7
9890	11.1	8.4	0.1	6.2	2.3	3.3	0.1	1.3	0.5	66.0	0.6
10000	10.1	6.6	0.1	5.6	2.0	1.7	0	1.1	0.4	71.6	0.6
10100	8.1	11.0	0	4.4	1.6	2.3	0	1.1	0.5	70.4	0.5
10210	4.4	7.5	0.1	2.6	0.8	1.1	0	0.6	0.3	82.2	0.3
10310	10.5	8.5	0.3	5.7	2.1	5.2	0.1	1.2	0.3	65.4	0.7
10370	8.3	12.1	0.1	4.7	1.6	6.8	0.1	1.2	0.3	64.4	0.5
10560	11.2	8.0	0.1	5.4	2.1	2.5	0.1	1.5	0.4	68.1	0.7
10660	10.9	8.2	0.3	5.7	2.2	2.2	0.1	1.3	0.4	68.0	0.6
10750	11.0	6.6	0.2	5.6	2.2	2.5	0.1	1.4	0.4	69.3	0.7

TABLE 15. Major Oxides Measured by XRF, in % by Weight for Wilmington Well E

Depth	Al_2O_3	CaO	Cr_2O_3	Fe_2O_3	K_2O	MgO	MnO	Na_2O	P_2O_5	SiO_2	TiO_2
9150	10.0	21.4	0.1	5.1	2.2	2.4	0	1.2	1.3	55.5	0.6
9210	12.0	5.1	0.1	6.2	2.6	1.7	0	1.5	0.7	69.4	0.8
9270	12.4	8.4	0.1	5.6	2.6	1.8	0	1.7	0.9	65.7	0.7
9330	6.3	13.3	0	3.1	1.3	1.5	0	0.7	0.5	72.7	0.4
9360	8.8	3.9	0.1	4.8	1.9	1.7	0	0.9	0.3	77.0	0.6
9380	8.2	4.6	0.1	4.3	1.6	1.3	0	1.0	0.3	78.1	0.5
9440	11.1	6.3	0.1	5.6	2.3	2.0	0	1.3	0.5	70.1	0.7
9500	9.3	8.0	0.1	5.0	1.9	1.6	0	1.1	0.4	72.0	0.6
9560	9.9	8.5	0.1	4.4	2.0	1.5	0	1.2	0.4	71.6	0.5
9620	11.1	8.5	0	3.2	2.0	4.5	0	0.7	0.4	69.0	0.4
9680	10.4	4.9	0	4.3	2.0	1.4	0	1.2	0.3	74.8	0.6
9700	9.5	12.4	0.1	8.2	1.9	5.3	0.2	1.1	0.4	60.3	0.6
9760	9.7	1.6	0.1	4.2	1.7	1.2	0	1.2	0.3	79.4	0.6
9820	10.1	9.8	0	4.6	2.0	1.8	0.1	1.2	0.4	69.4	0.7
9860	10.5	7.5	0.1	5.1	1.9	2.0	0	1.3	0.3	70.6	0.6
9980	18.9	2.9	0.1	7.3	3.7	2.5	0.1	1.9	0.5	60.8	1.1
10060	12.7	7.3	0	5.4	2.5	2.7	0.1	1.4	0.4	66.7	0.7
10160	11.1	5.5	0.1	5.8	2.2	2.3	0.1	1.2	0.3	70.8	0.7
10280	12.0	5.1	0.1	5.6	2.3	2.0	0.1	1.5	0.3	70.3	0.8
10320	12.9	5.4	0	5.8	2.6	2.3	0	1.6	0.4	68.2	0.8

APPENDIX D

CALCULATED SEDIEMENTARY COMPONENTS

TABLE 16. Sedimentary Components, after Isaacs' Corrections, in % by Weight for East Beverly Hills Well A

Depth	Detritus	Aluminosilicates	Detrital Quartz	Silica	Apatite	Dolomite	Calcite	Total
9430	82.7	62.0	20.7	9.1	0	6.7	15.4	113.9
9520	67.5	50.6	16.9	21.8	0.6	2.5	20.0	112.3
9670	73.1	54.8	18.3	15.5	0.3	3.7	20.7	113.3
9760	79.3	59.5	19.8	11.0	0.2	4.9	17.9	113.4
9820	73.9	55.4	18.5	11.5	0.5	7.2	26.4	119.5
9910	63.1	47.3	15.8	14.9	0.9	5.1	39.7	123.7
9970	62.9	47.2	15.7	18.2	1.4	3.2	34.0	119.8
10020	66.9	50.1	16.7	17.8	1.1	3.2	28.0	116.9
10050	54.5	40.9	13.6	26.8	1.7	3.0	34.3	120.4
10070	68.7	51.5	17.2	17.4	0.8	3.9	25.6	116.5
10080	62.0	46.5	15.5	18.4	1.6	3.5	35.7	121.2
10100	68.3	51.3	17.1	15.6	0.6	10.9	30.1	125.5

TABLE 17. Sedimentary Components, after Isaacs' Corrections, in % by Weight for West Beverly Hills Well B

Depth	Detritus	Aluminosilicates	Detrital Quartz	Silica	Apatite	Dolomite	Calcite	Total
3510	79.9	59.9	20.0	3.1	0.8	26.9	35.3	146.0
3540	71.1	53.3	17.8	13.2	1.4	11.8	30.3	127.8
3690	59.6	44.7	14.9	19.7	0.2	16.2	38.7	134.4
4110	40.7	30.6	10.2	6.7	0.3	81.1	100.5	229.3
4230	57.0	42.8	14.3	12.8	0.1	34.4	56.0	160.3
4320	43.4	32.6	10.9	23.0	0.5	40.3	63.2	170.5
4440	51.2	38.4	12.8	35.0	0.2	9.5	25.6	121.4
4530	53.6	40.2	13.4	38.4	0.1	3.4	15.2	110.6
4650	65.1	48.9	16.3	24.4	0.4	4.5	19.6	114.2
4710	37.0	27.7	9.2	40.3	1.5	17.5	42.0	138.4
4830	69.9	52.4	17.5	13.4	0.3	16.1	31.8	131.5
4920	80.6	60.5	20.2	7.8	0.2	8.9	22.1	119.6
5160	60.7	45.5	15.2	9.0	0.3	33.0	55.2	158.2
5250	83.4	62.5	20.8	7.5	-0.2	11.2	18.0	119.8
5370	87.4	65.6	21.9	6.7	0.0	6.4	12.6	113.1
5460	85.7	64.3	21.4	5.9	-0.1	10.1	16.9	118.4
5580	86.7	65.0	21.7	3.6	-0.2	8.6	18.6	117.3
5670	72.1	54.0	18.0	3.4	0.3	25.1	47.3	148.1
5880	75.7	56.8	18.9	4.8	0.3	11.1	37.0	128.9
6000	71.0	53.3	17.8	8.1	0.1	14.8	39.1	133.2
6210	77.7	58.3	19.4	7.2	0.0	15.8	28.0	128.7
6270	61.1	45.8	15.3	30.3	0.2	9.2	16.7	117.5
6420	71.2	53.4	17.8	18.6	0.1	7.3	19.7	117.0
6450	58.3	43.7	14.6	29.3	0.6	7.4	22.6	118.1

TABLE 17. Continued

Depth	Detritus	Aluminosilicates	Detrital Quartz	Silica	Apatite	Dolomite	Calcite	Total
6600	65.6	49.2	16.4	13.2	0.2	24.2	39.4	142.5
6690	73.1	54.8	18.3	14.7	0.2	6.8	23.3	118.1
6750	60.7	45.5	15.2	13.0	0.6	34.1	50.8	159.1
6780	58.9	44.2	14.7	17.2	0.6	18.7	45.1	140.5
6870	69.7	52.3	17.4	24.3	0.1	4.0	11.5	109.6
6960	60.8	45.6	15.2	23.4	0.3	16.2	29.9	130.6
7020	53.4	40.1	13.4	35.0	0.0	7.1	21.4	117.0
7080	57.5	43.1	14.4	31.3	0.6	2.8	21.4	113.5
7140	58.3	43.7	14.6	18.3	1.2	24.5	44.5	146.9
7200	53.6	40.2	13.4	25.3	1.2	10.7	38.9	129.7
7260	62.4	46.8	15.6	26.7	2.1	4.6	21.5	117.4
7290	69.8	52.4	17.5	14.4	3.3	6.3	31.2	125.0
7770	77.2	57.9	19.3	14.4	0.2	8.2	17.0	116.9
7920	79.8	59.8	19.9	13.6	0.4	5.4	13.6	112.7
7980	84.5	63.3	21.1	10.0	0.4	4.7	12.6	112.1
8040	79.4	59.5	19.8	12.0	-0.3	11.5	17.8	120.4
8070	77.8	58.4	19.5	14.2	0.0	10.8	16.5	119.3

TABLE 18. Sedimentary Components, after Isaacs' Corrections, in % by Weight for Inglewood Well C

Depth	Detritus	Aluminosilicates	Detrital Quartz	Silica	Apatite	Dolomite	Calcite	Total
7220	87.5	65.6	21.9	1.1	-0.5	6.0	19.8	113.9
7310	64.4	48.3	16.1	27.9	-0.1	4.3	14.6	111.0
7400	84.2	63.2	21.1	1.7	-0.4	5.0	25.6	116.1
7490	98.9	74.2	24.7	-0.5	-0.7	4.3	4.3	106.4
7580	86.3	64.7	21.6	2.5	-0.2	12.3	18.1	119.1
7640	78.6	58.9	19.6	0.7	-0.2	33.3	41.0	153.4
7670	93.3	70.0	23.3	1.2	-0.5	7.2	11.0	112.2
7760	85.7	64.3	21.4	2.6	0.0	5.9	21.4	115.6
7820	93.4	70.0	23.3	3.1	-0.6	5.4	7.8	109.1
7850	87.7	65.8	21.9	1.4	-0.3	5.6	20.6	115.0
7970	89.5	67.2	22.4	2.8	-0.5	6.2	13.6	111.7
8040	90.9	68.2	22.7	3.0	-0.6	9.1	10.9	113.3
8080	54.0	40.5	13.5	4.0	0.1	11.3	69.5	138.8
8120	98.2	73.6	24.5	1.4	-0.5	3.2	2.5	104.8
8160	41.9	31.4	10.5	2.3	0.9	81.2	111.6	237.9
8200	68.0	51.0	17.0	9.9	11.9	7.0	45.8	142.6
8280	40.8	30.6	10.2	34.5	4.0	3.1	44.4	126.9
8300	49.6	37.2	12.4	19.0	9.5	7.5	59.3	145.0
8320	73.8	55.3	18.4	12.1	3.8	6.8	28.1	124.5

TABLE 19. Sedimentary Components, after Isaacs' Corrections, in % by Weight for Wilmington Well D

Depth	Detritus	Aluminosilicates	Detrital Quartz	Silica	Apatite	Dolomite	Calcite	Total
9240	80.5	60.4	20.1	11.1	1.0	15.5	18.1	126.2
9360	92.8	69.6	23.2	4.2	-0.1	8.3	7.7	113.0
9700	72.6	54.4	18.1	21.3	0.6	3.7	11.5	109.8
9750	78.5	58.9	19.6	18.6	0.1	2.5	6.3	106.0
9800	70.9	53.2	17.7	24.9	0.1	4.6	9.2	109.5
9890	62.0	46.5	15.5	27.3	0.3	9.3	18.9	117.8
10000	56.4	42.3	14.1	36.4	0.2	2.7	12.0	107.6
10100	45.5	34.1	11.4	42.0	0.5	6.3	22.4	116.6
10210	24.8	18.6	6.2	66.7	0.3	2.7	14.6	109.0
10310	58.6	44.0	14.7	28.8	-0.1	18.7	23.7	129.6
10370	46.7	35.0	11.7	35.2	0.1	26.8	35.0	143.9
10560	62.5	46.9	15.6	29.0	0	5.8	15.8	113.1
10660	61.2	45.9	15.3	29.7	0.1	4.5	15.7	111.2
10750	61.4	46.1	15.4	30.9	0.1	6.1	13.6	112.2

TABLE 20. Sedimentary Components, after Isaacs' Corrections. in % by Weight for Wilmington Well E

Depth	Detritus	Aluminosilicates	Detrital Quartz	Silica	Apatite	Dolomite	Calcite	Total
9150	56.3	42.2	14.1	20.4	2.3	5.7	42.2	126.9
9210	67.3	50.5	16.8	27.3	0.7	1.9	9.1	106.3
9270	69.7	52.3	17.4	22.1	1.1	1.9	15.3	110.2
9330	35.5	26.6	8.9	50.6	0.6	3.8	25.4	115.8
9360	49.2	36.9	12.3	46.2	0.1	3.4	7.6	106.5
9380	45.6	34.2	11.4	49.5	0.2	1.8	8.1	105.3
9440	62.0	46.5	15.5	31.4	0.3	3.4	11.9	109.0
9500	52.3	39.2	13.1	39.3	0.2	2.5	14.5	108.9
9560	55.4	41.6	13.9	36.9	0.1	1.7	14.7	108.9
9620	62.2	46.6	15.5	30.1	0	15.1	21.7	129.2
9680	58.0	43.5	14.5	38.6	0	1.2	7.9	105.7
9700	53.1	39.8	13.3	27.2	0.2	19.4	31.5	131.4
9760	54.3	40.7	13.6	45.5	0.1	0.4	1.8	102.1
9820	56.7	42.5	14.2	34.0	0.1	2.9	17.7	111.3
9860	59.0	44.3	14.8	33.7	-0.1	3.9	13.9	110.5
9980	106.0	79.5	26.5	-5.5	-0.2	2.1	3.5	106.0
10060	71.3	53.5	17.8	22.1	-0.1	6.1	14.4	113.8
10160	62.4	46.8	15.6	31.8	-0.2	4.7	10.6	109.3
10280	67.1	50.3	16.8	28.3	-0.1	2.9	8.9	107.1
10320	72.1	54.1	18.0	23.1	-0.1	4.0	9.8	108.8

REFERENCES

REFERENCES

Activation Laboratories Ltd., 2013, 4C-XRF Fusion-XRF, http://www.Actlabs.com

Atwater, T.M., 1970, Implications of plate tectonics for the Cenozoic tectonic evolution of western North America: Geological Society of America Bulletin, v. 81, p. 3513-3536.

Aydin, A., 2000, Fractures, faults, and hydrocarbon entrapment, migration and flow: Marine and Petroleum Geology, v. 17, no. 7, p. 797-814.

Barron, J. A., 1986, Paleoceanographic and tectonic controls on deposition of the Monterey Formation and related siliceous rocks in California: Palaeogeography, Palaeoclimatology, Palaeoecology, v. 53, p. 27-15.

Barron, J.A., and Isaacs, C.M., 1999, Updated chronostratigrpahic framework for the California Miocene, *in* Isaacs, C.M., and Rullkotter, J., eds., The Monterey Formation: From rocks to molecules, New York, Columbia University Press.

Bartoush, E.J., 1938, Wilmington Oil Field, Los Angeles County, California: American Association of Petroleum Geologists Bulletin, v. 22, no. 8, p. 1048-1079.

Behl, R.J., 1999, Relationships between silica diagenesis, deformation and fluid flow in Monterey Formation cherts, Santa Maria Basin, Ca, *in* Eichhubl, P., ed., Diagenesis, deformation, and fluid flow in the Miocene Monterey Formation, Special Publication Pacific Section Society for Sedimentary Geology, 83, 77-83.

Biddle, K.T., 1991, The Los Angeles basin: an overview: *in* Biddle, K.T., ed., Active Margin Basins, American Association of Petroleum Geologists Memoir 52, p. 5-24.

Bilodeau, W.L., Bilodeau, S. W., Gath, E.M., Oborne, M., and Proctor, R.J., 2007, Geology of Los Angeles, California, United States of America: Environmental & Engineering Geoscience, v. 13, no. 2, p. 99-160.

Blake, G.H., 1991, Review of the Neogene Biostratigraphy and Stratigraphy of the Los Angeles basin and implications for basin evolution: *in* Biddle, K.T., ed., Active Margin Basin, American Association of Petroleum Geologists Memoir 52, p.135-184.

Blake, M.C., Campbell, R.H., Diblee, T.W., Howell, D.G., Nilsen, T.H., Normark, W.R., Vedder, J.C., and Silver, E.A., 1978, Neogene basin formation in relation to plate-tectonic evolution of the San Andreas fault system, California: American Association of Petroleum Geologists Bulletin, v. 62, no. 3, p. 344-372.

Bramlette, M. N., 1946. The Monterey Formation of California and the origin of its siliceous rocks: United States Geological Survey, Professional Paper 212, p. 57.

Brassell, S.C., 1992, Biomarkers in sediments, sedimentary rocks and petroleum: biological origins, geological fate and applications: Society for Sedimentary Geology, Geochemistry of Organic Matter in Sediments and Sedimentary Rocks, v. 27, p. 29-72.

Clarke, D.D.; 1987, The structure of the Wilmington oil field, *in* Oil Producing Areas in Long Beach: Santa Fe Springs, p. 43-55.

Critelli, S., Rumelhart, P.E., and Ingersoll, R.V., 1995, Petrofacies and provenance of the Puente Formation (Middle to Upper Miocene), Los Angeles basin, southern California: Implications for rapid uplift and accumulation rates: Journal of Sedimentary Research, v. A65, no. 4, p. 656-667.

Crouch, J.A., and Bukry, D., 1979, Comparison of Miocene provincial foraminferal stages to coccoliths in the California Continental borderland: Geology, v. 7, p. 211-215.

Curiale, J. C., and Odermatt, J.R., 1989, Short-term biomarker variability in the Monterey Formation, Santa Maria Basin: Organic Geochemistry, v. 14, p. 1-13.

Division of Oil, Gas, and Geothermal Resources, 1992, California oil and gas fields, volumes I, II, and III.

Durham, D., 1974, Geology of the southern Salinas Valley area, California: United States Geological Survey, Professional Paper 819, P. 111.

Durham, D.L., and Yerkes, R.F., 1964, Geology and oil resources of the eastern Puente Hills area, southern California: United States Geological Society Professional Paper 420-B, p. 62.

Elliot, P.E., Lockman, D., and Canady, W., 2009, Multiple uses for image logs within the Los Angeles basin: Society of Petrophysicists and Well Log Analysts 50th Annual Logging Symposium, Woodlands, TX.

.

Follmi, K.B., Garrison, R.E., and Grimm, K.A., 1991, Stratification in phosphatic sediments: Illustrations from the Neogene of California, *in* Einsele, G., Ricken, W., and Seilacher, A., eds., Cycles and events in stratigraphy: Berlin, Springer-Verlag, p.492-507

Follmi, K.B., Badertscher, C., de Kaenel, E., Stille, P., John, C.M., Adatte, T., and Steinmann, P., 2005, Phosphogenesis and organic-carbon preservation in the Miocene Monterey Formation at Naples Beach, California: The Monterey hypothesis revisited, Geological Society of America, v. 117, no. 5/6, p. 589-619.

Garrison, R.E., Hoppie, B.W., and Grimm, K.A., 1994, Phosphates and dolomites in coastal upwelling sediments of the Peru margin and the Monterey Formation (Naples Beach section), California, in Hornafius, J.S., ed, Field guide to the Monterey Formation between Santa Barbara and Gaviota, California: Bakersfield, Pacific Section, American Association of Petroleum Geologists, p. 67-84

Graham, S.A, and Williams, L.A., 1985, Tectonic, depositional, and diagenetic history of Monterey Formation (Miocene), central San Joaquin basin, California: American Association of Petroleum Geologists Bulletin, v. 69, p. 385-411

Hoots, H.W., 1931, Geology of the eastern part of the Santa Monica Mountains, Los Angeles County, California: United States Geological Society Professional Paper 165-C, p. 134-183.

Hoots, H.W., 1935, Marine oil shale, source of oil in Playa Del Rey field, California: American Association of Petroleum Geologists Bulletin, v. 19, no. 2, p. 172-205.

Hornafius, J.S., 1991, Facies analysis of the Monterey Formation in the northern Santa Barbara Channel, American Association of Petroleum Geologists, Bulletin 75, p. 894-909.

Ingersoll, R.V., Rumelhart, P.E., 1999, Three-stage evolution of the Los Angeles basin, southern California, Geology, v. 27, no. 7, p. 593-596.

Ingle, J.C. Jr., 1980, Cenozoic paleobathymetry and depositional history of selected sequences within the southern California continental borderland: in W. Sliter, ed., Studies in Micropaleontology, Foram, Res, Special Publication 19, p. 163-195, Washington DC, Cushman Foundation.

Ingle, J.C. Jr., 1981, Origin of Neogene diatomites around the north Pacific rim, *in* Garrison, R.E., and Douglas, R.G., eds. The Monterey Formation and related siliceous rocks of California: Los Angeles, Pacific Section, Society of Economic Paleontologists and Mineralogists, p. 159-179

Isaacs, C. M., 1980, Diagenesis is the Monterey Formation examined laterally along the coast near Santa Barbara, California: Stanford University unpublished Ph.D. thesis, p. 329.

Isaacs, C.M., 1981, Lithostratigraphy of the Monterey Formation, Goleta to Point Conception, Santa Barbara coast, California, *in* Isaacs, C.M., ed., Guide to the Monterey Formation in the California coastal area, Ventura to San Luis Obisbo: Los Angeles, Pacific Section, American Association of Petroleum Geologists, p. 9-23

Isaacs, C.M., 1983, Compositional variation and sequence in the Miocene Monterey Formation, Santa Barbara coastal area, California: *in* Larue, D.K. and Steel, R.J., eds., Cenozoic Marine Sedimentation, Pacific margin, USA. Pacific Section Society for Sedimentary Geology Special Publication 117-132.

Isaacs, C.M., 1984, Hemipelagic deposits in a Miocene basin, California, *in* Larue, D.K., and Steel, R.J., eds., Cenozoic Marine Sedimentation, Pacific margin, USA: Pacific Section Society for Sedimentary Geology Special Publication 15, p. 481-496.

Isaacs, C.M., 1985, Abundance versus rates of accumulation in fine-grained strat of the Miocene Santa Barbara basin, California: Geo-Marine Letters, v. 5, p.25-30.

Isaacs, C.M., 1987, Use of well cuttings for determining compositional trends in the Monterey Formation, California, [abs.]: American Association of Petroleum Geologists Bulletin, v. 71, p. 570-571.

Isaacs, C.M., 2001, Depositional framework of the Monterey Formation, California: *in* Isaacs, C.M., and Rullkotter, J., eds., The Monterey Formation: from rocks to molecules, New York, Columbia University Press, p. 1-30.

Isaacs, C.M., and Peterson, N.F., 1987, Petroleum in the Miocene Monterey Formation, California, *in* the Hein, J.R., ed, Siliceous sedimentary rock-hosted ores and petroleum: New York, Van Nostrand Reinhold, p. 83-116.

Isaacs, C.M., Jackson, L.L., Stewart, K.C., and Scott, N., 1989, Analytical reproducibility and abundances of major oxides, total carbon, organic carbon, and sedimentary components of Miocene and early Pliocene cuttings from the Point Conception Deep Stratigraphic Test well, OCS-Cal 78-164 No. 1, offshore Santa Maria basin, southern California: United States Geological Society Open-File Report 87-75, p. 1-26.

Isaacs, C.M., Tomson, J.H., Taggart, J.E., Jackson, L.L., 1990, Abundances of major elements and sedimentary components in Miocene and early Pliocene cuttings from a well in the South Elwood oil field area, offshore Santa Barbara-Ventura basin, southern California: United States Geological Survey Open-File Report 89-79, p. 1-26.

Isaacs, C.M.., Tomson, J.H., Stewart, K.C., and Jackson, L.L., 1992, Abundances of major elements and sedimentary components in cuttings from the Repetto, Sisquoc, and Monterey Formations, OCS P-0188 H-1 and H-2 wells, Hondo Oil Field, offshore Santa Barbara-Ventura Basin, southern California: United States Geological Society Open-File Report 92-383.

Isaacs, C.M., Medrano, M.D., Siems, D.F., and Mee, J.S., 1993, Abundances of major elements and sedimentary components in cuttings from the Foxen, Sisquoc, Monterey and Point Sal formations, OCS P-0315-1 Well, Point Arguello oil field, offshore Santa Maria basin, southern California: United States Geological Survey Open File Report 93-382, p. 1-32.

Isaacs, C.M., and Rullkotter, R., 2001, The Monterey Formation: from rocks to molecules, Isaacs, C.M., and Rullkotter, J., eds., New York, Columbia University Press.

Jacobson, J.B., and Lindblom, R.G., 1987, The East Beverly Hills, South Salt Lake and San Vicente fields- examples of urban oil development, Los Angeles, California: *in* Wright, T., and Heck, H., eds., Petroleum Geology of Coastal Southern California: American Association of Petroleum Geologists p. 32-39.

Jefferey, A.W.A., Alimi, H.M., and Jenden, P.D., 1991, Geochemistry of Los Angeles basin oil and gas systems: *in* Biddle, K.T., ed., Active Margin Basin, American Association of Petroleum Geologists Memoir 52, p.197-219.

Katz, B.J., and Elrod, L.W., 1983, Organic geochemistry of DSDP Site 467, offshore California, Middle Miocene to Lower Pliocene strata, Geochemica et Cosmochemica Acta, v. 47, p. 389-396.

Keller M. A. and Isaacs C. M., 1985, An evaluation of temperature scales for silica diagenesis in diatomaceous sequences including a new approach based on the Miocene Monterey Formation, California: Geo-Marine Letters, v. 5, p. 31-35.

Kennet, J.P., 1977, Cenozoic evolution of Antarctic glaciations, the circum-Antarctic Ocean, and the impact of global paleooceanography: journal of Geophysical Research, v. 82, p. 3843-3860.

Kleinpell, R.M., 1938, Miocene stratigraphy of California: American Association of Petroleum Geologists, p. 450.

Luyendyk, B.P., 1991, A model for Neogene crustal rotations, transtension, and transpression in southern California: Geological Society of America Bulletin, v. 103, p. 1528-1536.

Luyendyk, B.P., and Hornafius, J.S., 1987, Neogene crutal rotations, fault slip, and basin development in southern California, *in* Ingersoll, R.V., and Ernst, W.G., eds., Cenozoic basin development of Coastal California: Englewood Cliffs, New Jersey, Prentice-Hall, Inc, Rubey v. 6, p. 259-283.

MacKinnon, T.C., 1989, Origin of the Miocene Monterey Formation in California, in MacKinnon, T.C., ed., Oil in California Monterey Formation: Fieldtrip guidebook T311: Washington, D.C., American Geophysical Union, p. 1-10.

Mayuga, M.N., 1970, Geology and development of California's giant- Wilmington Oil Field, American Association of Petroleum Geologists Special Volumes M. 14, p.158-184.

Michael, E.G., 2001, Geochemical characterization of the Miocene Monterey Formation and oils in the Santa Barbara-Ventura and Santa Maria basins,, *in* Isaacs, C.M., and Rullkotter, J., eds., The Monterey Formation: from rocks to molecules, New York, Columbia University Press, p. 1-30.

Moore, D.M., and Reynolds, R.C. Jr., 1997, X-ray diffraction and the identification and analysis of clay minerals. 2nd ed. Oxford University Press, New York.

Nicholson, C., Sorlien, C., Atwater, T., Crowell, J.C., and Luyendyk, B.P., 1994, Microplate capture, rotation of the western Transverse Ranges, and initiation of the San Andreas transform as a low-angle fault system: Geology, v. 22, p. 491-495.

Norton, T.F., and Otott, G.E., 1996, The stratigraphy of the Wilmington oil field: *in* Clarke, D., Otott, G.E., and Phillips, C.C., eds., Old oil fields and new life: a visit to the giants of the Los Angeles basin, Pacific Section American Association of Petroleum Geologists, Guidebook, p. 23-35.

Otott, G.E., 1996, History of the Wilmington oil field- 1986-1996. *in* Clarke, D., Otott, G.E., and Phillips, C.C., eds., Old oil fields and new life: a visit to the giants of the Los Angeles basin, Pacific Section American Association of Petroleum Geologists, Guidebook, p. 17-22.

Peters, K.E., Magoon, L.B., Zenin, C.V., Liilis, P.G., 2007, Source-rock geochemistry of the San Joaquin Basin Province, California: in Petroleum Systems and Geologic Assessment of Oil and Gas in the San Joaquin Basin Province, California, p. 1-102

Philippi, G.T., 1975, The deep subsurface temperature controlled origin of the gaseous and gasoline- range hydrocarbons of petroleum: Geochimica et Cosmochimica Act, v. 39, p. 1359-1373.

Pisciotto, K.A., and Garrison, R.E., 1981, Lithofacies and depositional environments of the Monterey Formation, California: *in* Garrison, R.E., and Douglas, R.G., eds., The Monterey Formation and related siliceous rocks of California, Society for Sedimentary Geology, p. 97-122.

Redin, T., 1991, Oil and gas production from submarine fans of the Los Angeles basin, *in* Biddle, K.T., ed., Active margin basins: American Association for Petroleum Geologists Memoir 52, p. 239-259

Reid, A.A., and McIntyre, J.L., 2001, Monterey Formation porcelanite reservoirs of the Elk Hills field, Kern County, California, American Association of Petroleum Geologists Bulletin, v. 85, no. 1, p. 169-189.

Romero, A.M., and Philp, R.P., 2012, Organic geochemistry of the Woodford Shale, southeastern Oklahoma: How variable can shales be, American Association of Petroleum Geologists Bulletin, v. 96, no. 3, p. 493-517.

Rumelhart, P.E., Ingersoll, R.V., 1997, Provenance of the upper Miocene Modelo Formation and subsidence analysis of the Los Angeles basin, southern California: Implications for paleotectonic and paleogeographic reconstructions, Geological Society of America, v. 109, no. 7, p 885-899.

Schoellhamer, J.E., Vedder, J.G., Yerkes, R.F., and Kinney, D.M., 1981, Geology of the northern Santa Ana Mountains, California: USGS Professional Paper 420-D p. D1-D109.

Schwalbach, J.R., and Gorsline, 1985, Holocene sediment budgets for the basins of California Continental Broderland, Journal of Sedimentary Petrology, v. 55, p. 829-842.

Schweller, W.J., Gidman, J., Grant, C.W., and Reed, A.A., 1988, Lithofacies, depositional environments, and reservoir quality of Pliocene deep-sea fan sediments, Inglewood field, Los Angeles basin, California, Society for Sedimentary Geologists, Giant oil and gas fields, v. 1 and v. 2, p. 1-29.

Smith, B.C., 2011, Fundamentals of Fourier Transform Infrared Spectroscopy: Boca Raton, CRS Press, Taylor &Francis Group.

Speakman, S.A., 2011, An introduction to Reitveld Refinement using PANalytical X'pert HighScore Plus v3.0a: *in* Fundamentals of Rietveld Refinement: Massachusetts, Institute of Technology.

Srodon, J., Drits, V.A., McCarty, K., Hsieh, J.C., and Eberl, D.D., 2001, Quantitative x-ray diffraction analysis of clay-bearing rocks from random preparations: Clays and Clay Minerals, v. 49, no. 6, p. 514-528.

Teng, L.S., and Gorsline, D.S., 1989, Late Cenozoic sedimentation in California continental borderland basins as revealed by seismic facies analysis: Geological Society of America Bulletin, v. 101, p. 27-41.

Testa, S.M., 2007, The history of oil along the Newport-Inglewood structural zone- Los Angeles county, California: Petroleum History Institute, Oil Industry History, v. 8, no. 1, p. 9-35.

Tovell, W.M., 1942, Geology of the Nodular Shale and upper Miocene of the western Los Angeles basin: California Institute of Technology Master's Thesis.

Truex, J.N., 1974, Structural evolution of Wilmington, California, anticline: American Association of Petroleum Geologists Bulletin, v. 58, p. 2398-2410.

Tsutsumi, T., Yeats, R.S., and Huftile, G.J., 2001, Late Cenozoic tectonics of the northern Los Angeles fault system, California, Geological Society of America Bulletin, v. 113, p. 454-468.

USGS, 2012, Assessment of Potential Additions to Conventional Oil and Gas Reserves in Discovered Field of the United States from Reserve Growth, Fact Sheet 2012-3108.

Waples, D.W., Machihara, T., and Tsutomo, M., 1991, Biomarkers as organic-facies indicators: *in* Waples, D.W., and Machihara, T., eds., Biomarkers for geologists: a practical guide to the application of steranes and triterpanes in petroleum geology: American Association of Petroleum Geologists Special Volume, p. 41-61.

Walker, A.L., McCulloh, T.H., Peterson, N.F., and Stewart, R.J., 1983, Anomalously low reflectance of vitrinite, in comparison with other petroleum source-rock maturation indices, from the Miocene Modelo Formation in the Los Angeles basin, California, *in* Isaacs, C.M., ed., Petroleum generation and occurrence in the Miocene Monterey Formation, California, p. 185-190.

Wissler, S.G., 1943, Stratigraphic relations of the producing zone of the Los Angeles basin oil fields: California Division of Mines, Bulletin, n. 170, Part 2, p. 209-234.

Wissler, S.G., 1958, Correlation chart of producing zones of Los Angeles basin oil fields, *in* Higgins, J.W., ed., A guide to the geology and oil fields of the Los Angeles and Ventura regions: Pacific Section American Association of Petroleum Geologists, p. 59-61.

Woodring, W.P., Bramlette, M.N., and Kew, W.S., 1946, Geology and paleontology of Palos Verde Hills, California: USGS Professional Paper 207, p.145.

Woodring, W.P., Bramlette, M.N., and Kleinpell, R.M., 1936, Miocene stratigraphy and paleontology of Palos Verde Hills, California: AAPG Bulletin, v. 20, 9.125-149.

Woodfruff, F. and Savin, S.M., 1989, Miocene deepwater oceanography: Paleoceanography, v. 4, p. 87-140.

Wright, T.L, 1987, The Inglewood oil field, Petroleum Geology of Coastal Southern California; Pacific Section of American Association of Petroleum Geologists, p. 41-49.

Wright, T.L., 1991, Structural geology and tectonic evolution of the Los Angeles basin, California: *in* Biddle, K.T., ed., Active Margin Basins: American Association of Petroleum Geologists, p. 35-134.

Yeats, R.S., and Beall, J.M., 1991, Stratigraphic controls of oil fields in the Los Angeles basin: guide to maturation history, *in* Biddle, K.T., ed., Active margin basins: American Association for Petroleum Geologists Memoir 52, p. 221-237.

Yerkes, R. F., 1972, Geology and oil reserves in the western Puente Hills area, southern California: USGS Professional Paper 420-C, p. 63.

Yerkes, R.F., McCulloh, J.E., Schoellhamer, J.E., and Vedder, J.G., 1965, Geology of the Los Angeles basin, California: United States Geological Survey Professional Paper 420-A, p. 1-57

Yerkes, R.F., and Campbell, R. H., 1979, Stratigraphic nomenclature of the central Santa Monica Mountains, Los Angeles County, California: USGS Contributions to Stratigraphy, Bulletin 1457-E, p. E1-E31.